Università degli Studi di Pisa

Facoltà di Scienze Matematiche, Fisiche e Naturali

Ph.D. Thesis in Mathematics

Dr. **Marina Cosentino**

Connectance and Stability in Systems with a Large Number of Degrees of Freedom

Advisor: Prof. **Claude Froeschlé**
Internal Advisor: Prof. **Andrea Milani Comparetti**

Ph.D. Director: Prof. **Fabrizio Broglia**

A Dimitri

"La scienza è una scoperta.
Fai tutti i passi motivati, ben misurati, ma quello che scopri scopri!
Non è la conseguenza dei passi.
I passi ti portano su quel davanzale da cui vedi lo spettacolo della scoperta.
La scoperta è uno spettacolo e l'Autore di questo spettacolo è chi fa tutte le cose."

(L. Giussani)

Contents

Chapter 1

Introduction

In this thesis we investigate the properties of dynamical systems with a large number of degrees of freedom as a function of the number of couplings among the equations of motion. This parameter is called *connectance* and exists in the literature since the seventies, having been introduced in a pioneer numerical work by Gardner and Ashby [23] for a linear system. Since then this subject has been very little developed, both from the theoretical and the numerical point of view.

In spite of the reduced number of studies deserved to it, the notion of connectance is considered important for many applications, in particular ecology and economics. In these domains a common question is how the qualitative properties of interacting systems change when the number of interactions among degrees of freedom grows, i.e. when the dynamics becomes in some sense more complex. One can be interested to the transition from order to chaos, or more simply to the transition from stability to instability for a given equilibrium solution. For reasons of simplicity most studies discard the full richness of nonlinear dynamics and are restricted in fact to the analysis of local properties about equilibria.

Our aim is to review the relationships between dynamical properties and connectance, for what concerns both local (then linearized systems) and global nonlinear features. We investigate whether the connectance is a useful indicator to parameterize some characteristics of the system. For what concerns the nonlinear dynamics we concentrate on the conservative case, because in this domain there exists a wide range of well-established results, even if the non-conservative case can be very important for the applications.

Our results are mainly numerical and are intended to be a point of departure for further theoretical work. Nevertheless, they represent as well some firmer bases for those applications in which the notion of connectance is relevant.

Our thesis is structured as follows.

In Chapter 2 we summarize the theory of linear systems, which is applied to the study of local properties about equilibria.

Chapter 3 contains a review of the theory of conservative dynamical systems. In particular, we concentrate on the study of integrable and quasi-integrable dynamics. The classical KAM and Nekhoroshev theorems, concerning the stability of the actions in the non-integrable case, are analysed, and the notion of Hamiltonian chaos is introduced.

In Chapter 4 we introduce the notion of connectance from an historical point of view. We discuss the original numerical experiment of Gardner and Ashby [23], who first introduced the notion of connectance. Their study deals with a linear system, for which the connectance is simply defined as the fraction of non-zero off-diagonal elements in the corresponding matrix. The problem under investigation concerns how the probability of stability changes when the connectance is increased, for a large set of matrices. The non-connected case consists of a diagonal matrix with negative elements. The stability is evaluated by computing the eigenvalues, according to the classical result that a continuous systems is stable when the real part of all the eigenvalues is negative. All numerical experiments reported in the literature show that when the matrix elements are taken at random, the probability of instability grows with the connectance. Conversely, ecological considerations suggest that more "complex" systems (i.e. with large connectance) are more stable, giving rise to a decennial controversy. We briefly resume the implications of this debate, as well as its applications to population and market dynamics.

For the nonlinear case, we discuss the pioneer numerical experiment of Froeschlé [17], in which for a specific n-dimensional coupled symplectic mapping the relationship between connectance and chaos is investigated. Here the connectance is defined as in the linear case, given a matrix of coefficients which prescribe the couplings. Froeschlé found that the fraction of chaotic orbits ncreases not only with the number of degrees of freedom, but with the connectance as well. This study leaved many open question, but nevertheless it has not been further developed.

In Chapter 5 we reconsider the influence of the connectance on the stability from a local analysis point of view. A generic n-dimensional system is linearized about an equilibrium and the resulting matrix is considered. We take as a point of departure the classical Gardner and Ashby experiment, and we study numerically the probability of stability as a function of the connectance and of the statistical distribution of the matrix elements. While generically we confirm the decrease of stability with the connectance, we find some regimes for the coefficients in which a recover of stability at large connectance is obtained. This is a very surprising result,

which can have applications in ecology and economics. We investigate this special situation by studying experimentally the probability distribution of the eigenvalue with largest real part when the matrix is completely full. We discover some scaling laws as a function of the matrix parameters, for which a theoretical explanation does not exist yet. These results, obtained in particular for negative off-diagonal elements, can represent a suggestion for extending the theory of random matrices in a new direction.

In Chapter 6 we switch from the local analysis to the global investigation of many orbits in conservative nonlinear systems. We first explain the notion of chaoticity and discuss some tools to detect and measure chaos. We then study the influence of the connectance on the degree of chaoticity in two different models. The first one derives strictly from the original Froeschlé mapping [17], while the second is a variant of the classical Hamiltonian mean field system [1]. In both cases we deal with a coupled n-dimensional symplectic mapping in which a matrix of coupling coefficients is introduced. While in the linear context the values of these coefficients are distributed according to given statistical laws, here for simplicity they take only the values zero or one.

A linear model is completely defined by its matrix, so that the connectance is a non-ambiguous concept. In the nonlinear case, the connectance can be defined in many ways according to the structure of the equations. For this reason, along with a definition of connectance still given by the fraction of non-zero elements in the coupling matrix, we consider another indicator given by the fraction of direct couplings in the equations of motion. This quantity can be nevertheless difficult to evaluate a priori.

In the first model, the connectance does not measure directly the fraction of direct couplings, while it does in the second one. In both systems the probability of chaoticity always decreases with the percentage of direct dynamical couplings, as far as the number of effective degrees of freedom is not reduced due to special symmetries. The connectance is instead a less useful parameter, as it can be seen in the first model, for which the probability of chaoticity decreases with the connectance until it reaches a minimum, and then starts to increase. This happens because the minimum corresponds already to full dynamical coupling, and a further increase of the connectance leads in fact to a reduction of the number of degrees of freedom. This is due to the special structure of the couplings when the connectance is larger than a given value.

These results, which should be extended to a wider class of models, are a first step toward establishing a relation among the structure of couplings in a system and its generic properties. The connectance is one of the most economical parameters

that can be introduced in this sense. It still has predictive properties when intended as the fraction of direct dynamical couplings, and not simply as a trivial property of a matrix defining the model equations. Our results not only confirm the previous findings, but reveal that the relationship between connectance and dynamical properties is far from being completely understood. The problem remains open toward further studies, both theoretical and numerical.

Chapter 2

The stability of the equilibrium points in dynamical systems

A dynamical system is a mathematical model which expresses the variability of a situation changing with time. The time t can be represented as continuous, $t \in \mathbb{R}$, or discrete, $t \in \mathbb{Z}$.

It is well known that the notion of equilibrium plays a very important role in the study of the behaviour of a dynamical system. In particular, equilibria become interesting when their stability properties can be investigated.

In this Chapter we perform an analytic and qualitative study of the behaviour of the orbits about the equilibrium points in continuous systems. The fundamental question is whether an orbit with a given initial condition close to an equilibrium remains indefinitely close or if it escapes far away. Loosely speaking, in the first case we will say that the equilibrium is stable, in the second case that it is unstable. As a first step, we introduce the linearization of a generic system about an equilibrium point and discuss the behaviour of the solution of the relative linear equation, both in the plane case and for the n-dimensional case. The nature of these solutions will be used next to analyse the stability of the equilibrium points for the original system.

The notion of equilibrium discussed in this Chapter will be used in Chapters 4 and 5, in which the transition from stability to instability will be investigated as a function of the degree of the interactions among the n degrees of freedom of the system.

2.1 Linearization of a dynamical system about an equilibrium point

In this section we discuss the linearization of a dynamical system of n degrees of freedom about an equilibrium and the behaviour of the corresponding solutions. For simplicity we start with the case of the plane ($n = 2$) and we generalize then to the case of n degrees of freedom.

We consider a general system with n degrees of freedom

$$\begin{aligned} \mathbf{f} : \mathbb{R}^n &\to \mathbb{R}^n \\ \mathbf{x} &\mapsto \mathbf{f}(\mathbf{x}) = \dot{\mathbf{x}} \end{aligned} \tag{2.1}$$

If there exists an equilibrium solution $\mathbf{x}(t) = \mathbf{c}$, where $\mathbf{c}$ satisfies $\mathbf{f}(\mathbf{c}) = \mathbf{0}$, we consider the linear approximation about $\mathbf{c}$. In other words, we write $\mathbf{x} = \mathbf{c} + \tilde{\mathbf{x}}$ and we consider the Taylor expansion at the first order for $\mathbf{f}(\mathbf{c} + \tilde{\mathbf{x}})$, i. e.

$$f(\mathbf{c} + \tilde{\mathbf{x}}) = A\tilde{\mathbf{x}} + O(\tilde{\mathbf{x}}^2) \tag{2.2}$$

where A is the Jacobian matrix of $\mathbf{f}$ evaluated at $\mathbf{c}$,

$$A_{ij} = \frac{\partial f_i}{\partial x_j}|_{\mathbf{x}=\mathbf{c}}. \tag{2.3}$$

In this way we reduce ourselves to the study of the system $\dot{\tilde{\mathbf{x}}} = A\tilde{\mathbf{x}}$, i.e., by changing the name of the variable $\tilde{\mathbf{x}}$, to the system

$$\dot{\mathbf{x}} = A\mathbf{x}, \ \mathbf{x} \in \mathbb{R}^n, \tag{2.4}$$

where A is a linear real operator. The equation (2.4) with A in the form of (2.3) is called *variational equation* for the equation (2.1) related to the particular solution $\mathbf{x} = \mathbf{c}$.

A way to solve this equation consists in changing the coordinates to reduce it to the simplest possible form, called *canonical form*. The optimal case occurs when a new basis $\{\mathbf{u}_1, \ldots, \mathbf{u}_n\}$ can be introduced in which the linear operator A is diagonal. Calling M the change-of-basis matrix from the old coordinates to the new ones $\boldsymbol{\xi}$, i.e. $\mathbf{x} = M\boldsymbol{\xi}$, the equation (2.4) takes the form

$$\dot{\boldsymbol{\xi}} = \Lambda\boldsymbol{\xi}, \qquad \Lambda = M^{-1}AM \tag{2.5}$$

It is easy to demonstrate that the vectors $\mathbf{u}_1, \ldots, \mathbf{u}_n$ must satisfy the *eigenvalue equation* for the matrix A, i.e.

$$A\mathbf{u}_i = \lambda_i \mathbf{u}_i \tag{2.6}$$

where the eigenvalues λ_i are the diagonal elements of the matrix Λ.

This diagonalization procedure is always possible if there exist n distinct eigenvalues. Otherwise, the canonical form will not be necessarily diagonal, depending on the dimension of $Ker(A - \lambda I)$ [52].

In order to have non trivial solutions for the equation (2.6), λ must satisfy the *characteristic equation*

$$det(A - \lambda I) = 0 \tag{2.7}$$

which is an algebraic equation of the form

$$P_n(\lambda) = p_n\lambda^n + p_{n-1}\lambda^{n-1} + \ldots + p_0 = 0$$

with real coefficients $p_0, \ldots p_n$.

The solutions of the linear system (2.4) can be classified according to the solutions of the characteristic equation. In the following subsection we discuss in detail the case $n = 2$.

2.1.1 The nature of the solutions in the plane

For $n = 2$, the characteristic equation can be written as

$$\lambda^2 - \lambda TrA + detA = 0.$$

We classify the solutions according to the sign of the discriminant $\triangle = (TrA)^2 - 4detA$. We have then the three different cases:

- **Case 1**: $\triangle > 0$: two different real eigenvalues λ_1, λ_2;
- **Case 2**: $\triangle < 0$ two complex-conjugate eigenvalues; λ_1, λ_2
- **Case 3**: $\triangle = 0$ two coincident real eigenvalues.

Case 1 (two different real eigenvalues λ_1, λ_2). The eigenvectors too can be chosen real and the general solution is

$$\mathbf{x}(t) = \alpha_1 e^{\lambda_1 t}\mathbf{u}_1 + \alpha_2 e^{\lambda_2 t}\mathbf{u}_2 \ (\alpha_i \in \mathbb{R}). \tag{2.8}$$

We analyse now the qualitative behaviour of the orbits. Denoting with ξ and η the new variables, the solutions passing from ξ_0 and η_0 are

$$\xi(t) = \xi_0 e^{\lambda_1 t}, \ \eta(t) = \eta_0 e^{\lambda_2 t}. \tag{2.9}$$

If we represent the orbits in the plane (ξ, η), we obtain the dynamics displayed in Figure 2.1 and 2.2. When not both the eigenvalues are equal to zero, we can distinguish the following cases:

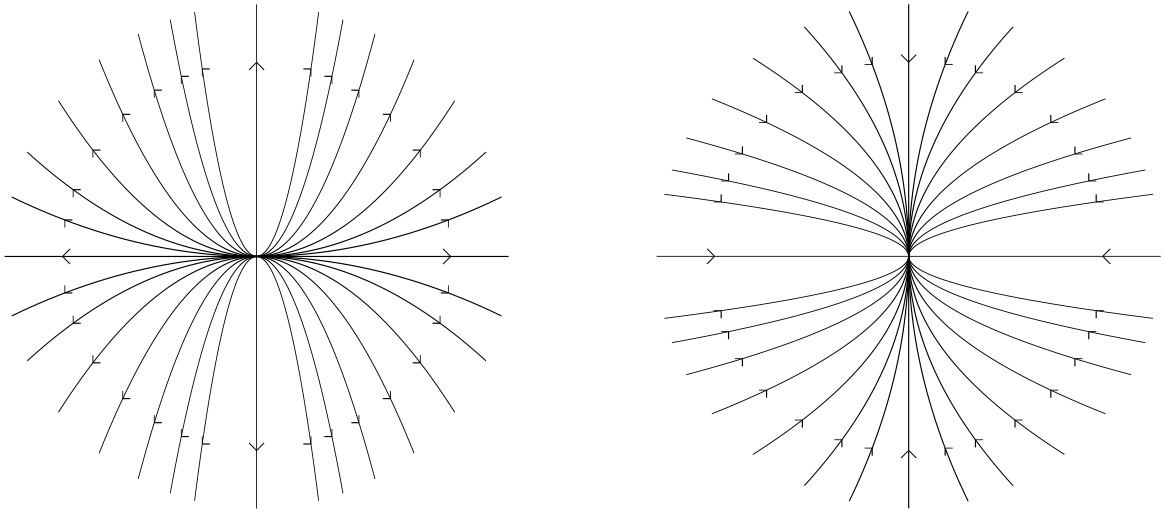

(a) (b)

Figure 2.1: Case of real different eigenvalues with equal sign. In (a) the eigenvalues are such that $\lambda_1, \lambda_2 > 0$ (unstable node). In (b) we have $\lambda_1, \lambda_2 < 0$ (stable node).

1. λ_1 and λ_2 with the same sign. By the elimination of the time in equation (2.9), we obtain $\frac{\eta}{\eta_0} = (\frac{\xi}{\xi_0})^{\lambda_2/\lambda_1}$. We observe that all the orbits cross the origin, the dynamics depending on the positive or negative sign of the eigenvalues:
   (a) if $\lambda_1, \lambda_2 > 0$ the orbits go out from the origin which is called *unstable node* (Figure 2.1a);
   (b) if $\lambda_1, \lambda_2 < 0$ the orbits go into the origin which is called *stable node* (Figure 2.1b).
2. λ_1 and λ_2 with different sign. The trajectories are still given by $\frac{\eta}{\eta_0} = (\frac{\xi}{\xi_0})^{\lambda_2/\lambda_1}$ and, when supposing $\lambda_1 < 0 < \lambda_2$, we obtain Figure 2.2. With the exception of the orbits lying on the axes, all the other ones come from infinity and go to infinity. The origin in this case is called *unstable saddle*.
3. One eigenvalue equal to zero. We assume $\lambda_1 = 0$ and we write the solutions:
$$\xi(t) = \xi_0, \ \eta(t) = \eta_0 e^{\lambda_2 t}.$$
The dynamics depends on the sign of λ_2: if $\lambda_2 < 0$ we obtain Figure 2.3a, while if $\lambda_2 > 0$ we obtain Figure 2.3b.

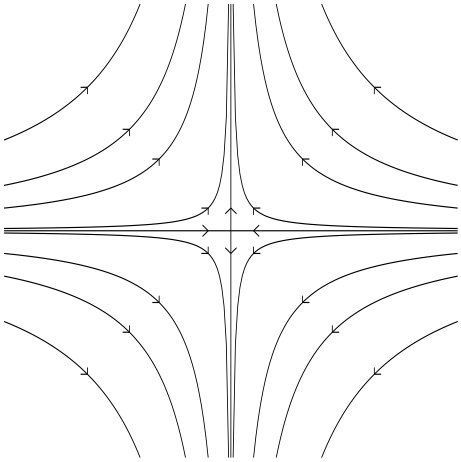

Figure 2.2: Case of real different eigenvalues with different sign, $\lambda_1 < 0 < \lambda_2$ (saddle).

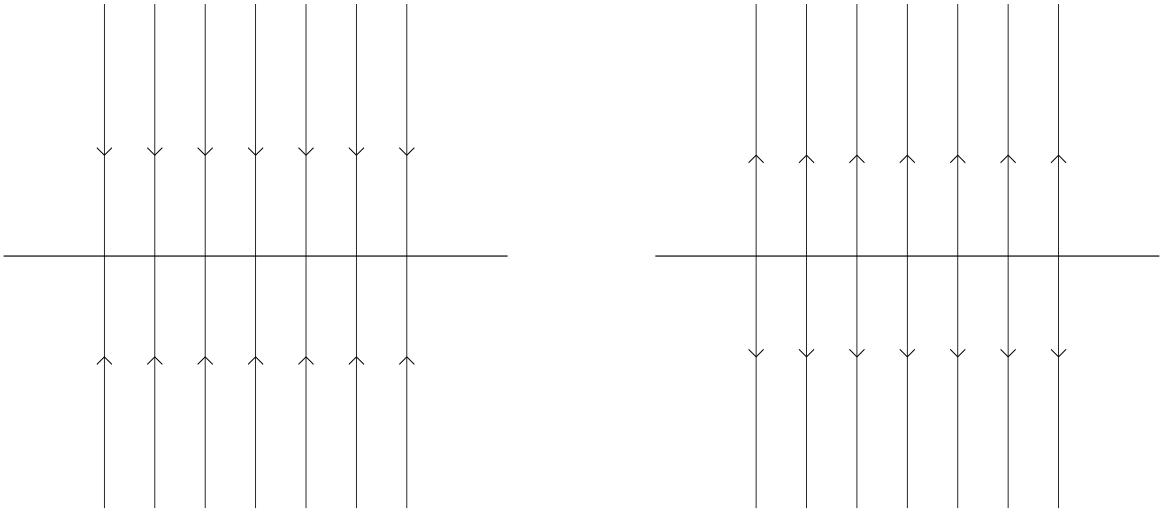

(a) (b)

Figure 2.3: Case of real different eigenvalues λ_1, λ_2 such that $\lambda_1 = 0$. In (a) λ_2 is negative, while in (b) λ_2 is positive.

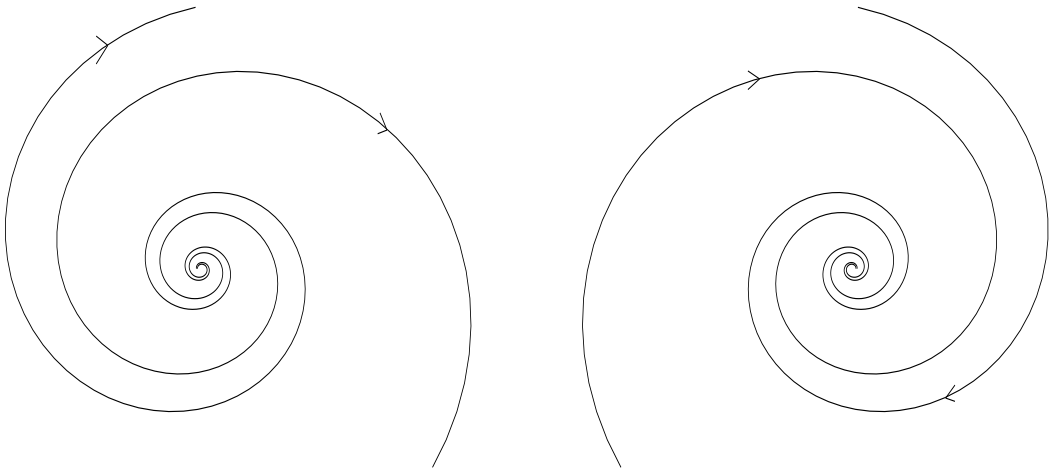

(a) (b)

Figure 2.4: Case of complex-conjugate eigenvalues with $Re\lambda \neq 0$. In (a) $Re\lambda$ is positive and one has a source (unstable), while in (b) $Re\lambda$ is negative and one has an unstable fo.

Case 2 (eigenvalues λ_1, λ_2 complex-conjugate). We denote $\lambda_1 = \lambda$, $\mathbf{u}_1 = \mathbf{u}$. We have then $\lambda_2 = \bar{\lambda}$ (complex-conjugate of λ_1) and $\mathbf{u}_2 = \bar{\mathbf{u}}$. In analogy with the previous case, the general solution can be written as

$$\mathbf{x}(t) = Ce^{\lambda t}\mathbf{u} + De^{\bar{\lambda} t}\bar{\mathbf{u}} \ (C, D \in \mathbb{C}) \tag{2.10}$$

and it is real for $D = \bar{C}$. If we want to express the real solution $\mathbf{x}(t)$ without using complex vectors and coefficients, we have to decompose $\mathbf{u}$ and λ in real and imaginary parts

$$\mathbf{u} = \mathbf{v}_1 + i\mathbf{v}_2, \ \lambda = \alpha + i\beta, \ \mathbf{v}_j \in \mathbb{R}^2, \ \alpha, \beta \in \mathbb{R} \tag{2.11}$$

and we have to write C in the exponential form, $C = \rho e^{-i\gamma}$, with ρ, γ arbitrary constants. The general solution can be written now in the form

$$\mathbf{x}(t) = \xi(t)\mathbf{v}_1 + \eta(t)\mathbf{v}_2 \tag{2.12}$$

where $\xi(t) = 2\rho e^{\alpha t} cos(\beta t + \gamma)$, $\eta(t) = -2\rho e^{\alpha t} sin(\beta t + \gamma)$. We obtain then the two different kinds of dynamics shown in Figure 2.4 and 2.5 . We distinguish the two different cases, depending whether the real part $Re\lambda$ is zero or not:

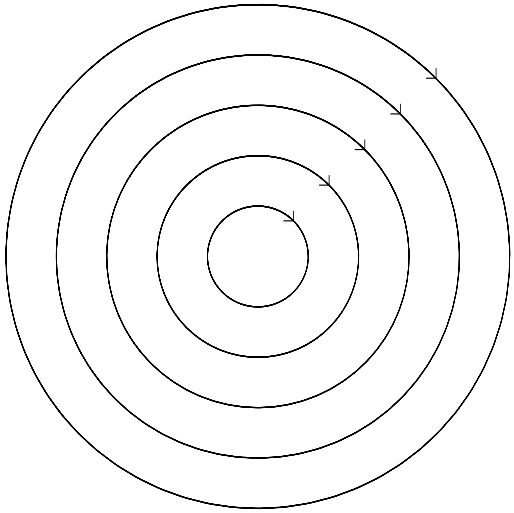

Figure 2.5: Case of complex-conjugate eigenvalues with $Re\lambda = 0$. One has a center.

1. $Re\lambda \neq 0$. The behaviour of the orbits is represented in Figure 2.4 and it depends on the positive or negative sign of $Re\lambda$. In the first case the amplitude of the curves increases, escaping from the equilibrium which is called *source* (Figure 2.4a). When $Re\lambda < 0$ the amplitude of the curves decreases, approaching the origin which is called *sink* (Figure 2.4b).

2. $Re\lambda = 0$. The behaviour of the orbits is represented in Figure 2.5. The orbits are circles and the origin is called *center*.

Case 3 It is the degenerate case in which the two eigenvalues are the same. Now the canonical form is not always diagonal, because a basis of eigenvectors does not necessarily exist. The nature of the solutions depends on the dimension of $ker(A - \lambda I)$. Without entering into the details (for a thorough discussion see [31]), we just resume the possible cases. Defining $\lambda = \lambda_1 = \lambda_2$, when $\lambda \neq 0$ we have:

1. $\dim(ker(A - \lambda I)) = 2$. The matrix Λ is given by

$$\Lambda = \begin{pmatrix} \lambda & 0 \\ 0 & \lambda \end{pmatrix}$$

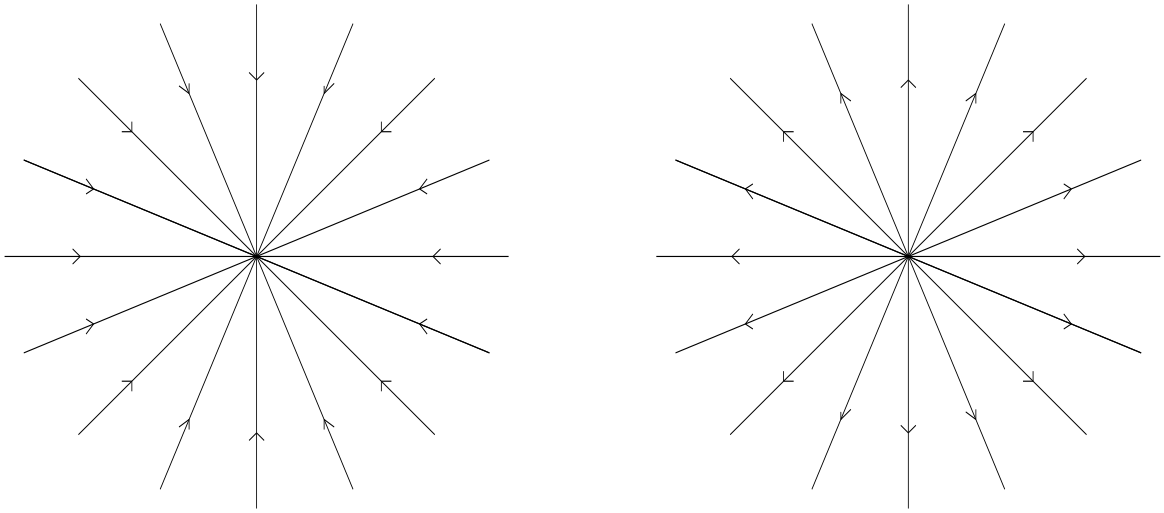

(a) (b)

Figure 2.6: The behaviour of the orbits in the phase plane for real and identical eigenvalues and degeneration of the eigenvectors. One has a star node stable (a) or unstable (b).

and the trajectories are represented in Figure 2.6 for $\lambda < 0$ or $\lambda > 0$. The origin is called *star node*.

2. $\dim(ker(A - \lambda I)) = 1$. The matrix Λ is given by

$$\Lambda = \begin{pmatrix} \lambda & 1 \\ 0 & \lambda \end{pmatrix}$$

and the trajectories are represented in Figure 2.7 for $\lambda < 0$ or $\lambda > 0$. The origin is called *degenerate node*.

Finally, when $\lambda = 0$ the matrix Λ in canonical form is simply

$$\Lambda = \begin{pmatrix} 0 & 1 \\ 0 & 0 \end{pmatrix}$$

and the ξ axis degenerates to equilibrium points, the trajectories being all straight lines parallel to the ξ axis.

(a) (b)

Figure 2.7: The behaviour of the orbits in the phase plane for identical eigenvalues. One has a degenerate node stable (a) or unstable (b).

2.1.2 The n-dimensional case

The generalization of the previous classification to the n-dimensional case is immediate when all the eigenvalues are distinct and different from zero. In this case, the corresponding eigenvectors form a basis and the space $\mathbb{R}^n$ can be decomposed in the direct sum of unidimensional subspaces, corresponding to the real eigenvalues, or two-dimensional subspaces, corresponding to the complex-conjugate eigenvalues. One recovers immediately the notions of node and saddle points for real eigenvalues, and of source, sink and center for complex ones. The cases in which at least one eigenvalue is zero, or the degenerate cases in which the eigenvalues are not all distinct, are more complicated. For a more detailed discussion one can refer to the book of Hirsch-Smale [31].

2.2 The stability of the equilibrium points

As said in the introduction of this Chapter, the notion of equilibrium points is important when their stability properties are considered. In fact there exist many

definitions of stability, which account for different situations and goals. We analyse some of these definitions, and for our purposes we consider stability for positive times only.

Definition 2.1 An equilibrium point $\bar{\mathbf{x}}$ of the differential equation $\dot{\mathbf{x}} = f(\mathbf{x})$ is said to be *stable* if for any neighborhood U of $\bar{\mathbf{x}}$ there exists a neighborhood V of $\bar{\mathbf{x}}$ such that any solution with initial condition in V remains in U for any $t \geq 0$.

Definition 2.2 An equilibrium point is said to be *unstable* if it is not stable.

Definition 2.3 An equilibrium point $\bar{\mathbf{x}}$ of the differential equation $\dot{\mathbf{x}} = f(\mathbf{x})$ is said to be *asymptotically stable* if
i) it is stable ;
ii) there exists a neighborhood V^* of $\bar{\mathbf{x}}$ such that any solution with initial condition in V^* tends to $\bar{\mathbf{x}}$ for $t \to +\infty$.

2.2.1 The 2-dimensional case

For the case of the linear equations in the plane, according to the previous definitions, a sink, a center or a node with negative eigenvalues are stable, while a saddle or a node with positive eigenvalues are unstable. The non-degenerate case in which one eigenvalue is zero is stable when the second eigenvalue is negative, unstable when the second one is positive. The degenerate cases are stable when the eigenvalue is negative, unstable when it is zero or positive.

For what concerns asymptotic stability, stable nodes, sinks and the stable degenerate cases are all asymptotically stable.

To resume our analysis for the origin in the linear equation $\dot{\mathbf{x}} = A\mathbf{x}$, it is evident that the properties of stability depend only on the sign of the real parts of the eigenvalues. More precisely one obtains:

- asymptotic stability, if and only if both eigenvalues have negative real part;
- instability, if and only if at least one eigenvalue has positive real part.

One can demonstrate that the properties of stability persist also for the original nonlinear system, unless $Re\lambda = 0$ or in the degenerate cases, in which the properties of the equilibrium can not be determined a priori.

2.2.2 The n-dimensional case

In the n-dimensional case, there exists the fundamental property:

Proposition 2.1 Given the linear equation $\dot{\mathbf{x}} = A\mathbf{x}$ in $\mathbb{R}^n$, the following holds:

- if all the eigenvalues of A have negative real parts, then the origin is asymptotically stable;
- if at least one of the eigenvalues has positive real part, then the origin is unstable.

We address now the problem of the nonlinear case. For $n = 2$, we just said that the correspondence between the behaviour of the nonlinear equation $\dot{\mathbf{x}} = \mathbf{f}(\mathbf{x})$ and of its linearization $\dot{\mathbf{x}} = A\mathbf{x}$ is not always guaranteed. Nevertheless, in the case of the proposition (2.1), the property of stability of the nonlinear problem are the same of its linearization and the following holds:

Proposition 2.2 Given the nonlinear equation $\dot{\mathbf{x}} = \mathbf{f}(\mathbf{x})$ in $\mathbb{R}^n$ and its linearization in the point $\mathbf{c}$, $\dot{\mathbf{x}} = A\mathbf{x}$, one has:

- if all the eigenvalues of A have negative real parts, then $\mathbf{c}$ is asymptotically stable;
- if at least one of the eigenvalues has positive real part, then $\mathbf{c}$ is unstable.

Chapter 3

The stability in conservative systems

In this Chapter we shift our attention to a notion of stability different from the one we examined in Chapter 2. We will deal with conservative systems, which admit a description in terms of an Hamiltonian function. In this context, we will examine the notion of integrable systems, such that some degrees of freedom (the action variables) are constant of motion. The concept of stability introduced in this Chapter has to be intended then as "stability of the actions", i.e. of their time-independent character, against perturbations of the Hamiltonian function which describes the dynamics. The two basic theorems we are going to discuss will be the KAM theorem and the Nekhoroshev theorem, which concern respectively the local stability (i.e. valid for a limited set of initial conditions in the action space) for an infinite time and the global stability over a limited time, but still useful in practice. When stability is loss, the notion of Hamiltonian chaos appears. The topology of the phase space is then of crucial importance to understand the dynamics.

Starting from continuous systems we will introduce also the notion of symplectic mappings, which in this context can usefully replace the notion of continuous dynamical systems, because they do not alterate the phase space topology.

All the definitions and theorems presented here constitute a preamble for the Chapter 6, in which the stability of the actions will be studied as a function of the interaction among the n degrees of freedom of the system.

3.1 Hamiltonian systems

A system of ordinary differential equations of type

$$\frac{d\mathbf{r}}{dt} = \mathbf{F}(\mathbf{r}) \tag{3.1}$$

is said to be in *Hamiltonian form* if $\mathbf{r}$ is a $2n$-uple and, denoting by $x_1, ..., x_n$ and $v_1, ..., v_n$ its $2n$ components, there exists a function $H(v_1, ..., v_n, x_1, ..., x_n)$ such that the equations (3.1) can be rewritten as

$$\begin{cases} \dot{v}_i = -\frac{\partial H}{\partial x_i} \\ \dot{x}_i = \frac{\partial H}{\partial v_i} \end{cases} \tag{3.2}$$

for $i = 1, ..., n$. The function H is called *the Hamiltonian*, the equations (3.2) *Hamiltonian equations* and the variables $x_1, ..., x_n$ and $v_1, ..., v_n$ are respectively called *coordinates* and *momenta*. The system is said to be *autonomous* if the Hamiltonian does not depend on the time and this is the case we will consider in the following. The *Hamiltonian flow* is the time evolution of coordinates and momenta described by (3.2) and has the following specific properties:

1. *Conservation of volume.* As it is well known, for a system of equations of type (3.1), the volume δV of an infinitesimal set of initial conditions evolves with time according to the equation

$$\frac{1}{\delta V}\frac{d\delta V}{dt} = \sum_{i=1}^{m} \frac{\partial F_i}{\partial r_i} \equiv div\mathbf{F} \tag{3.3}$$

where m is the number of components of $\mathbf{r}$ and $\mathbf{F}$. For a Hamiltonian system $H(v_1, ..., v_n, x_1, ..., x_n)$, where $m = 2n$, $\mathbf{r} = (v_1, ..., v_n, x_1, ..., x_n)$ and

$$\mathbf{F} = (-\frac{\partial H}{\partial x_1}, ..., -\frac{\partial H}{\partial x_n}, \frac{\partial H}{\partial v_1}, ..., \frac{\partial H}{\partial v_n}) \tag{3.4}$$

it is simple to check that $div\mathbf{F} = 0$. This means that the volume is preserved by Hamiltonian flow. This property is very important, because it implies that a cloud of initial conditions can never shrink nor inflate. In particular, it also implies that Hamiltonian dynamics can not have *attractors*, namely manifolds of dimension smaller than the number of degrees of freedom towards which the flow may collapse.

2. *Time evolution of a function along a Hamiltonian flow.* Given a function $f(\mathbf{v}, \mathbf{x}, t)$ defined on the phase space, with $\mathbf{v}$ and $\mathbf{x}$ evolving according to Hamilton equation (3.2), one gets by differentiation

$$\frac{df}{dt} = grad_{\mathbf{x}} f \cdot \dot{\mathbf{x}} + grad_{\mathbf{v}} f \cdot \dot{\mathbf{v}} + \frac{\partial f}{\partial t} = \{f, H\} + \frac{\partial f}{\partial t} \tag{3.5}$$

where $\{,\}$ denote the Poisson bracket.

3. *Conservation of H.* The rate of change of H versus time can be written, by differentiation of $H(\mathbf{v}, \mathbf{x}, t)$ and by applying (3.5), as

$$\frac{dH}{dt} = \{H, H\} + \frac{\partial H}{\partial t} = \frac{\partial H}{\partial t}. \tag{3.6}$$

In other words, the autonomous Hamiltonians do not change of value along the flow that they generate, namely they are *constants of motion.*

3.1.1 The concept of integrability and the action-angle variables

The solution of a system of differential equations

$$\frac{dr_i}{dt} = F_i(\mathbf{r}), \text{ with } i = 1, ..., n \text{ and } \mathbf{r} \equiv (r_1, ..., r_n) \tag{3.7}$$

can be written in an implicit form as a system of integral equations

$$\int_{\mathbf{r}(0)}^{\mathbf{r}(t)} \frac{dr_i}{F_i(\mathbf{r})} = \int_0^t dt = t. \tag{3.8}$$

The system (3.7) is therefore said to be *integrable*, if the integrals at the left hand side of (3.8) can be explicitely computed and the resulting relationships $F_i'(\mathbf{r}(t)) - F_i'(\mathbf{r}(0)) = t$ (where F_i' is the primitive of $1/F_i$) can be inverted, giving $\mathbf{r}(t)$ as an explicit function of t.

Using this definition of integrability, it is very difficult to conclude whether a given system of differential equations is integrable or not. If the solutions of the integrals are not found, it is hard to know if this is due to a genuine lack of integrability of the system, or simply to a lack of skill in finding the primitive function. This is precisely the situation which occurred until the end of the XIX^{th} century, when mathematicians believed that every Hamiltonian system was integrable. For Hamiltonian systems, a partial help comes from the *Liouville theorem*, which states that a n-degrees of freedom Hamiltonian is integrable if it admits n independent constants of motion $\Phi_1, ..., \Phi_n$, such that the Poisson bracket $\{\Phi_i, \Phi_j\}$ is zero for

$i \neq j$. Although it is easier to find constants of motion than to actually solve the Hamiltonian equations, there is no general recipe on how *all* constants of motion can be found. In particular, if only m constants of motion are known, with $m < n$, it is hard to know whether additional constants of motion are still to be found or really do not exist. For instance, for several years celestial mechanics has been looked for a third constant of motion of the three degrees of freedom Hamiltonian describing the dynamics of a star in a cubic galactic potential, until Hénon and Heiles [30] numerically showed that such a third constant of motion does not exist. Conversely, the Toda lattice Hamiltonian has been long conjectured to be non-integrable, until Michel Hénon [29] found the last missing constant of motion.

Luckily nowadays the situation is not so desperate as it was before the work of Poincaré [50] (Section 3.1.3). There exists a criterion of non-integrability – that is the appearance of chaos, which will be discussed in Section 3.2.1 – that can be used both analytically and numerically.

For what concerns the integrable Hamiltonian systems, of crucial importance is the *Arnold-Liouville theorem*, an extension of Liouville theorem provided by Arnold in 1963 [3]. In the context of Liouville theorem and if the n-dimensional surface implicitly defined by the constants of motion $\Phi_1, ..., \Phi_n$ is *compact*, Arnold proved that it is possible to introduce new variables which transform the Hamiltonian in a simpler form, without changing the Hamiltonian equations. The variables which satisfy the last request are called *canonical* and the transformation *canonical transformation*. The new canonical ($\mathbf{p}$,$\mathbf{q}$) are such that

- the coordinates $q_1, ..., q_n$ are *angles*, cyclically defined on an interval $[0, 2\pi]$ and the canonical transformation from the original momenta and coordinates is $2\pi -$ *periodic* on the angles $q_1, ..., q_n$;
- in the new variables, the Hamiltonian depends on the momenta $\mathbf{p}$ only, i. e. $H \equiv H(\mathbf{p})$.

The momenta $\mathbf{p}$ are usually called the *actions* of the system. A set of canonical variables $(\mathbf{p}, \mathbf{q})$, where the coordinates $\mathbf{q}$ are angles, are generally called *action-angle variables*.

3.1.2 Integrable dynamics and quasi-periodic motions

We said that an integrable system can be generally represented, using the action-angle variables, by a Hamiltonian H_0 depending on the actions $\mathbf{p}$ only. The equations

of motion are simply:

$$\begin{cases} \dot{p}_i = -\partial H_0/\partial q_i(\mathbf{p}) = 0 \\ \dot{q}_i = \partial H_0/\partial p_i(\mathbf{p}) = \omega_i(\mathbf{p}) \end{cases} \tag{3.9}$$

$1 \leq i \leq n$, from which follows that the actions p_i are constants of motion, while the angles q_i have constant time derivative ω_i. Since the coordinates q_i are angles, the time derivatives ω_i are in fact their *frequencies*.

Therefore each trajectory evolves on what is called in topology a *n-dimensional torus* (denoted by T^n) and this motion is called *translation on the torus*. The motion given by an integrable Hamiltonian is then a circulation of the angles with constant frequencies on a torus defined by constant values of the action $\mathbf{p}$. The tori $\mathbf{p}$=*constant* are therefore *invariant* for the dynamics, in the sense that a trajectory starting on a torus will never leave it and so the phase space is said to be *foliated in invariant tori*. Moreover, the motion of the angles on a torus depends qualitatively on the frequencies $\omega_i(\mathbf{p})$.

In Figure 3.1 it is shown the simple case $n = 1$. One can see how the trajectory on each torus is influenced by the frequency ω. In particular, it lies either on a discrete set of points (when the frequency is rational, and the orbit is periodic) or fills densely the torus (when the frequency is irrational).

If we consider the case $n = 2$, one has the following

Proposition 3.1 An orbit on a torus T^2 of frequencies $\boldsymbol{\omega} = (\omega_1, \omega_2)$ is periodic if and only if ω_2/ω_1 is a rational number; if the previous ratio is irrational then the orbit is dense on T^2.

We enunciate then hereafter some definitions and properties concerning the relationship between the frequencies and the resulting motion in the generic n-dimensional case ($n \geq 2$).

Definition 3.1 If the equation $\mathbf{k} \cdot \boldsymbol{\omega} = \sum_{i=1}^{n} k_i \omega_i = 0$, $\mathbf{k} = (k_1, ..., k_n) \in \mathbb{Z}^n$ admits as a unique solution the vector $\mathbf{k} = (0, ..., 0)$, then the frequencies are said to be *non-resonant*.

Definition 3.2 If there exist $n-1$ independent linear vectors $\mathbf{k}$ such that $\mathbf{k} \cdot \boldsymbol{\omega} = 0$, then the frequencies are said to be *completely resonant*.

Definition 3.3 The subset $\mathcal{M}_{\boldsymbol{\omega}} = \{\mathbf{k} \in \mathbb{Z}^n : \mathbf{k} \cdot \boldsymbol{\omega} = 0\}$ is called *the module of the resonance*, the number $m = dim\mathcal{M}_{\boldsymbol{\omega}}$ *multiplicity of the resonance* and $\boldsymbol{\omega}$ *resonance of multiplicity m*.

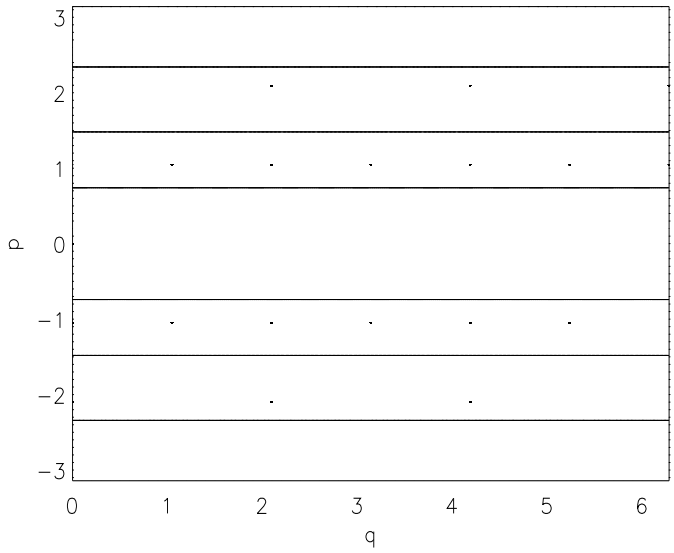

Figure 3.1: The phase space $(\mathbf{p}, \mathbf{q})$ of an integrable system for rational and non-rational frequencies.

Definition 3.4 The quantity $|\mathbf{k}| \equiv |k_1| + ... + |k_n|$ is called the *order of the resonance.*

Proposition 3.2 Let $\mathbf{T}^n$ a n-dimensional torus described by the coordinates $(q_1, ..., q_n)$ and let $\bar{\mathbf{q}}(t) = \bar{\mathbf{q}}(0) + \bar{\boldsymbol{\omega}} t \ (mod 2\pi)$ an orbit on the torus. Let $\mathcal{M}_{\bar{\boldsymbol{\omega}}}$ the module of the resonance associated to $\bar{\boldsymbol{\omega}}$. We obtain then

1. the orbit is *periodic* if and only if $dim\mathcal{M}_{\bar{\boldsymbol{\omega}}} = n - 1$, i. e. $\bar{\boldsymbol{\omega}}$ is completely resonant.

2. if $dim\mathcal{M}_{\bar{\boldsymbol{\omega}}} = 0$, i. e. $\bar{\boldsymbol{\omega}}$ is non-resonant, then the orbit is *dense* on the torus and the motion is called *quasi-periodic.*

3. if $0 < dim\mathcal{M}_{\bar{\boldsymbol{\omega}}} < 1$ then the orbit covers densely the torus of dimension $n - dim\mathcal{M}_{\bar{\boldsymbol{\omega}}}$ and the orbit is always called *quasi-periodic.*

In general, the frequencies depend on the considered torus, namely on the values of the actions $\mathbf{p}$. In the case where the Hamiltonian is linear in the actions, however, the frequencies result to be independent of $\mathbf{p}$. In this case the system is said to be

isochronous. More generally, a Hamiltonian system is called *degenerate* if

$$det\left(\frac{\partial^2 H_0}{\partial p_i \partial p_j}\right) = 0. \tag{3.10}$$

If the system is degenerate, then there exists at least one direction in the action space along which the frequencies do not change. Conversely, if the system is non-degenerate, at least one frequency must change for any arbitrary small displacement in the action space. In the latter case, the resonant tori are dense in the phase space, namely arbitrarily close to any point $\mathbf{p}^*$ in the action space there is a point $\mathbf{p}$ such that the equation $\mathbf{k} \cdot \boldsymbol{\omega} = 0$ is satisfied by a non-zero integer vector $\mathbf{k}$. We will see that in the perturbation theory this property has a relevant importance.

3.1.3 Quasi-integrable systems and perturbation theory

A Hamiltonian system is said to be $quasi - integrable$ if, using a suitable set of action-angle variables, its Hamiltonian function can be written as

$$H(\mathbf{p}, \mathbf{q}) = H_0(\mathbf{p}) + \epsilon H_1(\mathbf{p}, \mathbf{q}), \tag{3.11}$$

where ϵ is a small parameter and $\partial H_0/\partial \mathbf{p}$ and H_1 are intended to be of order unity. It is therefore natural to regard H_0 as the *integrable approximation* and H_1 as its *perturbation*. In fact, the flow generated by H_0, namely

$$\mathbf{p} = constant \,\text{and}\, \mathbf{q} = \boldsymbol{\omega}_0 t + \mathbf{q}(0)$$

approximates at order ϵ the real dynamics generated by H_1, in the sense that it deviates from the real trajectory by a quantity of order ϵ in a time of order unity, and by a quantity of order unity in a time of order $1/\epsilon$. Unfortunately, if one is interested in a very accurate description of the dynamics or in its qualitative behaviour on timescales longer than $1/\epsilon$, the knowledge of the flow generated by H_0 is not enough and one has to look for much better approximations of the real dynamics. This is the goal of *perturbation theory*. First of all, we inquire if there exists a canonical transformation $(\mathbf{p}, \mathbf{q}) \to (\mathbf{p}', \mathbf{q}')$ which transforms the Hamiltonian $H(\mathbf{p}, \mathbf{q})$ into an integrable one $H'(\mathbf{p}')$. In order to understand better this point we give a simple example for which this transformation exists. We consider a system with n degrees of freedom, where H_0 is a system of uncoupled oscillators, i. e.

$$H_0(\mathbf{p}) = \sum_{l=1}^{n} \omega_l p_l \tag{3.12}$$

and H_1 is an analytic function depending only on the angles q_i, i. e.

$$H_1(\mathbf{q}) = \sum_{\mathbf{k}\in\mathbb{Z}^n} c_{\mathbf{k}} e^{i\mathbf{k}\cdot\mathbf{q}} \tag{3.13}$$

where the coefficients $c_{\mathbf{k}}$ are constant.

We use then the following transformation:

$$p_l = p'_l - \sum_{\mathbf{k}\in\mathbb{Z}^n} \frac{c_{\mathbf{k}} k_l}{\mathbf{k}\cdot\boldsymbol{\omega}} e^{i\mathbf{k}\cdot\mathbf{q}}. \tag{3.14}$$

We can simply verify that this transformation is canonical, because it preserves the fundamental Poisson brackets. In the new variables we obtain the following Hamiltonian which is integrable:

$$H'(\mathbf{p}') = \sum_{l=1}^{n} \omega_l p'_l. \tag{3.15}$$

It remains to demonstrate that the previous transformation is allowed, studying the condition of existence of the denominators and of convergence of the series. The first request implies that all the frequencies $\omega_1, ..., \omega_n$ are not resonant ($\sum_{i=1}^n k_i \cdot \omega_i \neq 0$). The second request adds the fact that the frequencies $\boldsymbol{\omega}$ must be sufficiently far from resonance. In particular it is sufficient to assume that the frequencies satisfy the so called *diophantine condition*:

$$|\mathbf{k}\cdot\boldsymbol{\omega}| > \frac{\gamma}{|\mathbf{k}|^\tau} \,\forall\, \mathbf{k} \in \mathbb{Z}^n \tag{3.16}$$

with some real positive γ and τ. With this assumption, we can estimate the series:

$$\begin{array}{l} |\sum_{\mathbf{k}} \frac{c_{\mathbf{k}} k_l}{\mathbf{k}\cdot\boldsymbol{\omega}} e^{i\mathbf{k}\cdot\mathbf{q}}| \leq \sum_{\mathbf{k}} \frac{|c_{\mathbf{k}}||\mathbf{k}|}{|\mathbf{k}\cdot\boldsymbol{\omega}|} |e^{i\mathbf{k}\cdot\mathbf{q}}| \leq \\ \leq \frac{1}{\gamma} \sum_{\mathbf{k}} |c_{\mathbf{k}}||\mathbf{k}|^{\tau+1} |e^{i\mathbf{k}\cdot\mathbf{q}}| \leq \frac{1}{\gamma} \sum_{\mathbf{k}} e^{-|\mathbf{k}|\sigma} |\mathbf{k}|^{\tau+1} |e^{i\mathbf{k}\cdot\mathbf{q}}| \end{array} \tag{3.17}$$

where we have used the fact that, being H_1 analytic, $|c_{\mathbf{k}}| \leq e^{-|\mathbf{k}|\sigma}$ for all $\mathbf{k} \in \mathbb{Z}^n$ and for some positive σ, which is the radius of analyticity of H_1 in the complex plane. Now we can simply demonstrate the convergence on the complex space with $\mathrm{Im}(\mathbf{q}) < \sigma - \delta$, $\forall\ \delta < \sigma$. Indeed on this domain, $|e^{i\mathbf{k}\cdot\mathbf{q}}| \leq e^{|\mathbf{k}|(\sigma-\delta)}$ and therefore (3.17) is bounded by

$$\frac{1}{\gamma} \sum_{\mathbf{k}} |\mathbf{k}|^{\tau+1} e^{-|\mathbf{k}|\delta} \tag{3.18}$$

which is convergent.

Summing up, we can assert that the two fundamental requests for the existence of the canonical transformation are the following:

1. the frequencies $\boldsymbol{\omega}$ must be diophantine;

2. this property must hold *everywhere* in the phase space.

This last property is fulfilled in the case considered above, since the Hamiltonian we have considered is linear in the actions and, by consequence, the frequencies are the same over all the action-space. Therefore, if the frequencies are diophantine, the system is integrable. However this property is not true for general Hamiltonians: already in the simple model of uncoupled *rotators*, where $H_0 = \sum_l c_l p_l^2/2$, the frequencies are function of p. We give then the rigorous result, known as Poincaré theorem.

Theorem 3.1 (**Poincaré**)
Let $H(\mathbf{p},\mathbf{q}) = H_0(\mathbf{p}) + \epsilon H_1(\mathbf{p},\mathbf{q})$ with $(\mathbf{p},\mathbf{q}) \in D \times \mathbb{T}^n$, D open set of $\mathbb{R}^n$ and assume:
i) H_0 is non-degenerate, more precisely

$$det\left(\frac{\partial^2 H_0}{\partial p_i \partial p_j}\right) \neq 0$$

in an open subset D_0 of D;
ii) the Fourier series of H_1 is essentially full. More precisely, denoting

$$H_1(\mathbf{p},\mathbf{q}) = \sum_{\mathbf{k}\in\mathbb{Z}^n} c_{\mathbf{k}}(\mathbf{p}) e^{i\mathbf{k}\cdot\mathbf{q}} \tag{3.19}$$

for any $\mathbf{k} \in \mathbb{Z}^n$ there exists $\mathbf{k}'$ parallel to $\mathbf{k}$ such that $c_{\mathbf{k}'} \neq 0$ in D_0. Then a function χ solving (3.19) in D_0 does not exist.

3.1.4 Kam Theorem

The considerations made in the last section show that it is not possible to eliminate globally the angles in a non-degenerate quasi-integrable Hamiltonian system because of the dense presence of the resonances. A possibility is to eliminate the angles only for those values of $\mathbf{p}$ corresponding to frequencies which are diophantine. A simple Hamiltonian that, although non-integrable in general, admits one exact solution in this sense is:

$$H(\mathbf{I},\boldsymbol{\varphi}) = H_0(\mathbf{I}) + H_1(\mathbf{I},\boldsymbol{\varphi}) \text{ with } ||H_1|| = O(||\mathbf{I}||^2), \tag{3.20}$$

where $\mathbf{I}$ and $\boldsymbol{\varphi}$ are conjugate action-angle variables. In fact, for $\mathbf{I}= \mathbf{0}$, the equations of motion are

$$\begin{cases} \dot{\mathbf{I}} = \mathbf{0} \\ \dot{\boldsymbol{\varphi}} = \partial H_0/\partial \mathbf{I}(\mathbf{0}) \end{cases} \tag{3.21}$$

and the solution correspondent to the initial condition $(\mathbf{I}, \boldsymbol{\varphi}) = (\mathbf{0}, \boldsymbol{\varphi}_0)$ is $\mathbf{I} = \mathbf{0}$ and $\boldsymbol{\varphi} = (\partial H_0/\partial \mathbf{I})(\mathbf{0})t + \boldsymbol{\varphi}_0$. Therefore, the torus $\mathbf{I} = \mathbf{0}$, $\boldsymbol{\varphi} \in \mathrm{T}^n$ is invariant for the flow of (3.20), because every orbit starts on the torus and never leaves it. This simple example leads to the original approach followed by Kolmogorov in 1954 [33]. He proved that, given a quasi-integrable Hamiltonian $H(\mathbf{p}, \mathbf{q}) = H_0(\mathbf{p}) + \epsilon H_1(\mathbf{p}, \mathbf{q})$ and a value of $\mathbf{p}_0$ such that

1. $\boldsymbol{\omega}_0 = (\partial H_0/\partial \mathbf{p})(\mathbf{p}_0)$ satisfies the diophantine condition (3.16), with some real positive constant γ and τ;

2. H_0 is non degenerate in $\mathbf{p}_0$, i. e.:

$$det \left(\frac{\partial^2 H_0}{\partial p_i \partial p_j} \right) \neq 0$$

then there exists $\bar{\epsilon}(\boldsymbol{\omega}_0)$ such that $\forall\ \epsilon < \bar{\epsilon}$ there exists a canonical transformation $(\mathbf{p}, \mathbf{q}) \rightarrow (\mathbf{I}, \boldsymbol{\varphi})$ which allows to write the Hamiltonian in the form (3.20), with $(\partial H_0'/\partial \mathbf{I})(\mathbf{0}) = \boldsymbol{\omega}_0$.

The Kolmogorov theorem implies that quasi-integrable systems admit, for small enough perturbations, invariant tori in correspondence with the diophantine frequencies. The Hamiltonian equations can be integrated if restricted to these tori. The theorem has been extended and improved by Moser in 1962 [46] and Arnold in 1963 [2], and for this reason it is known as the *KAM theorem*. For the same reason the invariant tori are usually called *KAM tori*.

The main points of the theorem are the following:

1. the dynamics of the integrable part H_0 gives a foliation of the phase space in invariant tori, the actions $\mathbf{p}$ being constant and the angles $\mathbf{q}$ circulating linearly with time, with frequencies $\boldsymbol{\omega}_0(\mathbf{p})$;

2. when a small perturbation $\epsilon H_1(\mathbf{p}, \mathbf{q})$ is added, the KAM theorem ensures that the tori with diophantine frequencies persist invariant for the flow of the complete Hamiltonian $H_0 + \epsilon H_1$;

3. for the invariant torus, new local action-angle variables $\mathbf{I}, \boldsymbol{\varphi}$ can be introduced, such that the Hamiltonian is transformed in the form (3.20). In these variables, the motion on the torus is very simple: the action $\mathbf{I}$ are constants on the invariant torus and the angles $\boldsymbol{\varphi}$ circulate linearly with time. In the original variable ($\mathbf{p}$,$\mathbf{q}$) the motion on the torus can be computed by composing all the transformations that have been required to give the Hamiltonian the form (3.20). Since each of these transformations is periodic in the angles, the relationship between $(\mathbf{p}, \mathbf{q})$ and $(\mathbf{I}, \boldsymbol{\varphi})$ is of type $\mathbf{p} = \mathbf{P}(\mathbf{I}, \boldsymbol{\varphi})$, $\mathbf{q} = \mathbf{Q}(\mathbf{I}, \boldsymbol{\varphi})$, with functions $\mathbf{P}$ and $\mathbf{Q}$ periodic in $\boldsymbol{\varphi}$, and $\mathbf{Q}^{-1}$ periodic in $\mathbf{q}$. Therefore on the torus the angles $\mathbf{q}$ are no longer linear functions of time, but still have constant frequencies. The actions $\mathbf{p}$ have oscillations that are periodic in the angles $\mathbf{q}$, being $\mathbf{p} = \mathbf{P}(\mathbf{I}, \mathbf{Q}^{-1}(\mathbf{q}))$, and quasi-periodic with time, the angles having non-resonant frequencies. For a given frequency vector, the perturbed invariant torus is *translated* and *distorted* in the phase space with respect to the unperturbed torus, however it is not possible to *rectify* all tori with the same analytic transformation. The situation is illustrated in Figure 3.2;

4. the size of ϵ determines the fraction of tori which remain invariant. In the theorem ϵ must be smaller than a fixed threshold, which is of the order of γ^4 [33]. Therefore, increasing ϵ, the number of invariant tori is reduced and only those with large enough γ can survive. Moreover, if ϵ is too large, no invariant tori persist.

Even if the KAM theorem does not provide any information on the perturbed dynamics away from the invariant tori, we can expect that most of them are destroyed and their orbits show a "chaotic" behaviour. In this sense the KAM theorem does not give a solution and the problem of description of chaotic dynamics requires the study of resonant dynamics, which is explained next. Nevertheless the existence of KAM tori plays a very important role in the dynamics of the global system. To understand better this fact, it is useful to look for a graphic representation of the KAM theorem, which is the purpose of the next section.

3.1.5 A graphic representation of the KAM theorem in low dimension: the Poincaré section

If we consider a Hamiltonian system with two degrees of freedom, it is simple to visualize its dynamics by using the *Poincaré section*. We consider the restriction of the Hamiltonian $H(p_1, p_2, q_1, q_2)$ to the trajectories which satisfy $H(p_1, p_2, q_1, q_2) = C$ for some constant C. The phase space is $4D$, but the conservation of the energy forces the motion to evolve in a three-dimensional space. We reduce now the dimension

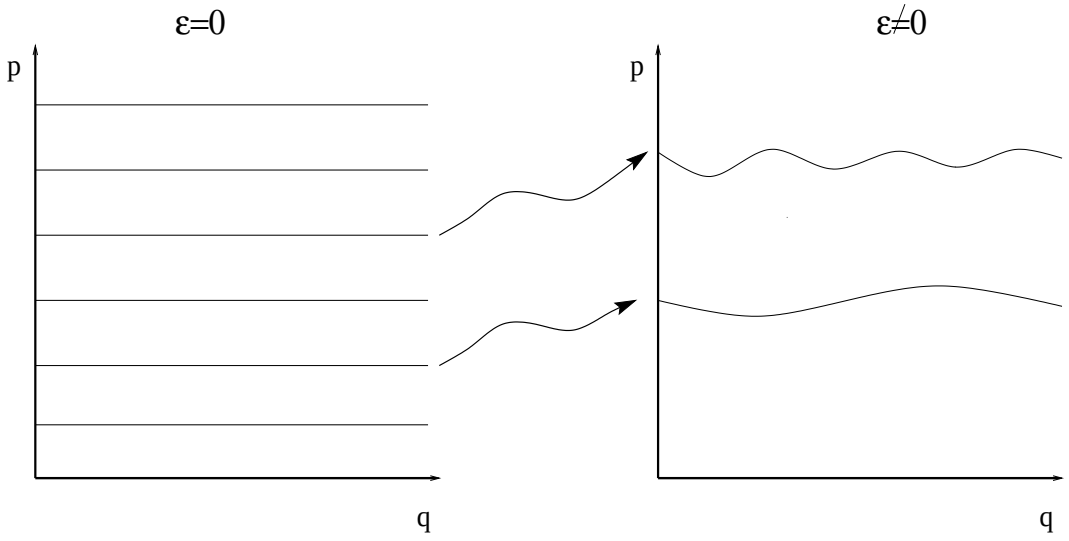

Figure 3.2: The phase space of the integrable and of the perturbed Hamiltonian. A torus with diophantine frequencies persists invariant for the flow, but it is deformed and translated with respect to the unperturbed one.

of the system by choosing a two-dimensional surface Σ transverse to most of such trajectories. Since in general the actions of the system have only small oscillations, while the angles circulate between 0 and 2π, we can choose Σ as the surface defined by a constant value of one angle, for instance setting $q_2 = 0$. For a given value of C, the values of p_1 and q_1 on the surface $q_2 = 0$ unambiguously determines the value of the remaining action p_2, which can be computed by solving the implicit equation $H(p_1, q_1, p_2, 0) = C$. Now, by numerical integrations of the motion we can calculate the successive intersection of each trajectory with the surface Σ and consider only those generated when the trajectory pierces the surface in a given direction, for instance $\dot{q}_2 > 0$. The sequence of points p_1, q_1 that each trajectory marks on Σ gives an unequivocal image of the time evolution of the trajectory in phase space (Figure 3.3). If a trajectory lies on a KAM torus, the sequence of points p_1, q_1 must lie on a one dimensional curve. In fact, on a KAM torus the actions are periodic functions of the angles, so that – denoting by $p_1 = P(q_1, q_2)$ the periodic relationship between p_1 and (q_1,q_2) – on the surface of section $q_2 = 0$ the points p_1, q_1 must lie on the curve $p_1 = P(q_1, 0)$. Moreover, because the angles have non-resonant frequencies, at each intersection with the surface $q_2 = 0$ the angle q_1 has to assume a different value on the interval $[0, 2\pi]$ and, with time passing, the sequence of points on the

surface of section must densely fill the curve $p_1 = P(q_1, 0)$. As a consequence, if the Poincaré section is computed for long enough time, the KAM tori appear as solid curves crossing the entire interval $[0, 2\pi]$.

An example of Poincaré section for a system with two degrees of freedom is displayed on Figure 3.4. One can see an invariant torus, appearing as a solid line. In general, each KAM torus divides the phase space in two parts that are disconnected for the dynamics. As a consequence, the trajectories can not pass from one side of the invariant torus to the other without crossing it: this is impossible by definition of invariance. In the case of $n > 2$ this is not true and this is due to the co-dimension of the KAM tori with respect to the phase space. In fact, in the case of n degrees of freedom the dimension of the phase space is $2n$ and the conservation of the Hamiltonian forces the motion to evolve in a $2(n-1)$-dimensional space. A KAM torus has dimension n, so the co-dimension is $n-1$. This implies that the phase space is divided in two disconnected parts only if $n = 2$.

For $n = 3$, the situation becomes more complicated and the Poincaré section in the phase space does not allow a useful visualization. Instead, because the dynamics is determined by the values more or less rational of the frequencies, it is instructive to analyse the frequency space. Taking for simplicity a two-degrees of freedom system again, the frequency space is a plane, but on a surface of constant Hamiltonian it becomes a line, parameterized by the ratio ω_1/ω_2 (Figure 3.5).

The KAM tori are fixed points over the frequencies line, which correspond to the diophantine values. Conversely, the chaotic trajectories are characterized by frequencies which move with time, so they move on the line. Each KAM torus divides the frequency space into two disconnected parts. The trajectories which do not lie on invariant tori can wander on the frequency line, but can not pass through diophantine ratios.

Now, in the case $n = 3$, the frequency space is two-dimensional and we choose the ratio ω_1/ω_3 and ω_2/ω_3 as coordinates. Again, KAM tori are represented by dots in this frequency plane, while the trajectories that are not on invariant tori may wander on the frequency plane. It is immediately evident from Figure 3.6 that the trajectory can slalom among KAM tori and "diffuse" , in principle, everywhere. In reality, we will see in Section 3.2.2, that the slalom among KAM tori takes an extremely long time.

3.2 Area-preserving mappings

The intersection of a trajectory with a Poincaré section is an example of a discrete dynamical system (called in this case *Poincaré map)*. We saw that many character-

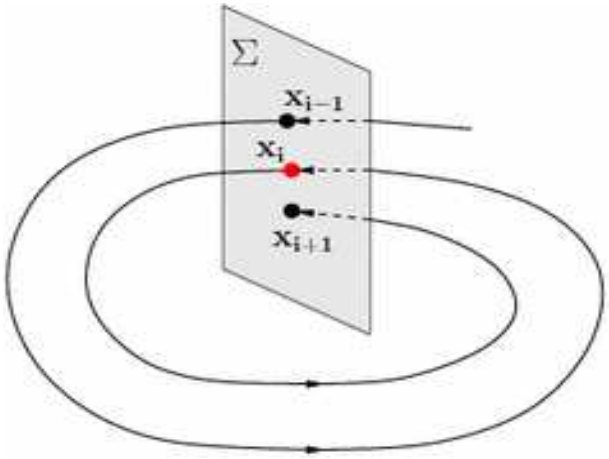

Figure 3.3: Example of a Poincaré section Σ. The orbit intersects subsequently the surface, in the same direction, at the points x_i.

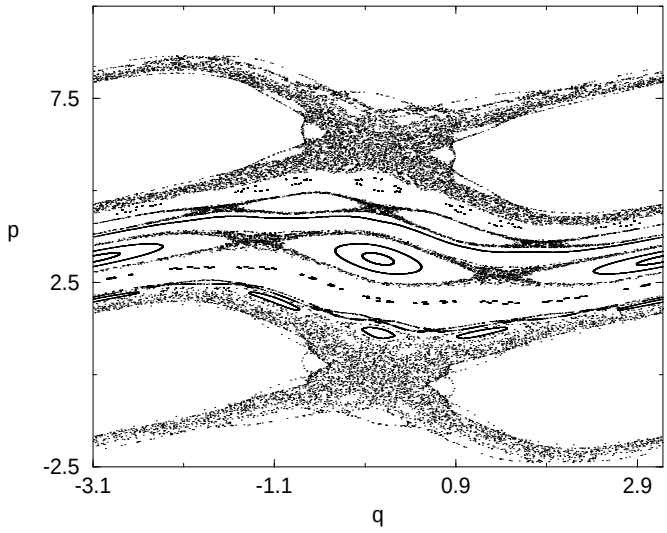

Figure 3.4: Invariant torus bound chaotic layers in Hamiltonian systems with two degrees of freedom, originating at $(q, p) = (-3.1, 3.75)$

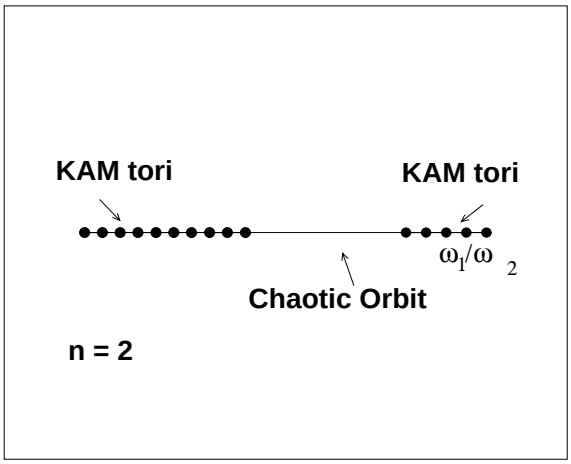

Figure 3.5: KAM tori and chaotic orbits in the frequency space in the case of two degrees of freedom.

istics of the topology of the phase space in a Hamiltonian system can be understood by examining the corresponding Poincaré map. If one has to study only the general properties of the Hamiltonian dynamics, without focalizing on a specific system, he can more easily analyse the dynamics of a discrete map which derives from a time-continuous Hamiltonian. Such maps, called symplectic, have been largely used in the literature like a real numerical laboratory. Let us just recall the standard map [9],[15] and the Hénon's quadratic map [28].

To be more precise, we give the following

Definition 3.5 Let $W \in \mathbb{R}^{2n}$ an open set, and $\psi : W \to W$ an application of class C^1. The application (map) ψ is said *symplectic* if its Jacobian matrix J satisfies the relation

$$J^T E J = E \tag{3.22}$$

where E is the $2n \times 2n$ block matrix

$$E = \begin{pmatrix} 0 & I \\ -I & 0 \end{pmatrix},$$

I being the $n \times n$ unit matrix.

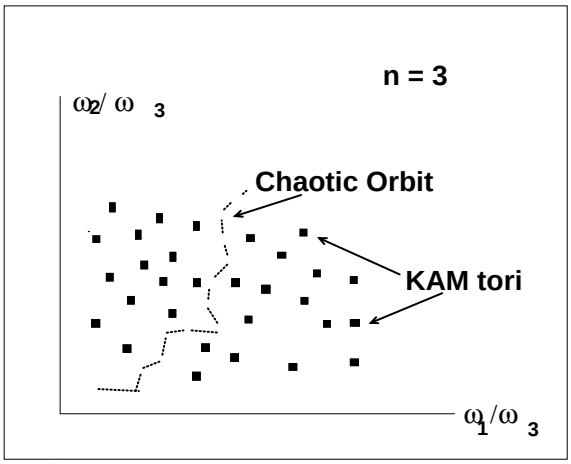

Figure 3.6: KAM tori and chaotic orbits in the frequency space in the case of three degrees of freedom.

When $n = 1$, the symplecticity condition is equivalent to the request that $detJ = 1$, i.e. the map is area-preserving.

It turns out that any $2n$-symplectic map is Hamiltonian, in the sense that there exists a Hamiltonian such that the transformation generated by the map is the section at discrete times of the flow generated by the Hamiltonian in the $2n$-dimensional phase space.

We give here a general procedure to construct a symplectic map from a continuous Hamiltonian system. In particular, we derive the well-known *standard map* from the equations of the pendulum.

Let us consider its Hamiltonian:

$$H = \frac{p^2}{2} - \cos q. \tag{3.23}$$

We can associate to the corresponding equation of motion

$$\begin{cases} \dot{q} &= \frac{\partial H}{\partial p} = & p \\ \dot{p} &= -\frac{\partial H}{\partial q} = & -\sin q \end{cases} \tag{3.24}$$

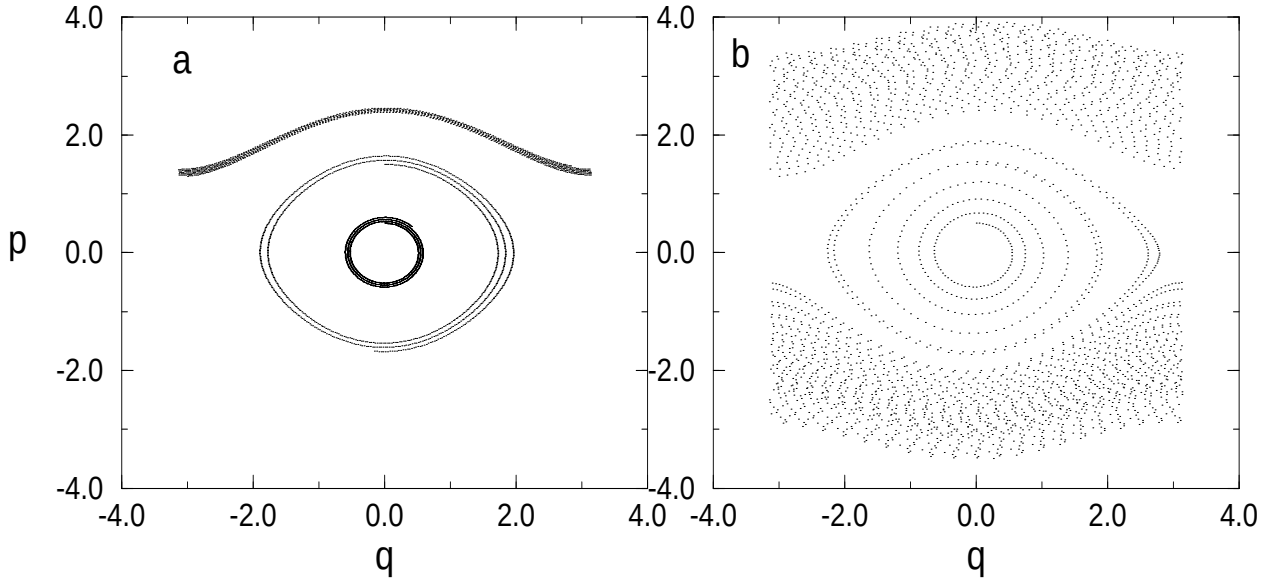

Figure 3.7: The phase portrait of the pendulum for different values of Δt when using the Euler integration method. Even for a small Δt ($\Delta t = 0.02$, a),the area is not conserved. For a larger Δt ($\Delta t = 0.1$, b), the global pattern is completely lost.

the mapping T_1:

$$T_1 = \begin{cases} q_1 &= q_0 + p_0 \Delta t \\ p_1 &= p_0 - \Delta t \sin q_0 \end{cases} \tag{3.25}$$

which is nothing but the explicit Euler method to compute orbits of ordinary differential equations. If we consider the phase space diagram obtained with T_1, even with a small value of Δt ($\Delta t = 0.02$), the system appears slowly expanding (Figure 3.7a). Instead, for a larger value of Δt ($\Delta t = 0.1$), the expansion is drastic (Figure 3.7b). If we compute the determinant of the Jacobian matrix J we obtain $|J| = 1 + \Delta t^2 \cos q_0$ which is not equal to one, therefore the mapping is not area-preserving.

Let us make a slight change in the mapping by taking an implicit Euler scheme in the equation for p, which leads to the mapping T_2:

$$T_2 = \begin{cases} q_1 &= q_0 + p_0 \Delta t \\ p_1 &= p_0 - \Delta t \sin q_1 \end{cases} \tag{3.26}$$

Again if $\Delta t \to 0$ the discretization is consistent with the initial system of equations. This method is known as *leap-frog*. The determinant of the Jacobian matrix is now

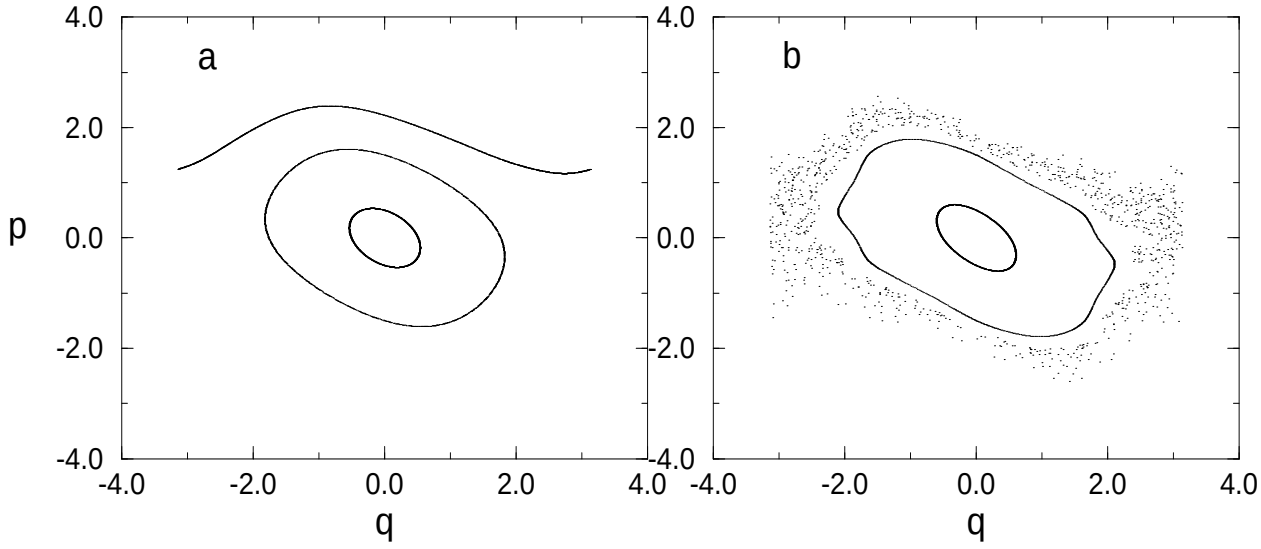

Figure 3.8: The phase portrait of the pendulum for different values of Δt when using the leap-frog integration method. For a small Δt ($\Delta t = 0.002$, a), the invariant curves are well preserved. Even for a larger Δt ($\Delta t = 0.1$, b), the invariant curves are only distorted but not completely destroyed.

equal to 1, so we obtained an area-preserving (and then symplectic) map for any Δt. Thanks to the area-preserving property, even for large values of Δt ($\Delta t \simeq 0.1$) the phase space diagram of the map is qualitatively in agreement with that of the pendulum (Figure 3.8).

The procedure to obtain a symplectic map can be better understood if one splits the Hamiltonian in two parts: $H = H_1 + H_2$ with $H_1 = p^2/2$ and $H_2 = -\cos q$. The Euler explicit method applied successively to H_1 and H_2 gives rise to the two mappings:

$$T_2' = \begin{cases} q_1 &= q_0 + p_0 \Delta t \\ p_1 &= p_0 \end{cases} \tag{3.27}$$

and:

$$T_2'' = \begin{cases} q_2 &= q_1 \\ p_2 &= p_1 - \sin q_1 \Delta t \end{cases} \tag{3.28}$$

which are both area-preserving, because only one variable is advanced at each time. The composite mapping $T_2 = T_2' \circ T_2''$, which is the final standard map, is still area-preserving.

By the variable change $p\Delta t \to p$ and taking $\epsilon = -\Delta t^2$, the symplectic standard map is commonly written as

$$T = \begin{cases} p_{i+1} &= p_i + \epsilon \sin(p_i + q_i) \quad (\mathrm{mod} 2\pi) \\ q_{i+1} &= p_i + q_i \quad (\mathrm{mod} 2\pi) \end{cases} \tag{3.29}$$

The standard map (3.29) obtained this way is then symplectic, but the Hamiltonian from which it derives is not simply related to the one of the pendulum, from which we started the procedure. Actually, it cannot be written in an explicit form. It can be easily shown that if $\epsilon = 0$ the standard map reduces to the Poincaré section at $q_2 = 0$ of the integrable Hamiltonian system $H_0(p_1, p_2, q_1, q_2) = p_1^2/2 + 2\pi p_2$, so when $\epsilon \neq 0$ it will represent the Poincaré map of a non-integrable perturbed system $H_0 + \epsilon H_1$. ϵ plays then the role of the perturbation parameter.

3.2.1 The visualization of the KAM theorem using the standard map

To visualize the KAM theorem, we use then the standard map (3.29). We show the phase portraits for different values of ϵ and analyse them in the light of the KAM theory. In Figure 3.9 we have chosen 20 initial conditions on the axis $q = 0$, with initial p regularly spaced on the interval $[-\pi, \pi]$.

In the case where ϵ is small ($\epsilon = 0.2$, Figure 3.9a) every initial condition generates an orbit lying on a KAM torus. This implies that the volume filled by tori KAM is large. The tori are significantly distorted with respect to the case $\epsilon = 0$ and this distortion leaves an "empty region" around $p = 0$. This is a *resonant region* and the trajectories there do not cross the axis $q = 0$, so that they can not be computed with our choice of initial conditions. The dynamics in the resonant region will be investigated in the light of the Nekhoroshev Theorem (Section 3.2.2). We finally note that, while most of the KAM tori appear as solid curves in Figure 3.9a, the one passing through $p = -2.24$ on the axis $q = 0$ appears as a dotted curve. This is because the time required to fill the torus densely with respect to the graphic resolution depends on the frequencies on the torus. The closer are the frequencies to a rational ratio, the longer is this time.

In Figure 3.9b, the value of ϵ is increased to 0.6. The dynamical structure changes significantly. Only 14 initial conditions generate trajectories lying on KAM tori. The initial conditions with $p = \pm 2.84$ and $p = \pm 1.36$ generate trajectories

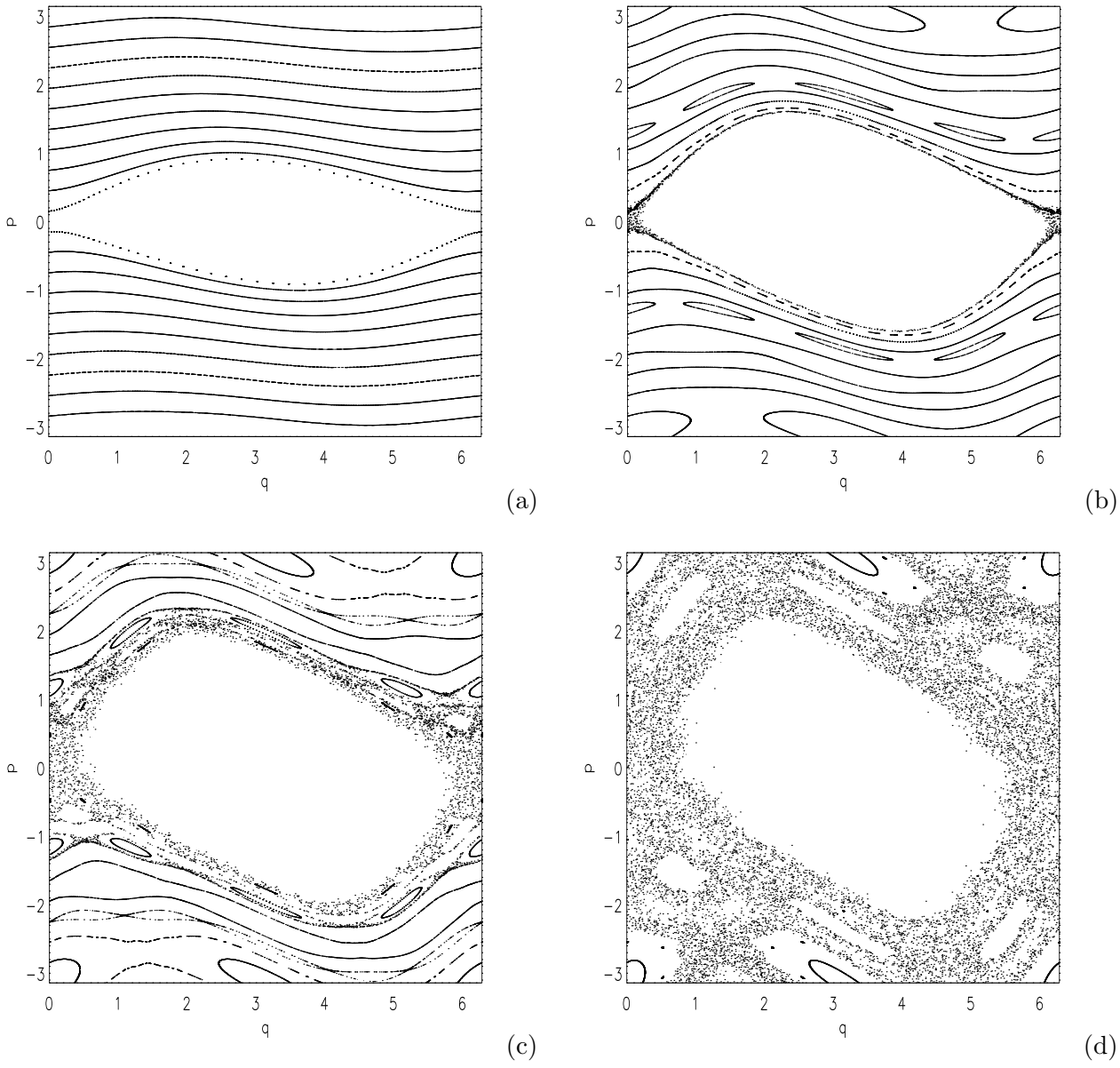

Figure 3.9: The phase portrait of the standard map for different values of ϵ. (a): $\epsilon = 0.2$, (b): $\epsilon = 0.6$, (c): $\epsilon = 0.9$, (d): $\epsilon = 1.2$. When increasing ϵ, the KAM tori become more distorted and more rare, while chaotic regions become more and more extended.

still lying on invariant curves, but these curves have a topological structure which is different from that of KAM tori: they appear as chains of closed circles called *islands*. These invariant curves correspond to the resonant dynamics. Finally, the iterations of the initial conditions $p = \pm 0.15$, $q = 0$ do not lie on a curve, but they are scattered over an area of larger dimension. Here KAM tori are destroyed, the actions being not periodically related to the angles. This is called a *chaotic region* and it is related to the resonant dynamics. We will analyse in detail the concept of *chaos* in Chapter 6, when introducing the Lyapunov Exponents.

In Figure 3.9c, only 4 initial conditions generate trajectories on KAM tori, showing that the volume filled by KAM tori shrinks when increasing the value of ϵ ($\epsilon = 0.9$). Chaotic zones appear also around some chains of island and not only around the central *empty region* as it was the case of Figure (3.9b). As said in Section 3.1.5, the surviving KAM tori separate the (p,q)-space in disconnected regions, so the dynamical evolution of the trajectories in the chaotic regions is bounded. For instance, the trajectory starting with $p = -0.15$ will never reach the region with $p < -2.5$, because a KAM torus can not be crossed.

Finally, in Figure 3.9d, we choose $\epsilon = 1.2$ and all KAM tori have disappeared. The chaotic regions have merged together, and now dominate the phase space portrait of the system. It is not possible to distinguish the evolutions of different initial conditions in the chaotic zone. The action p can assume any value during the evolution of chaotic trajectories.

3.2.2 The Nekhoroshev Theorem

The theorem which we are going to explain, proved by Nekhoroshev in 1976 [47], is a result on the stability of the actions as the KAM theorem and it is, in a certain way, complementary to it. It concerns too a quasi-integrable Hamiltonian of the form (3.11), but H must have a supplementary hypothesis of convexity which will be explained in the following. The result is valid for all initial conditions, conversely to the KAM theorem in which the initial conditions must correspond to diophantine frequencies. In order to obtain this global result, valid for all actions, the Nekhoroshev theorem replaces the concept of stability normally used in mathematics (namely over an infinite time), with the concept of *stability over long time*, but we will see that this is not penalizing for most practical applications.

The theorem can be stated in the following form:

Theorem 3.2 (**Nekhoroshev**)
Let $H(\mathbf{p}, \mathbf{q}) = H_0(\mathbf{p}) + \epsilon H_1(\mathbf{p}, \mathbf{q})$ be analytic in a domain $D \equiv W \times \mathbb{T}^n$, with $W \subset \mathbb{R}^n$ open and bounded. Let be H_1 such that $||H_1|| \leq 1$.

Given $\Delta \in \mathbb{R}$, in the following we define by $W - \Delta$ the set of points $\mathbf{p}$ which are contained in W together with a neighborhood of radius Δ.

Consider the matrix $C(p)$ defined by $C_{ij}(\mathbf{p}) = \frac{\partial^2 H_0}{\partial p_i \partial p_j}(\mathbf{p})$ and assume the convexity hypothesis:

$$C(\mathbf{p})\mathbf{v} \cdot \mathbf{v} \neq 0 \ \forall \mathbf{p} \ \in \ W \text{ and } \forall \mathbf{v} \ \in \ \mathbb{R}^n \backslash \mathbf{0}. \tag{3.30}$$

Then, there exist positive constants ϵ_*, α, β, a, b such that for any $\epsilon < \epsilon_*$ one has:

$$||\mathbf{p}(t) - \mathbf{p}(0)|| \leq \Delta \equiv \alpha \epsilon^a,$$

for all $\mathbf{p}(0) \in W - \Delta$ and for all $|t| \leq T(\epsilon)$, where

$$T = \beta \left(\frac{\epsilon_*}{\epsilon} \right)^{\frac{1}{2}} exp \left(\frac{\epsilon_*}{\epsilon} \right)^b. \tag{3.31}$$

The Nekhoroshev theorem does not exclude the possibility of chaotic motions. Indeed, the action $\mathbf{p}$ can possibly change in a chaotic way: the theorem just states that these changes are bounded by a quantity $\alpha \epsilon^a$ up to the time T. Slow drift can force the actions to change more than $\alpha \epsilon^a$ with respect to the initial conditions only after a time larger than T, as sketched in Figure 3.10. The important point is that the stability time T grows exponentially with respect to $\frac{1}{\epsilon}$. Therefore, as soon as ϵ is small, the stability time becomes extremely long and can possibly exceed the physical lifetime of the system, thus providing a result of practical stability.

A fundamental approach to the theorem, based on a geometric interpretation of it, put in evidence a particular structure in the phase space, called *geography of the resonances*. The fundamental idea is to expand the Hamiltonian in Fourier series of the angles, and truncate the series by taking the terms containing resonances only up to a given order K. We recall that the order of a resonance of the type $\mathbf{k} \cdot \boldsymbol{\omega} = 0$ is defined as $|\mathbf{k}| = \sum_{i=1}^n |k_i|$. On one hand, the number of resonances up to a given order is finite and each subset of the action space contains only a finite number of corresponding resonant lines. On the other hand, the analyticity of the Hamiltonian implies that the neglected terms in the truncated series, corresponding to resonances of order larger than K, have a size not exceeding $exp(-K\sigma)$. It can be shown that the threshold K can be chosen as large as $1/\epsilon^b$, so that this remainder (termed here R_K) turns out to be exponentially small in $1/\epsilon^b$. This is a key point to obtain a stability time $T(\epsilon)$ depending exponentially on $1/\epsilon^b$ as in (3.31). We consider for simplicity a system with three degrees of freedom and we analyse the frequency space, by drawing its structure.

As a first step we define a *non-resonant domain*, as the set of frequencies which are far enough from all resonances up to order K. More precisely, this domain is

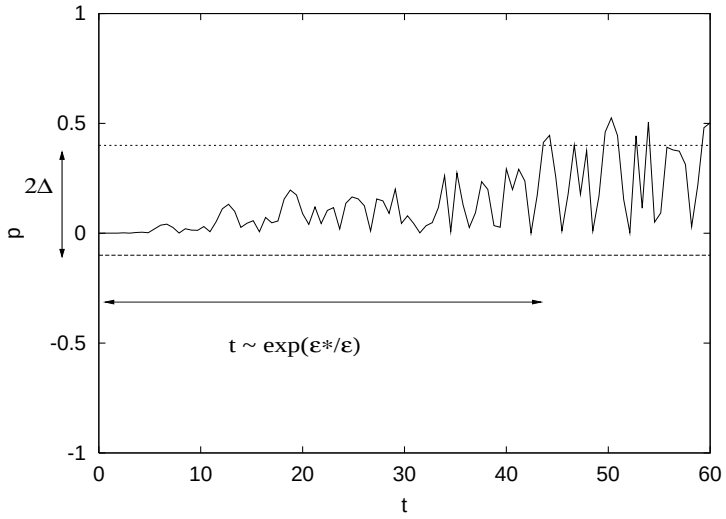

Figure 3.10: Evolution of the actions with respect to time in the Nekhoroshev regime.

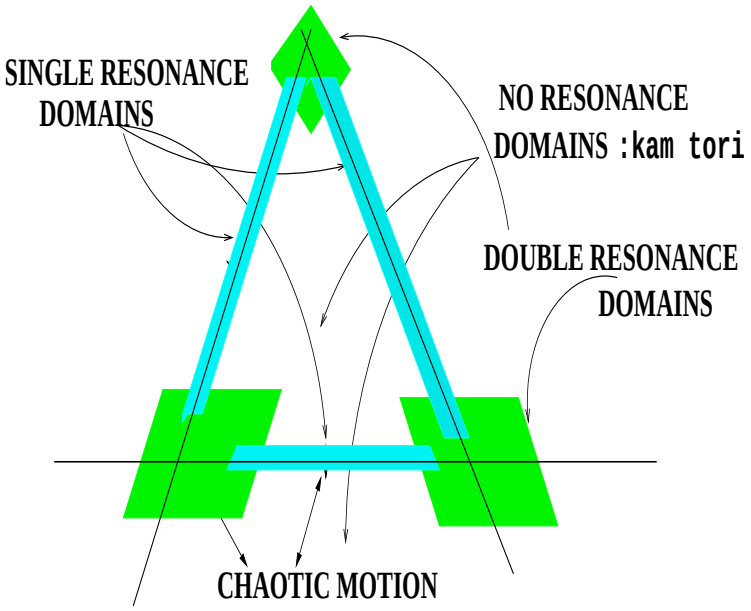

Figure 3.11: Geography of the resonances in the frequency space for a system with three degrees of freedom.

defined as the set of frequencies $\boldsymbol{\omega}$ such that $|\mathbf{k}\cdot\boldsymbol{\omega}| > \sqrt{\epsilon}$ for all $\mathbf{k}$ with $|\mathbf{k}| \leq K$. In Figure 3.11 this is the white disconnected domain, bounded by the blue stripes. All the terms in the truncated Hamiltonian are not-resonant in such a domain, because the denominator $\mathbf{k}\cdot\boldsymbol{\omega}$ has a lower limit larger than zero. We can then integrate the Hamiltonian, if we cut off the remainder R_K, which is exponentially small. By neglecting the flow represented by R_K, we can conclude that the frequencies are fixed in the non-resonant domain.

The second step consists in the analysis of the domains called *single resonance domains*, i.e the blue stripes in Figure 3.11. By definition, in these domains there exists only one single resonance of order smaller than K. Then one reduces the Hamiltonian to having only one resonant term and a remainder R_K, which is, again, exponentially small. Neglecting the remainder, such a Hamiltonian is still integrable, but depends on one resonant angle, so that the actions are no longer fixed. They change, driven by the resonant harmonic, along what is usually called the *fast drift direction*. Now, for a convex Hamiltonian, one can prove that the fast drift direction is transversal to the resonant lines, so in Figure 3.11 it will be orthogonal to the blue stripes. Therefore, following indefinitely the fast drift direction, the motion would enter the non-resonant domain. But this is impossible, because in the non-resonant domain the frequencies are fixed, as explained above. On the other hand, transversal motion with respect to the fast drift direction can be forced only by the non-integrable remainder R_K, so that it is exponentially slow. This slow motion is usually called *Arnold diffusion* and the set of lines of the type $\mathbf{k}\cdot\boldsymbol{\omega}= 0$ are known as *Arnold Web*.

One can better understand the transversality of the motion, by analysing a system with two degrees of freedom. We consider the Hamiltonian

$$H(p_1, p_2, q_1, q_2) = \frac{1}{2}(p_1^2 + p_2^2) + \epsilon cos(q_1 - q_2) \tag{3.32}$$

and we analyse the integrable part $H_0 = \frac{1}{2}(p_1^2 + p_2^2)$.

The motion must follow the level curves of the Hamiltonian, which on the plane (p_1, p_2) are represented on Figure 3.12a. We calculate the resonant lines of the Hamiltonian (3.32). The two frequencies are $\omega_1 = \frac{\partial H}{\partial p_1} = p_1$ and $\omega_2 = \frac{\partial H}{\partial p_2} = p_2$. From the condition $k_1\omega_1 + k_2\omega_2 = 0$, we obtain the resonant lines $p_1 = -\frac{k_2}{k_1}p_2$. The motion follows the level curves in Figure 3.12a which are bounded and then it must be transversal to the resonant lines, which cross the origin. As a consequence, the motion is limited and this fact derives from the hypothesis of convexity of H_0.

We consider now a non-convex Hamiltonian, for example

$$H(p_1, p_2, q_1, q_2) = \frac{1}{2}(p_1^2 - p_2^2) + \epsilon cos(q_1 - q_2). \tag{3.33}$$

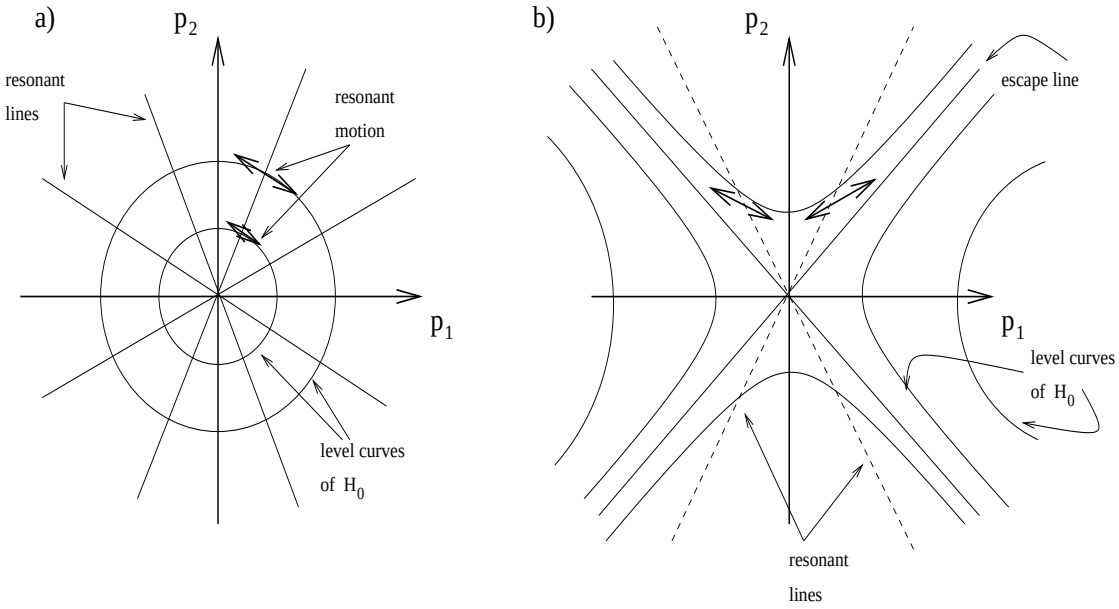

Figure 3.12: Dynamics in the action space for a convex (a) and non-convex Hamiltonian (b).

The resonances are still the lines $p_1 = -\frac{k_2}{k_1}p_2$ but the level curve are now open. The resonances transversal to the resonance lines have a limited motion, but this is not true for the resonances which coincide with the level curves, represented as solid straight lines in Figure 3.12b. The motion can then escape, by following these open lines.

We now come back to the geography of the resonances and we analyse the third step in the geometric interpretation of the Nekhoroshev theorem. This step consists in analysing the *double resonance domains*, centered around the resonance crossing (the resonances of multiplicity 2), i.e the green zones in Figure 3.11. In such domains, the Hamiltonian has two independent resonant terms of order smaller than K. Then, one can expect that these domains are characterized by strongly chaotic motions and that frequencies can move in any direction of the plane around the resonance crossing. However, again, this chaotic motion is bounded. Indeed, if the frequencies moved far enough from the double resonance point, they would enter either the non-resonant domain or one of the single resonant domains. This is impossible, since in the non-resonant domain frequencies are fixed and in the single resonance domains frequencies can change only along the fast drift direction.

In conclusion, neglecting the exponentially small remainder R_K, for each initial condition, the motion is confined within one of the resonance domains. As a consequence, frequencies and actions can change by at most a quantity equal to the radius of the double resonance domains . Nekhoroshev proved that this radius is proportional to ϵ^a, for some positive $a < 1$.

Moreover, in order to have a consistent picture as in Figure 3.11, the number of resonances of order smaller than K must not be too large, otherwise there would not be a place for the non-resonant domain and the construction of Figure 3.11 would not possible. The fact that the largest resonance domains are of order ϵ^a gives an upper bound of type $\frac{1}{\epsilon^b}$ on the choice of K.

Finally, we take into account the exponentially small remainder R_K. It is evident that the remainder can force diffusion in every direction of frequency space, but only with exponentially small speed. Then the result concerning bounded motion, deduced by neglecting R_K, will be true in principle only up to exponentially long times.

The construction of the Nekhoroshev theorem can be iterated in order to explore the dynamical structure of the system also for what concerns resonances of order larger than Nekhoroshev's threshold $K \sim \frac{1}{\epsilon^b}$. In the non-resonant domain defined above (denoted hereafter by G_K), after the elimination of the resonances up to order K, in the new action-angle variables $(\mathbf{p}', \mathbf{q}')$, the Hamiltonian has the form:

$$H'(\mathbf{p}', \mathbf{q}') = H'_0(\mathbf{p}') + \epsilon H'_1(\mathbf{p}', \mathbf{q}') \quad \text{with } \epsilon H'_1(\mathbf{p}', \mathbf{q}') = R_K(\mathbf{p}', \mathbf{q}'). \tag{3.34}$$

This is again a convex system, but the new perturbation is exponentially small with respect to the original one, being $\epsilon' \sim \exp(-\frac{1}{\epsilon^b})$. Then, applying the Nekhoroshev theorem to this Hamiltonian, one proves the global stability of motion in G_K for super-exponentially long times, namely up to $T \sim exp(exp(\frac{1}{\epsilon^b}))$ [45]. Moreover, one finds a new non–resonant domain $G_{K'}$, characterized by the absence of resonances up to order K'. On $G_{K'}$ one can introduce new action-angle variables so to transform the Hamiltonian into the sum of an integrable part and a remainder $R_{K'}$, the latter super-exponentially small. This procedure can be iterated and it is proved to be convergent to a set of invariant KAM tori of large volume [45].

If the perturbation parameter was too large, the resonances overlap. In this case there is no place for a non-resonant domain and invariant tori no longer exist. The overlapping of resonances allows orbits to pass from one resonance to another, in a fast so-called *Chirikov diffusion* (Figure 3.13).

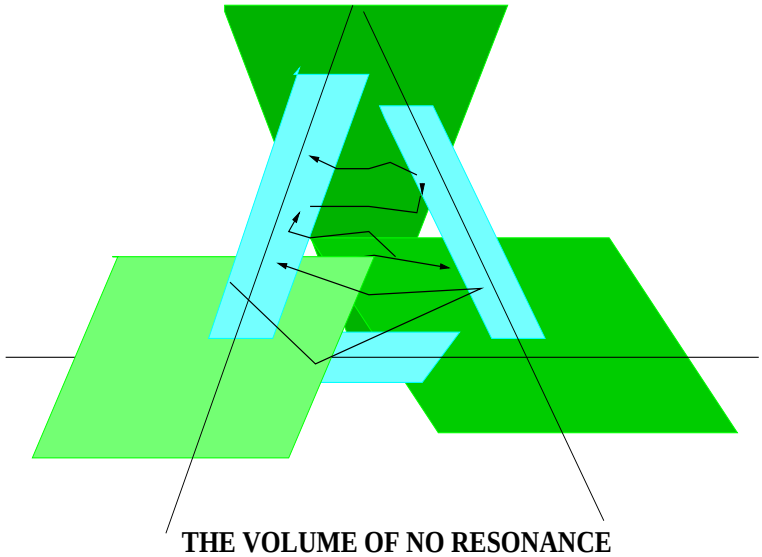

Figure 3.13: Chirikov regime: overlapping of resonances.

3.2.3 The transition from the Nekhoroshev to the Chirikov regime

As we said in the introduction, the crucial question about the stability of the actions in a Hamiltonian system is related to the structure and density of invariant tori which foliate the phase space. This is in fact the geometrical representation of the Nekhoroshev theorem. We recall that in a quasi-integrable system with Hamiltonian:

$$H(\mathbf{p},\mathbf{q}) = H_0(\mathbf{p}) + \epsilon H_1(\mathbf{p},\mathbf{q}), \tag{3.35}$$

non degenerate and convex, an eventual instability of the actions obeys the following exponential law:

$$||\mathbf{p}(t) - \mathbf{p}(0)|| \leq \alpha\epsilon^a, \qquad \text{for} \quad |t| \leq t_0\, e^{(\epsilon_*/\epsilon)^b}\ , \tag{3.36}$$

where $\alpha, t_0, \epsilon_*, a, b$ are suitable positive constants. We say that a system is in a Nekhoroshev regime when the diffusion of the actions is exponentially slow or equivalently when the phase space is dense of tori.

For large values of the perturbation parameter, this description fails and diffusion becomes a rapid phenomenon according to the well-known Chirikov criterion of overlapping of resonances [9]. The transition from the Nekhoroshev to the Chirikov

regime is a smooth process involving firstly the superposition of small resonances and then going from a slow Nekhoroshev diffusion to a fast Chirikov one. Therefore, such a slow diffusion is not easily recognized using even very long numerical integrations. This transition will be discussed in Chapter 6 when numerical tools for the detection of chaos will be developed.

Chapter 4

The connectance

4.1 An introduction to the problem of the "connectedness"

In the last thirty years many studies have been devoted to the investigation of the relationships between the properties of dynamical systems and their number of degrees of freedom. In the seventies the problem of looking for the transition from ordered to chaotic motion when increasing the number of interacting particles in nonlinear systems has been studied both analytically and numerically, leading to the conclusion that the measure of the chaotic domain with respect to the whole phase space volume increases very rapidly with the number of degrees of freedom [16],[6],[4].

We recall in particular the work of Froeschlé and Scheidecker [16], and the one by Benettin, Froeschlé and Scheidecker in the same years [4]. These authors took as a model problem an isolated one-dimensional self-gravitating system, consisting of n plane infinitely-extended-parallel sheets with uniform density. They studied its chaoticity when increasing the number of degrees of freedom, i. e. the number of sheets, and confirmed that the measure of the chaoticity of the system increases with the number of degrees of freedom. The authors remarked nevertheless that this result could possible be different if the system were not maximally "connected", in other words if each degree of freedom was not directly coupled with each other. This remark brings us directly to the problematic of the "connectedness", i. e. whether changing the fraction of direct couplings among degrees of freedom in a dynamical system could affect its properties.

In particular, a problem which has been largely studied is the relation between connectedness and stability in linear systems, for which there exist a wide range of

applications in many contexts, from ecology to economics.

In Section 4.2 we will analyse the use of connectedness in nonlinear systems, while in Section 4.3 and 4.4 we will move our attention to the linear case. The notion of "connectedness", which so far has not been rigorously defined, will be precised in the following and termed *connectance*, how it is customary in the literature.

4.2 The connectance in the nonlinear case

In this Section we analyse in detail the previous problematic and describe two different ways of "connecting": the simple model of Fermi-Pasta-Ulam [49], [25], [14] and a specific model consisting of a two-dimensional mapping introduced by Froeschlé in 1978 [17]. We will see that in the first case the connectedness is not a relevant parameter for the properties of the systems, while in the second one it plays a decisive role.

4.2.1 Fermi-Pasta-Ulam

The model of Fermi-Pasta-Ulam (FPU) consists in a chain of $n+2$ particles over a straight line (n moving particles, two fixed ones at the ends) interacting each other with nonlinear strength. The corresponding Hamiltonian is:

$$H(\mathbf{x},\mathbf{y}) = H_2(\mathbf{x},\mathbf{y}) + H_3(\mathbf{x}) + H_4(\mathbf{x}) \tag{4.1}$$

with

$$H_2 = \frac{1}{2}\sum_{j=1}^{n} y_j^2 + \frac{1}{2}\sum_{j=0}^{n}(x_{j+1}-x_j)^2,$$

$$H_3 = \frac{\alpha}{3}\sum_{j=0}^{n}(x_{j+1}-x_j)^3, \;\; H_4 = \frac{\beta}{4}\sum_{j=0}^{n}(x_{j+1}-x_j)^4.$$

Here $x_1, ..., x_n$ are the displacement with respect to the equilibrium position and $x_0 = x_{n+1} = 0$ are the fixed ends.

The normal coordinates are introduced via the canonical transformations (see Section 3.1)

$$x_j = \sqrt{\frac{2}{n+1}}\sum_{k=1}^{n} q_k sin\frac{jk\pi}{n+1}, \;\; y_j = \sqrt{\frac{2}{n+1}}\sum_{k=1}^{n} p_k sin\frac{jk\pi}{n+1}$$

(q_k, p_k) being the new coordinates and momenta. The quadratic part of the Hamiltonian in the normal coordinates is given by the form

$$H_2 = \sum_{j=1}^{n} E_j, \;\; E_j = \frac{1}{2}(p_j^2 + \omega_j^2 q_j^2) \tag{4.2}$$

with harmonic frequencies

$$\omega_j = 2sin\frac{j\pi}{2(n+1)}. \tag{4.3}$$

The problem, as first stated in the paper of Fermi, Pasta and Ulam [14], is concerned with the dynamical evolution of the harmonic energies E_j, as defined in (4.2). According to classical statistical mechanics the time average of each harmonic energy should be the same (equipartition), at least in the harmonic approximation, i. e.

$$\overline{E_j} = lim_{T\to\infty}\frac{1}{T}\int_0^T E_j(t)dt = \frac{E}{n}$$

where E is the total energy. Conversely, instead of a gradual, continuous flow of energy from the first mode to higher modes, the system showed an entirely different behaviour and this was a very surprising result which threw Fermi, Pasta and Ulam. This problematic has been widely studied in the literature [32], [13], [22] and will not be discussed in detail here. We are interested instead to the role of the connectedness in the FPU. It is clear that in this simple model each particle interacts with the near one, then the particles are not maximally connected, but they influence directly the behaviour of their neighborings only. A possible question is whether increasing the connectedness could influence or not the properties of the system.

In 1985 two studies on this subject were made by Giansanti, Pettini, Vulpiani [25] and by Paladin and Vulpiani [49]. The authors investigated the role played by an increase of connectedness respectively on the problem of the equipartion and on the chaoticity of the system. They defined the *connectance* as the average number of neighbor interacting masses in the chain. The original Hamiltonian is transformed into:

$$H = \sum_{i=1}^{n}[\frac{1}{2}y_i^2 + \frac{1}{2}(x_{i+1} - x_i)^2 + \frac{1}{2}\sum_{j\neq i}\frac{1}{4}\beta_{ij}(x_i - x_j)^4] \tag{4.4}$$

with $x_i = x_{i+n}$. The symmetric nonlinear coupling was defined by

$$\begin{aligned} &\beta_{ij} = \beta N_c, \text{ if } j \in [i - N_c, i + N_c] \\ &\beta_{ij} = 0, \text{ if } j \notin [i - N_c, i + N_c] \end{aligned} \tag{4.5}$$

where β is a positive constant and N_c is called the connectance number; in particular for $N_c = 1$ one obtains the standard first-neighbor case. They obtained that the

connectance has no relevant effect both on the equipartition and on the value of the Lyapunov exponent (see Chapter 6) for a given chaotic orbit.

The connectance can have instead some influence on the volume of the chaotic zone in the phase space. This will be discussed in the next Section, where we analyse another dynamical model, in which the degrees of freedom are connected differently from the FPU.

4.2.2 The Froeschlé 2n-dimensional mapping

A model different from the FPU which, even with a similar choice for the coupling coefficients, allows more complexity in connecting the various degrees of freedom, was studied by Froeschlé in 1978 [17]. In this paper he considered a n-dimensional symplectic mapping T built from n two-dimensional area preserving mappings. The mapping T is defined as :

$$\begin{cases} X_i = x_i + a_i \sin(x_i + y_i) + b \sum_{j=1}^{n} \alpha_{ij} \sin(\sum_{k=1}^{n} \alpha_{jk}(x_k + y_k)) \\ Y_i = x_i + y_i, \end{cases} \quad \forall i = 1, ..., n \tag{4.6}$$

The coefficients α_{ij} are such that α_{ij}=α_{ji} and

$$\begin{cases} \alpha_{ij} = 1 \quad \text{for } j - i < N_c \\ \alpha_{ij} = 0 \quad \text{for } j - i \geq N_c \end{cases} \tag{4.7}$$

with $j \geq i$. The interactions (which act as perturbations) are switched on or off by setting to 0 or 1 the elements of the upper or lower diagonals of this matrix. The *connectance* N_c is then defined as the number of non-zero upper and lower diagonals, so to quantify the number of direct interactions. The larger is the number of coefficients α_{ij} equal to 1, the larger is the number of direct couplings among the degrees of freedom. When $N_c = 1$, the mapping is the product of n two-dimensional mappings T_i,

$$T_i = \begin{cases} X_i = x_i + (a_i + b) \sin(x_i + y_i) \\ Y_i = x_i + y_i \end{cases} \tag{4.8}$$

When N_c=n the connectance between the mappings is maximal and each mapping interacts directly with the others with the same strength.

The author did not study the equipartition of energy, as in FPU, but he was mainly concerned with the emergency of chaos in such a coupled system. He measured the size of the non-chaotic zone about a given elliptic equilibrium point and found that it depends not only on the number of degrees of freedom but also on the

connectance. Fixed $n = 15$, for $N_c = 3, 6$ the size of the integrable zone remains more or less constant, while for $N_c = 9$ this integrable region has completely disappeared. This suggests that there exists a critical value of N_c which determines a drastic transition from an integrable to a chaotic regime. The author investigated the dependence of this critical value on the dimension of the system as well, finding that if n is quite large ($n \geq 20$) it seems to become independent of n.

Moreover, he focused his attention on the strength of interaction. For $N_c = \frac{1}{2}(n+2)$ if n is even and for $N_c = \frac{1}{2}(n+1)$ if n is odd, each mapping interacts directly with the others but not with the same strength. If we take for example $n = 3$, we have $N_c = 2$ and then the zero coefficients α_{ij} are only α_{13} and α_{31}. We have then for X_1 the equation:

$$\begin{aligned} X_1 &= x_1 + a_1 \sin(x_1 + y_1) + b\{\alpha_{11} \sin(\alpha_{11}(Y_1) + \alpha_{12}(Y_2)) + \\ &\quad \alpha_{12} \sin(\alpha_{21}(Y_1) + \alpha_{22}(Y_2) + \alpha_{23}(Y_3))\} \\ &= x_1 + a_1 \sin(x_1 + y_1) + b\{\sin(Y_1 + Y_2) + \sin(Y_1 + Y_2 + Y_3)\}. \end{aligned} \tag{4.9}$$

The problem at this point is twofold.

On one hand, even if $\alpha_{13} = 0$ the first and the third particle interact among them. In general having a zero element α_{ij} is not a sufficient condition to avoid a direct coupling between the particles i and j, so the coefficients do not really represent the interactions between the degrees of freedom. While in FPU it was simple to count the number of interactions, in the model of Froeschlé this is not so immediate.

The second problem, which is more complicated, concerns the "multiplicity" of the interactions. If we turn our attention to the previous example, we can see that the first particle interacts once with the third particle (the equation for X_1 contains X_3 with the coefficient equal to 1) and twice with the second particle (the equation for X_1 contains X_2 with the coefficient equal to 2). This shows that the "intensity" of the interaction is not always the same and in general it is not possible to connect each particles with all the others with the same strength of interaction. Thanks to these simple examples we can realize that it is not trivial to define the connectance unambiguously in the nonlinear case.

The situation is much more clear in the linear case in which the connectance corresponds exactly with the interaction among the degrees of freedom. We will analyse this problematic in detail in the next Sections.

4.3 The connectance in the linear case: the matrix of connectance

If we fix our attention to a linear system, it becomes simple to introduce a tool to measure the interactions among the degrees of freedom. If we consider the linear system

$$\dot{\mathbf{x}} = M\mathbf{x} \tag{4.10}$$

where M is a real $n \times n$ matrix, we can define the *connectance* C as the fraction of the non-zero off-diagonal elements $m_{i,j}$ of the matrix M. Its value is given then by the expression:

$$C = \frac{C_1}{n^2 - n}$$

where C_1 is the number of non-zero off-diagonal terms. In all cases the diagonal self-coupling terms are taken different from zero. The connectance varies then in the interval $[0, 1]$: if $C = 0$, M is a diagonal matrix, while if $C = 1$, all the elements are different from zero. A matrix element $m_{i,j} \neq 0$ denotes a direct interaction between the variables i and j, while if $m_{i,j} = 0$ there is no direct interaction.

Once defined the connectance, two issues must be analysed: how to dispose the elements in the matrix for a fixed connectance and how to assign the values of the non-zero elements.

For what concerns the positioning of the elements, two strategies will be considered in the following. The first one, called *ordered connectance*, consists in progressively connecting by starting from a diagonal matrix and filling completely the most internal non-zero upper and lower diagonals. For example, if $n = 3$ and $C = \frac{4}{6}$, the only possibility is the following one:

$$M_1 = \begin{pmatrix} m_{11} & m_{12} & 0 \\ m_{21} & m_{22} & m_{23} \\ 0 & m_{23} & m_{33} \end{pmatrix}.$$

This way of connecting is very particular and, in fact, does not allow to have many values of C if n is not sufficiently large. For example, when $n = 3$ the connectance can take only the values $C = 0, 4/6, 1$. The ordered connectance is then not optimal for a study concerning the transition from weakly connected to fully connected systems when the number of degrees of freedom is small.

The second strategy, which we call *non-ordered connectance*, consists in choosing randomly the location of the non-zero elements outside the main diagonal. For

example, always for $n = 3$ and $C = \frac{4}{6}$, two different possibilities can be:

$$M_2 = \begin{pmatrix} m_{11} & m_{12} & m_{13} \\ m_{21} & m_{22} & 0 \\ m_{31} & 0 & m_{33} \end{pmatrix} \qquad M_3 = \begin{pmatrix} m_{11} & m_{12} & m_{13} \\ m_{21} & m_{22} & 0 \\ 0 & m_{32} & m_{33} \end{pmatrix}.$$

In this way we have more possible values for the connectance, but we do not decide "a priori" the position of the interactions.

Clearly the two kinds of connectance correspond to different problems, and in the following we will analyse both cases.

The second problematic concerns the possible values for the filled elements of the matrix. We recall that in the paper of Froeschlé they can assume only the value 1, while in the pioneer work of Gardner and Ashby (Section 4.3.1) the elements are drawn in a random way from some given interval. Both ways of choosing the elements will be examined in Chapters 5 and 6.

4.3.1 The results of Gardner and Ashby

The first study concerning the role of the connectance in the study of linear systems was made by Gardner and Ashby in 1970 [23]. They considered the linearization of a dynamical system about an equilibrium point, reducing it to a system of ordinary differential equations

$$\dot{\mathbf{x}} = M\mathbf{x} \tag{4.11}$$

where M is a real $n \times n$ matrix. The connectance C was defined here for the first time as the fraction of non-zero non-diagonal elements in the matrix, and was taken randomly, according to our definitions in the previous Section. The non-zero elements of the matrix were chosen as random uniform variables belonging to some interval. In particular, the diagonal terms were taken in the interval $[-1, -0.1]$, so that the individual variables i were assumed to be intrinsically stable. The off-diagonal ones belonged instead to $[-1, +1]$.

According to the classical result that the system is stable when all the eigenvalues of M have negative real part, they computed the eigenvalues of a set of $N = 1000$ matrices and tested them for stability, when changing the connectance. They defined the *probability of stability* $\alpha(n, C)$ as the fraction of stable systems among all the N randomly chosen ones. The curve of Gardner and Ashby is reproduced in Figure 4.1.

$\alpha(n, C)$ was computed for $n = 4, 7$ and 10 and in general it depends both on the connectance and on the dimension of the system. For $C = 0$ the resulting diagonal matrix is evidently stable. For a given n, $\alpha(n, C)$ decreases monotonically with C

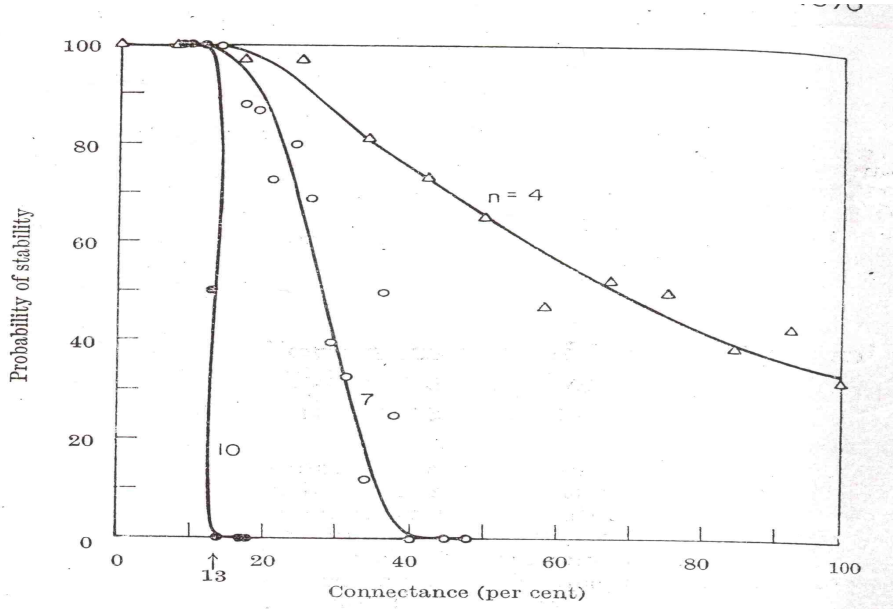

Figure 4.1: Gardner and Ashby experiment: probability of stability $\alpha(n, C)$ as a function of the connectance C for $n = 4, 7, 10$.

and when increasing n the probability $\alpha(n, C)$ drastically drops to 0 even for low values of C. In other words, the larger is n, the greater is the rate of decrease. Gardner and Ashby argued that there should exist a critical value C_{crit} for large n, so that $\alpha(n, C < C_{crit}) \sim 1$ and $\alpha(n, C > C_{crit}) \sim 0$. A sudden change of behaviour should occur in the vicinity of C_{crit}.

4.4 The connectance: an interdisciplinary tool

Since Gardner and Ashby's work the concept of connectance in linear systems has been applied to many contexts, in particular ecology and economics. For the ecologists community the connectance, intended as the number of links among living species, gives in fact some measure of the complexity in an ecological system, while in economics the connectance can be applied to the study of the equilibria of interdependent markets.

4.4.1 Application to ecology

Linear systems are used in ecology to modelize the dynamical behaviour of a so-called *food web*. Loosely speaking, a food web is defined as the multitude of relationships between species in a biotic community. This concept is translated into mathematical language as follows. Let i and j denote two biological species and x_i and x_j the number of organisms belonging to species i and j. In a system with n species, the set of all possible relationships among them is modeled at the lowest order by a $n \times n$ Jacobian matrix of interaction coefficients $m_{i,j}$ that describe the impact of each species i on the growth of each species j. The connectance associated to this matrix is understood as "complexity" in this context. In food webs the type of relationship between the species i and j can be classified according the signs of the entries of the matrix: if $m_{i,j} > 0$, i increases owing to the existence of j, whereas if $m_{i,j} < 0$, j effects i negatively. There are four possible relationships:

$m_{i,j} < 0\,,\ m_{j,i} < 0 \rightarrow$ negative feedback
$m_{i,j} > 0\,,\ m_{j,i} < 0 \rightarrow$ predator/prey
$m_{i,j} > 0\,,\ m_{j,i} > 0 \rightarrow$ cooperation
$m_{i,j} < 0\,,\ m_{j,i} > 0 \rightarrow$ prey/predator

In 1972 May [41] reconsidered Gardner and Ashby's results in a food web context. By analytic considerations, he extended Gardner and Ashby's work to an infinitely large number of variables, agreeing with the fact that randomly generated food webs decrease in stability as they increase in complexity.

In 1974 Daniels and Mackay [12] repeated the same numerical calculations of Gardner and Ashby, but they found a slightly different result. They confirmed the decrease of stability when increasing the connectance, but the transition from stability to instability was not so sharp and the critical value C_{crit} conjectured by Gardner and Ashby was not found. Moreover, in Figure 4.2 we can see that their curves (the solid lines) are more stable than Gardner and Ashby ones (the dotted lines).

This contradictory result was furtherly studied in 1986 by Martens [40]. He restricted his attention on the case of $C = 1$ and showed that Daniels and Mackay were not wrong. In his paper he resumed the debate among the previous different results and concluded that the discrepancy is due to a numerical instability in the computation of the eigenvalues.

In fact, we confirme ourselves the stability results found by Daniels and Mackay by a numerical experiment which will be described in Section 5.1.

The fundamental point of all these results is the decrease of stability when increasing the connectance. This was paradoxical to many ecologists who experience

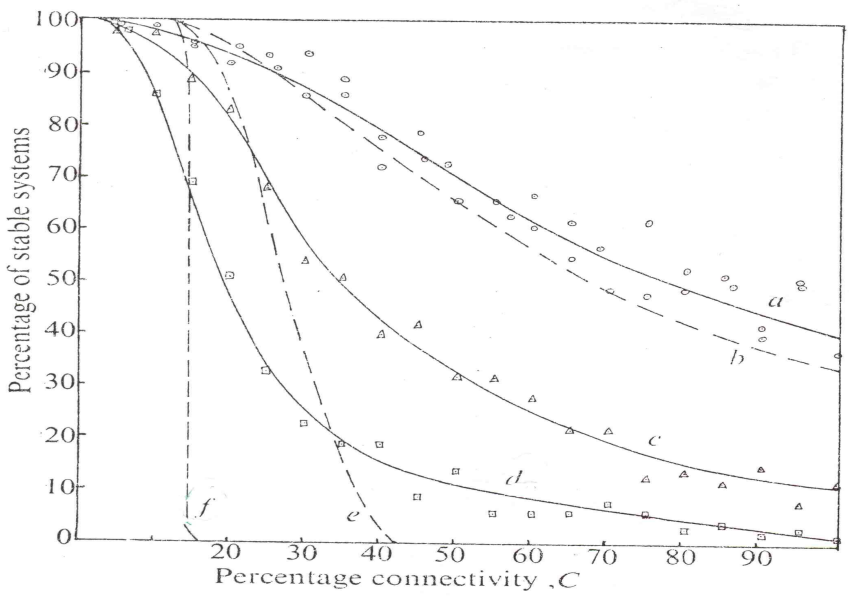

Figure 4.2: Percentage of stable systems versus connectance according to Daniels and Mackay: comparison between their results (solid lines, a, c, d) and those of Gardner and Ashby (dotted lines, b, e, f). a,b: n=4; c,e: n=7; d,f: n=10.

the opposite pattern in nature. It seems in fact that in real food webs complexity helps to increase stability rather than to diminish it. A way out of this paradox was to reconsider the dynamics of real food webs, by taking more complex networks, characterized by structured interactions, species "strategy" and dynamical characteristics that would allow complex communities to persist. This is translated into choosing the matrix elements in more complicated ways, not simply as random numbers in a given interval. May himself in 1999 [42] commented on the actual state of food webs theory, affirming that real ecosystems are not randomly constructed and therefore his results do not apply to real-world networks, which are much more structured.

As an example of a recent study which couples modern ecological considerations to mathematical modeling, in 2000 Wilmers, Sinha and Brede [55] reconsidered the dynamics of interactions in food webs. They examined the stability properties of differents food web configurations and added hierarchical structures to them. In particular, they compared the case of food webs characterized by completely random interactions with systems in which a high percentage of prey - predator relationships

is imposed. In this latter case, which is supposed to be dominant in nature, off-diagonal symmetric elements in the Jacobian matrix are taken with opposite sign. They repeated the Gardner and Ashby's experiment with these two choices of food webs and found that for a given value of C ($C = 0.11$) the "realistic" prey - predator food web has a larger probability of stability than the random one. Their result is shown in Figure 4.3, where stability is plotted against the standard deviation of the interacting coefficients for $C = 0.11$. Standard deviation and connectance are in fact functions of each other, so for a given standard deviation it corresponds a given connectance. The problem is that in all their experiments they never found an increase of stability with the connectance, as expected by the ecologists. This is the fundamental point, and until now in ecology no simple linear model has been found allowing an increasing of the stability with the connectance.

4.4.2 Application to economics

Another field concerning the relationship between connectance and stability in linear systems is economics, with regards to the stability of equilibria of interdependent

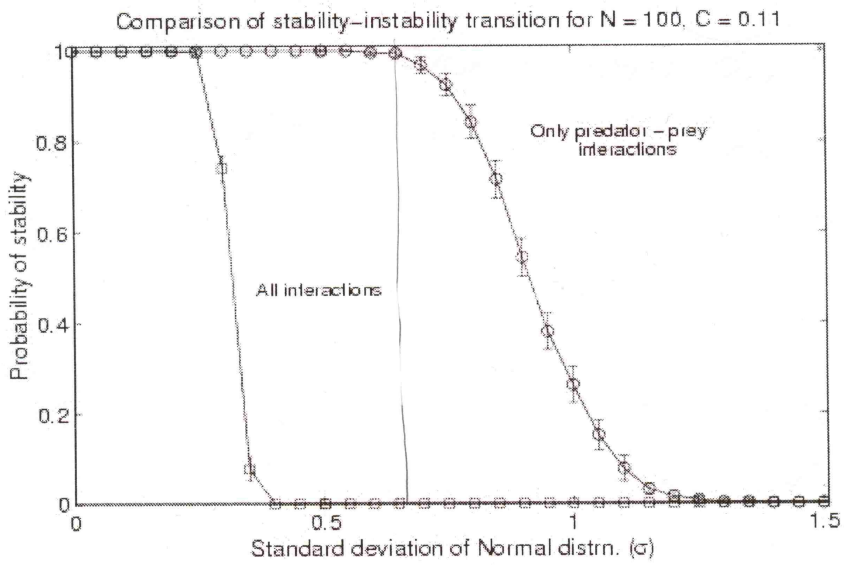

Figure 4.3: Wilmers, Sinha and Brede experiment: stability of food webs with hierarchical structures for $C = 0.11$ and $n = 100$ as a function of the standard deviation of the interaction coefficients.

markets. A study on this subject was done by Froeschlé and Longhi in 1987 [21] and then deepened by Froeschlé, Lega and Lohinger [20] and Cosentino, Lega and Froeschlé [11]. They studied the stability-connectance relation in an economic system of n goods characterized by a vector of prices $\vec{p} = (p_1, ..., p_n)$. The time evolution of prices is regulated by the market law of supply and demand. They defined the excess demand E_i as the difference between the global demand and the global supply for the good i obtained for a given vector of prices: $E_i = E_i(\vec{p})$. Then, the evolution of prices with time is defined by the set of equations:

$$\dot{p_i} = g_i[E_i(\vec{p})] \ \forall i = 1, .., n \tag{4.12}$$

where g_i is a regular increasing function which is 0 at the origin. The vector $\vec{p^*} = (p_i^*, ..., p_n^*)$ such that $E_i(\vec{p^*}) = 0 \ \forall i$ is said to be the vector of prices in general equilibrium. By linearizing the set of equations (4.12) we get:

$$\dot{\vec{P}} = M(\vec{p^*})\vec{P} \tag{4.13}$$

where $\vec{P} = (\vec{p} - \vec{p^*})$ and M is the Jacobian matrix of $\vec{g}$, i.e. the matrix which defines the relationships between the n independent markets. The authors simplified then the problem taking $g_i[E_i(\vec{p^*})] = b_i E_i(\vec{p^*})$, with $b_i > 0$ $(\forall i)$, which for the elements of M gives $m_{i,j} = b_i \partial E_i(p^\star)/\partial p_j$. The diagonal elements $m_{i,i}$ represent the influence exerted by a variation of the price of the good i on its global demand, while the off-diagonal terms $m_{i,j}$ represent the influence exerted by a variation in the price of the good j on the global demand for the good i. To fix the terminology, if $m_{i,j} > 0$ the good j is said to be a *substitute* of the good i, while if $m_{i,j} < 0$ the good j is said to be *complementary* to the good i.

Substitute goods play in some sense the same role: as an example, honey (good i) and sugar (good j) are sustituable and this is reflected in the fact that an increase of the price of sugar results in an increase of the demand for honey (interaction modeled by a positive $m_{i,j}$).

Complementary goods are for example spaghetti (good i) and sauce (good j): an increase of the price of sauce will produce a decrease in the demand for spaghetti (interaction modeled by a negative $m_{i,j}$).

Froeschlé and Longhi [21] studied then the stability α of the linear system $\dot{\mathbf{x}} = M\mathbf{x}$ as a function of the connectance, a problem perfectly analogous to the one studied in the food webs context. In particular, they studied the effects of substitutability/complementarity on the stability, i.e. the effect of varying the fraction of off-diagonal elements with positive/negative signs in the matrix M. They not only confirmed the results of Mackay and Daniels, but they searched the conditions

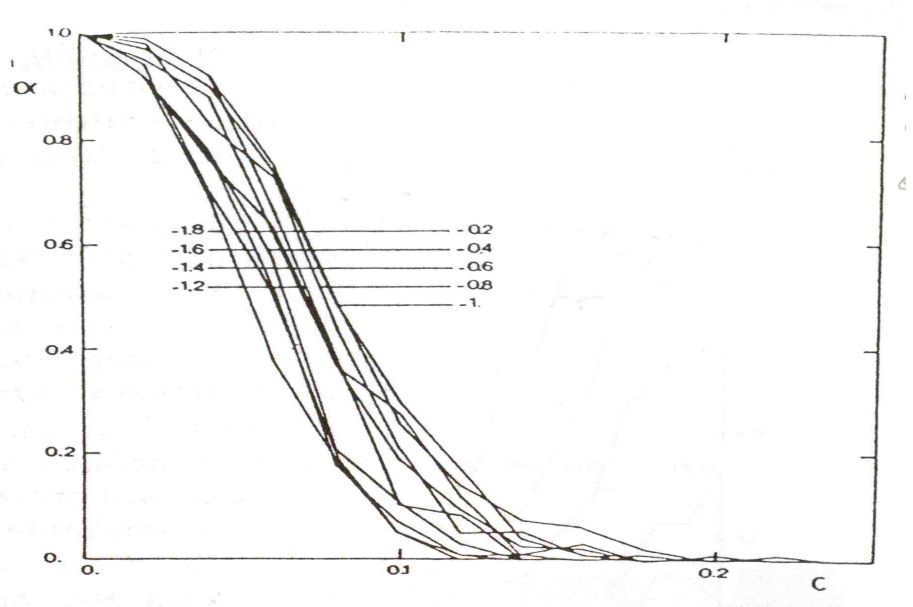

Figure 4.4: Probability of stability α as a function of the connectance C for different percentages of substitutable and complementary goods. The off-diagonal terms are uniformly distributed in the interval $[b, 2+b]$. The value of b is printed near each curve. For $b = -1.8$ we have a mean of 10% of complementarity, while for $b = -0.2$ we have a mean of 90% of substitutability. We have the maximal stability for $b = -1$ which is equivalent to a mean of 50% of substitutable goods.

for maximal stability finding that the maximal stability is obtained for 50 % of substitutable goods. By choosing the off-diagonal terms as random variables in a given interval, this coincides with taking this interval symmetric with respect to 0. The result is plotted in Figure 4.4.

This result seemed in contradiction with the general equilibrium theory, for which total substitutability is considered a sufficient condition for stability. In fact there is no contradiction, because the general theory of equilibria supposes tacitly the so-called Walras law, which states that in a market of $n+1$ goods in which one plays the role of money and has no dynamical role, for any vector $\vec{p}$ of prices

$$\sum_{i=1}^{n+1} p_i E_i(\vec{p}) = 0. \tag{4.14}$$

Froeschlé and Longhi demonstrated that the Walras law implies the condition that

for every line of the matrix M, the sum of their elements is smaller than zero, i.e.

$$\sum_{j=1}^{n} m_{i,j} < 0 \quad \forall\, i = 1 \dots n. \tag{4.15}$$

Then, if we want to have any chance to satisfy the Walras law, we have to impose this restriction to the matrix.

Froeschlé and Longhi remarked that coupling this condition with the total substitutability implies that the matrix M satisfies the quasi-diagonal dominance criterion [43]. This criterion is a necessary condition for the stability of the system and states the following:

Quasi-diagonal dominance criterion

Given a $n \times n$ matrix M, if the diagonal terms $m_{i,i}$ are negative and there exists a set of positive numbers $w_i > 0, i = 1 \dots n$ such that:

$$w_i |m_{i,i}| > \sum_{j \neq i} w_j |m_{i,j}| \;\; \forall i = 1, \dots, n \tag{4.16}$$

then all the eigenvalues of M are negative.

Equation (4.16) implies that the relevant parameters for stability are the diagonal terms with respect to the sum of the modules of the off-diagonal terms, i.e the relative size of the intervals from which the diagonal and off-diagonal terms are drawn. With the restriction (4.15), the matrix M satisfies exactly the condition (4.16) with all the weights equal to 1 and then the equilibrium is stable.

In Figure 4.5 is displayed the same experiment as in Figure 4.4, but with the constraint (4.15) imposed. The off-diagonal terms belong to the interval $[b, 2 + b]$, with b going from -2 to -0.2, so for $b = -2$ all goods are complementary and for $b = -0.2$ there is 90% of substitutability. According to the previous discussion, one can see how in this case increasing the substitutability raises the probability of stability, because the chance of having a matrix satisfying the quasi-diagonal criterion is augmented.

Since this work, in the economics community it become common to try to adjust the parameters of an economic system to achieve the quasi-diagonal dominance condition in order to stabilize equilibria. In Section 5.2, we will show that this procedure is not optimal, because this criterion for stability is far from being sharp. Moreover, we will point out the relationship with this condition and a more general series of results known as Geršgorin (or Geršgorin-like) theorems.

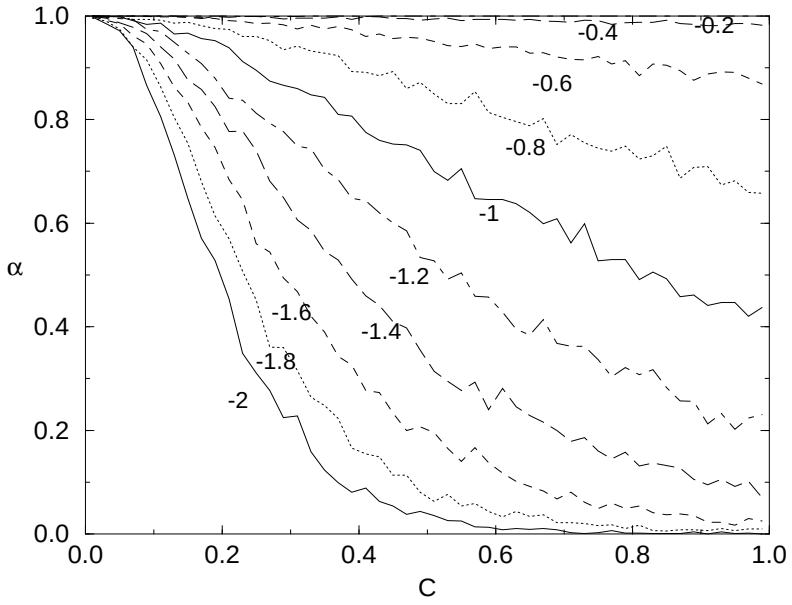

Figure 4.5: Probability of stability as a function of the connectance for different percentages of substitutable goods and the condition (4.15) imposed. The dimension is $n = 20$ and the diagonal elements belong to the interval $[-2.5, -0.1]$. The off-diagonal terms are uniformly distributed in the interval $[b, 2 + b]$. The value of b is printed near each curve. For $b = -2$ all the goods are complementary (and the stability is minimal), while for $b = -0.2$ we have a mean of 90% of substitutability (maximal stability).

Chapter 5

Linear stability and connectance

In this Chapter we reconsider the experiment of Gardner and Ashby discussed in Chapter 4, taking randomly constructed linear systems and studying their probability of stability as a function of the connectance. We present some new results, which are related to some open issues faced by both the ecology and the economics communities. On one side, we critically revise the relevance of the quasi-diagonal dominance criterion as a guide to enforce stability, and we point out how this criterion is part of a more general framework known as Geršgorin Theorem. On another side, we perform a general study on the influence of the distribution of the interaction coefficients on the stability behaviour of interacting systems. In particular, we will show as in appropriate regimes the stability can actually increase with the connectance, a fact which has been excluded so far. This behaviour is characteristic of systems termed in ecology *competitive*, i.e. such that the interaction coefficients among species are all negative. We finally address the dependence of the connectance/stability relationship on the size of the system and on the main value of the interaction strength. These results are published in [10].

5.1 Linear stability and connectance: basic statements

We briefly recall the main definitions and issues related to the connectance problem. Given a n-dimensional dynamical system $\dot{\mathbf{x}} = f(\mathbf{x})$, we focus our attention to the study of its linear stability about an equilibrium point. Linearization leads to a system of ordinary differential equations

$$\dot{\mathbf{x}} = M\mathbf{x} \tag{5.1}$$

where M is a real $n \times n$ matrix.

We choose as definition for the *connectance* C the one introduced in Section 4.3, coinciding with Gardner and Ashby's one. C is then the fraction of non-zero off-diagonal elements $m_{i,j}$ of the matrix M. In general the connectance will be chosen *non-ordered*, apart for a single experiment in which a comparison with the *ordered* case is performed.

We calculate the probability of stability over a given set of N matrices as a function of C. In all the following experiments we take $N = 1000$ if not otherwise specified, and 101 values of the connectance between 0 and 1. For each matrix we compute the eigenvalues in order to say if the system is stable or not, considering the system as stable if all its eigenvalues have negative real part. As discussed in Chapter 2, this is equivalent to select all systems which are asymptotically stable. We define the *probability of stability* α as the fraction of stable systems among all the N randomly chosen ones.

The non-zero elements of the matrices satisfy the relations :

$$\begin{cases} m_{i,i} = u[a_1, a_2] & \forall i, i = 1, ..., n \\ m_{i,j} = u[b_1, b_2] & \forall i, j \;\; j \neq i, i, j = 1, ..., n \end{cases} \tag{5.2}$$

where $u[x_1, x_2]$ denotes a random uniform variable belonging to the interval $U = [x_1, x_2]$. We denote U_D and U_{OD} the intervals from which we draw the diagonal and off-diagonal terms respectively. The diagonal elements will be taken always negative, to ensure stability when $C = 0$.

As an introduction, we perform a first experiment by choosing the same conditions as Gardner and Ashby, i.e. we take $U_D = [-1, -0.1]$ and $U_{OD} = [-1, 1]$ and three values of the matrix dimension: $n = 4, 7, 10$. The result is plotted in Figure 5.1. We can observe the same discrepancy with the Gardner and Ashby experiment (Figure 4.1) as explained in the previous Chapter.

To obtain a more complete result, we calculate the probability of stability for a larger number of degrees of freedom. We take then the same $U_D = [-1, -0.1]$ and $U_{OD} = [-1, 1]$ and ten values of the matrix dimension $n = 10, 20, 30, ...100$. It is evident that α depends both on the connectance and on the dimension of the system. For $C = 0$ the resulting diagonal matrix is evidently stable. For a given n, α decreases monotonically with C and when increasing n the probability α drastically drops to 0 even for low values of C (Figure 5.2). In the following Chapters we will see as this behaviour is in fact non universal, but it depends on the way of choosing the matrix coefficients.

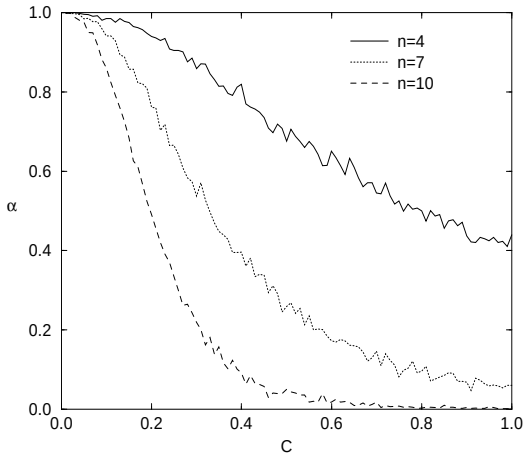

Figure 5.1: Probability of stability α as a function of the connectance for three different values of n ($n = 4, 7, 10$) and diagonal interval $U_D = [-1, -0.1]$, off-diagonal interval $U_{OD} = [-1, 1]$.

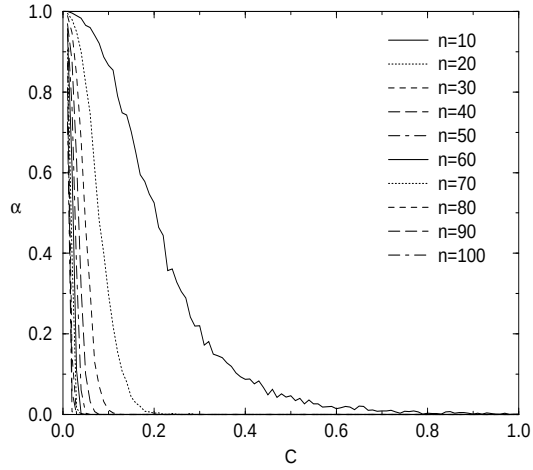

Figure 5.2: Probability of stability α as a function of the connectance for different dimensions n of the system and diagonal interval $U_D = [-1, -0.1]$, off-diagonal interval $U_{OD} = [-1, 1]$.

5.2 The diagonal dominance criterion revisited. The Geršgorin Theorem and its practical applicability

We saw in Section 4.4 that the quasi-diagonal dominance criterion has been used (especially in economics) as a guide to predict a priori the probability of stability for a given equilibrium, or even to optimize the coupling coefficients among degrees of freedom in order to maximize the stability for a given connectance.

This criterion derives in fact from a more general set of theorems [53], from which is nevertheless difficult to extract practical informations when n is large. The only one which can be easily used is the Geršgorin theorem [24] which states the following:

Geršgorin theorem

For any $n \geq 2$, let $M = [m_{i,j}] \in \mathbb{C}^{n\times n}$ a $n \times n$ complex matrix and let $\sigma(M) = \{\lambda \in \mathbb{C} : det[M - \lambda I_n] = 0\}$ denote its spectrum. Let define by

$$G_i(M) = \{z \in \mathbb{C} : |z - m_{i,i}| \leq r_i\}, \;\; r_i = \sum_{j\neq i} |m_{i,j}|, \;\; i = 1 \ldots n \tag{5.3}$$

the i^{th} Geršgorin disk in the complex plane.

Then the set of the eigenvalues of M is contained in the union of these disks:

$$\sigma(M) \subseteq \bigcup_{i=1}^{n} G_i(M). \tag{5.4}$$

In Figure 5.3 there is the geometric representation for a matrix $M_{4\times 4}$ with real elements.

A more complete result is given by the following

Generalized Geršgorin theorem

Given a matrix $M = [m_{i,j}] \in \mathbb{C}^{n\times n}$ and $\mathbf{w} = [w_1, ..., w_n]^T > 0 \in \mathbb{R}^n$, consider the matrix product $W^{-1}MW = [\frac{m_{i,j}w_j}{w_i}]$ where $W := diag[w_1, ..., w_n]$. Since M and $W^{-1}MW$ are similar matrices, $\sigma(M) = \sigma(W^{-1}MW)$.

By setting now

$$r_i^{\mathbf{w}} := \sum_{j\neq i} w_j |m_{i,j}|/w_i, \quad \forall i \in \mathbb{N} \tag{5.5}$$

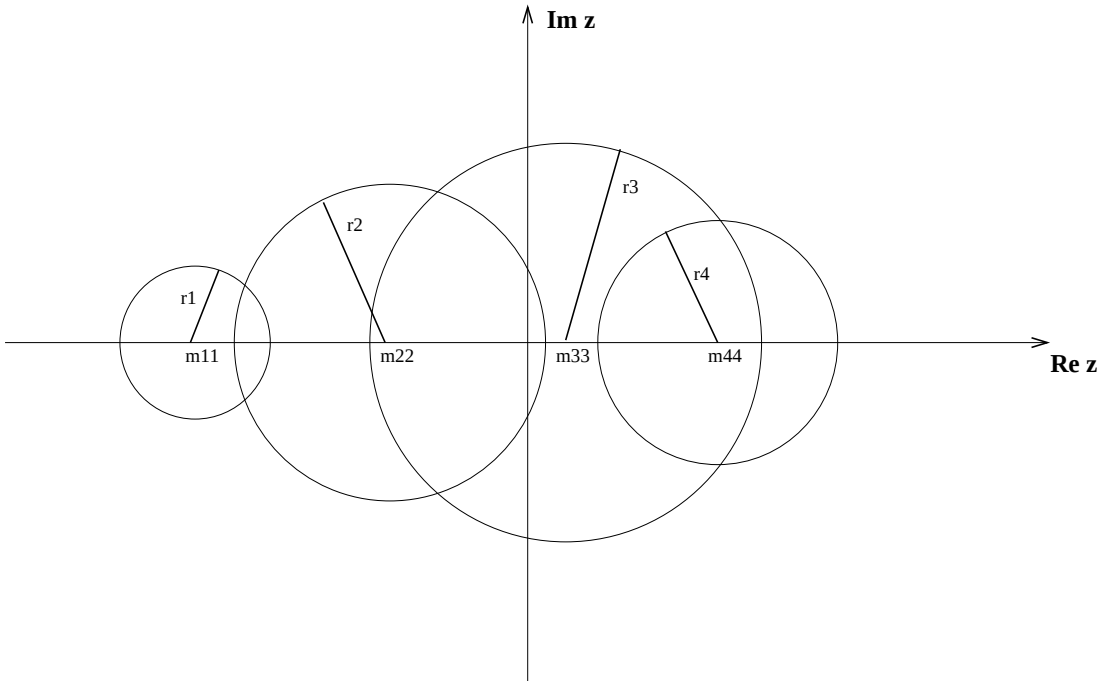

Figure 5.3: Geometric representation in the complex plane of the Geršgorin theorem for a matrix $M_{4\times 4}$ with real elements. The set of eigenvalues is contained in the union of the disks.

the Geršgorin theorem, applied to $W^{-1}MW$, gives

$$\sigma(M) = \sigma(W^{-1}MW) \subseteq \bigcup_{i=1}^{n} \{z \in \mathbb{C} : |z - m_{i,i}| \leq r_i^{\mathbf{w}}(M)\} =: \mathcal{G}^{\mathbf{w}}(M). \tag{5.6}$$

As this eigenvalue inclusion holds for each $\mathbf{w} = [w_1, ..., w_n]^T > 0 \in \mathbb{R}^n$, we have

$$\sigma(M) \subseteq \bigcap_{\mathbf{w}>0} \mathcal{G}^{\mathbf{w}}(M) \tag{5.7}$$

i.e. the spectrum is included in the infinite intersection of the unions of all Geršgorin disks, every disk being built with a weighted radius. We will call *Geršgorin criterion for stability* the condition that the intersection on the right-hand side of (5.7) lies on the negative complex plane.

From this theorem it can be readily derived the quasi-diagonal dominance sufficient condition (4.16) for stability. In fact, if (4.16) is satisfied for a set of weights $\bar{\mathbf{w}}$, then $\mathcal{G}^{\bar{\mathbf{w}}}(M)$ lies on the negative complex plane, so the whole spectrum lies on the negative complex plane and the matrix is stable.

It turns out that, when the off-diagonal terms are all positive, the inclusion in equation (5.7) becomes an equality, i.e.

$$\sigma(M) = \bigcap_{\mathbf{w}>0} \mathcal{G}^{\mathbf{w}}(M) \tag{5.8}$$

so the Geršgorin criterion (and the quasi-diagonal dominance one) becomes a necessary and sufficient condition for stability [51]. This is in general not true if the sign of the off-diagonal terms is not positive defined.

As explained in Section 4.4, for some applications such as economics [21] a classical strategy to maximize the likelihood of equilibria stability consists in forcing the system to satisfy the quasi-diagonal dominance, but considering only a single set of weights $\widetilde{\mathbf{w}}$ (usually $\tilde{w}_i = 1 \; \forall \, i$). We can suspect that, even in the necessary and sufficient case for which the equality (5.8) is satisfied, this procedure consisting in replacing the intersection $\bigcap_{\mathbf{w}>0} \mathcal{G}^{\mathbf{w}}(M)$ with a single set $\mathcal{G}^{\widetilde{\mathbf{w}}}(M)$ is far from being sharp. You could in fact expect that a matrix is very often stable even when $\mathcal{G}^{\widetilde{\mathbf{w}}}(M)$ does not lie on the negative complex plane. We check this issue by taking a set of off-diagonal positive definite matrices of size $n = 50$ with $U_{OD} = [0, 0.1]$ and $U_D = [-1, -0.1]$, and evaluating the finite intersection over 10^p randomly distributed weights $w_i \in (0, 1)$, for $p = 3, 4, \ldots, 8$. In Figure 5.4 we plot the fraction γ for which the finite intersection lies on the negative complex plane, compared to the real fraction of stable matrices α. It is evident that when increasing p the curves $\gamma(C)$ converge extremely slowly to the real stability curve $\alpha(C)$, so this approximate criterion gives very little information and it is difficult to made it sharp by choosing a large number of weights. The result does not get better when the w_i belong to a larger interval (not shown), nor taking simply all the w_i equal to one (Figure 5.4, dark dashed line).

A second aspect concerns the discrepancy between the spectrum $\sigma(M)$ and the intersection $\bigcap_{\mathbf{w}>0} \mathcal{G}^{\mathbf{w}}(M)$ when the inclusion (5.7) is not an equality, i.e. when the sign of the off-diagonal terms is not positive defined. At this purpose, we calculate $\alpha(C)$ for $n = 100$, $U_D = [-1, -0.1]$ and three off-diagonal intervals having the same distribution for the module of their elements: $U_{OD} = [-0.1, 0]$, $U_{OD} = [-0.1, 0.1]$ and $U_{OD} = [0, 0.1]$. In these three cases the intersection $\bigcap_{\mathbf{w}>0} \mathcal{G}^{\mathbf{w}}(M)$ is likely to be the same. The result is plotted in Figure 5.5. We remark that in the first two cases

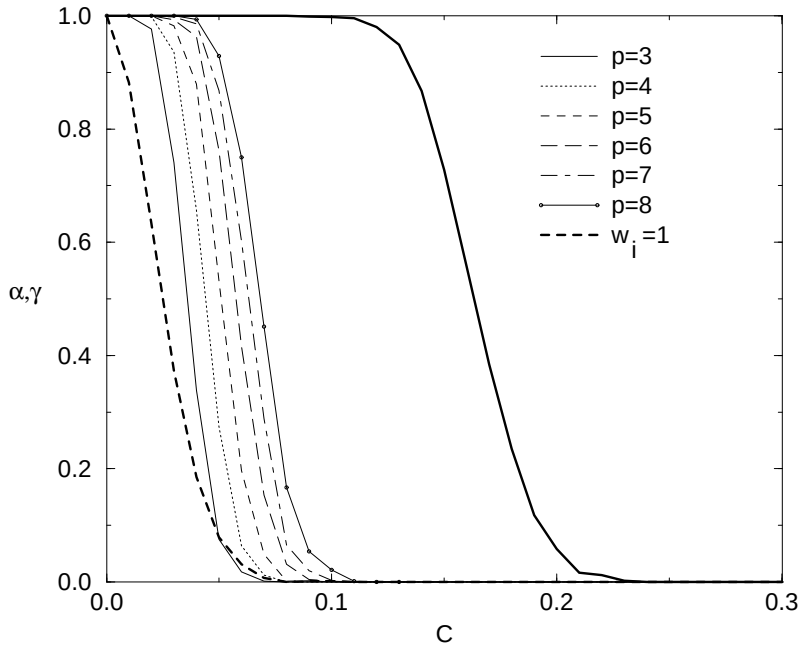

Figure 5.4: Light lines: probability of stability γ as a function of the connectance according to the quasi-diagonal dominance criterion for 10^p weights $w_i \in (0, 1)$ and different values of p. Dark dashed line: same with all the weights equal to 1. Dark solid line: probability of stability α from direct eigenvalues computation.

the fraction of stable matrices largely exceeds the one calculated in the third case, which in turns coincides with the prediction of the Geršgorin criterion. In other words, when the matrix elements are not positive the sharpness of the Geršgorin criterion in checking for stability is very small, making it an inefficient guide to enforce stability of equilibria.

It is interesting to remark that for $U_{OD} = [-0.1, 0]$ α shows a non-monotonic dependence on C, becoming larger when the matrix is fully connected. This behaviour is not possible when the off-diagonal matrix elements are drawn from a positive interval $U_{OD} = [0, b_2]$. In this case matrices with a size n and a connectance C will have the same stability properties if the parameter nCb_2 is kept constant, the right-hand side of equation (4.16) scaling statistically as nCb_2. This implies that

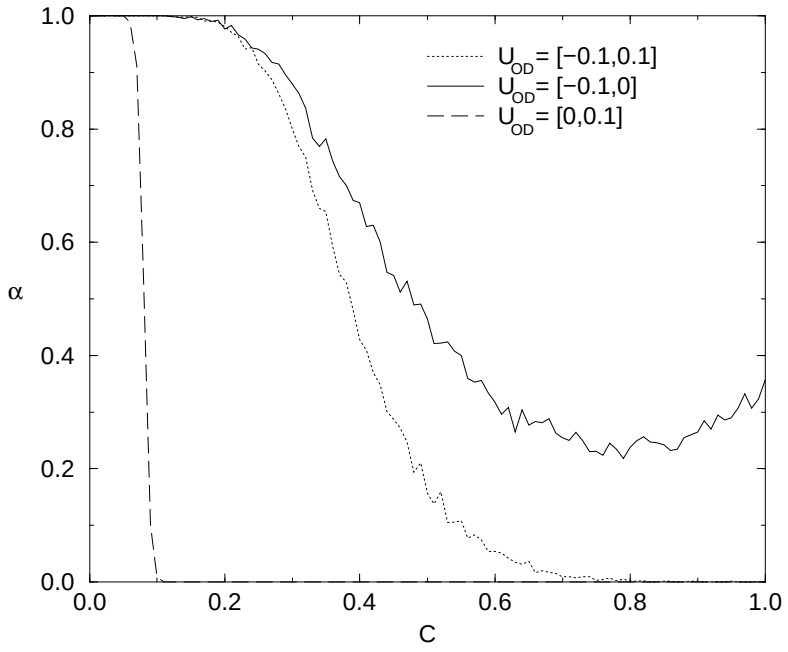

Figure 5.5: Probability of stability α as a function of the connectance for $n = 100$, diagonal interval $U_D = [-1, -0.1]$ and off-diagonal intervals $U_{OD} = [-0.1, 0.1]$ (dotted line), $U_{OD} = [-0.1, 0]$ (solid line), $U_{OD} = [0, 0.1]$ (dashed line).

the probability of stability can just decrease when increasing C, n or the amplitude of U_{OD}. The counter-intuitive behaviour seen for $U_{OD} = [-0.1, 0]$ will be termed *stability recover phenomenon* in the following. Its appearance, characteristic of competitive systems only, will be extensively studied in the following Sections along with the conditions for its realization.

We analyse now the connectance-stability behaviour in a case of ordered connectance. We consider two cases: positive off-diagonal elements ($U_{OD} = [0, 0.1]$), for which the Geršgorin criterion for stability is necessary and sufficient, and negative off-diagonal elements ($U_{OD} = [-0.1, 0]$), for which the stability recover phenomenon appears. Moreover, we take $U_D = [-1, -0.1]$ and $n = 100$. The stability curves are plotted in Figure 5.6, along with the corresponding results for the non-ordered connectance. One can remark how in both cases for the ordered connectance the

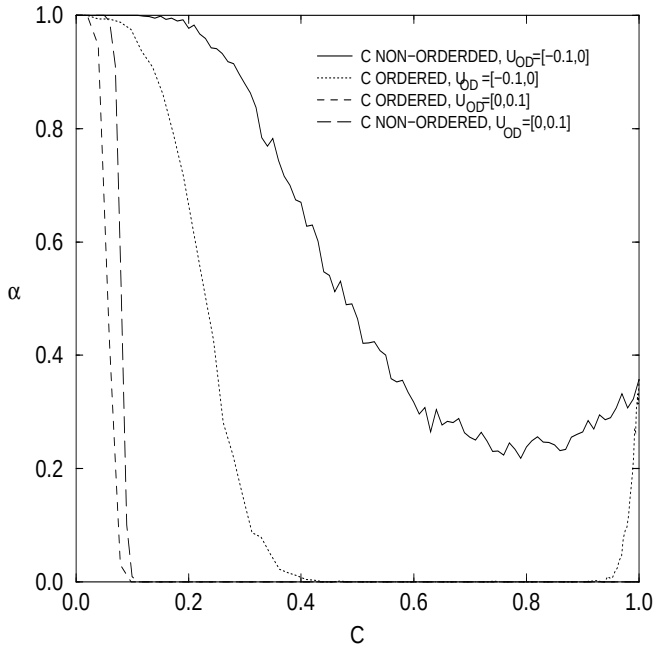

Figure 5.6: Probability of stability $\alpha(C)$ for the ordered and the non-ordered connectance. The dimension is $n = 100$ and the diagonal and off-diagonal intervals are $U_D = [-1, -0.1]$ and $U_{OD} = [-0.1, 0]$, $U_{OD} = [0, 0.1]$.

probability of stability is smaller than for the non-ordered one. We analyse this result when $U_{OD} = [0, 0.1]$. In this case we recall that in order to check for stability it is sufficient to analyse the position of the Geršgorin disks in the complex plane (see Figure 5.3). Take then a given value of the connectance. For the ordered case, the number of non-zero elements on each line of the matrix is fixed, so the distribution of the radii is expected to be uniform, while for the non-ordered case there is a range of possibilities, going from matrices with all the lines equally filled to matrices with some empty lines and some full lines, so there is a non-uniform distribution for the radii. This is true even when the weights are considered. Fix then a connectance value and a matrix which is unstable for the ordered case. Many non-ordered cases will correspond to it, some still unstable, but some stable, because now it can happen that the largest radii fall all on the left in Figure 5.3. So it is not surprising

that the non-ordered case has a larger stability than the ordered one.

When $U_{OD} = [-0.1, 0]$ this properties is even more evident, but the previous simple argument is not directly applicable, the Geršgorin criterion not being necessary and sufficient. Because we are interested to cases in which the stability is as large as possible, in the following we will treat the case of non-ordered connectance only.

5.3 The stability recover phenomenon: the choice of the coefficients

5.3.1 Stability properties when the diagonal or the off-diagonal terms are fixed

First of all, we want to investigate the behaviour of the function $\alpha(C)$ for C close to 1. To this purpose, we analytically address the simple fully-connected case in which the matrix M is given by:

$$\begin{cases} m_{i,i} = a \quad \forall i \qquad\qquad i = 1, ..., n \\ m_{i,j} = b \quad \forall i, j \quad j \neq i \quad i, j = 1, ..., n. \end{cases}$$

This matrix has $n-1$ eigenvalues equal to $a-b$, while the n^{th} one equals $a+(n-1)b$. This can be rapidly shown by taking a matrix B with all elements equal to b. B has at least one eigenvalue equal to 0 (because $detB = 0$) with multiplicity $n-1$ (because $rank(B) = 1$, so $ker(B) = n - 1$). The other eigenvalue equals then $Tr(B) = nb$. One remarks now that adding to a matrix the same value d to its diagonal, the eigenvalues are augmented by the same quantity d. Then we recover the eigenvalues for M by adding $a - b$ to the diagonal of B.

A necessary and sufficient condition for the stability is then $|a| > |b|$ if $a, b < 0$, and $|a| > (n-1)|b|$ if $a < 0, b > 0$. If all the matrix elements are negative, the stability condition is independent of the dimension n and much less restrictive than the Geršgorin criterion. It obviously coincides with this latter for $a < 0$ and $b > 0$, for $w_i = 1$ in this specific case.

We address now numerically the more general case of $a, b < 0$ taken randomly in a given interval and C between 0 and 1.

We first take the same off-diagonal values $b = -0.09$ and use different diagonal intervals $U_D = [a_1, -0.1]$ with $a_1 = -0.1, -0.2, -0.5, -1$. The stability curves $\alpha(C)$ for $n = 100$ are plotted in Figure 5.7 (light lines). In this case characterized by diagonal elements drawn from a non-zero amplitude interval $U_D = [a_1, a_2]$ such that $a_2 < b$, α is still 1 for $C = 1$ and raises suddenly from 0 when C approaches 1.

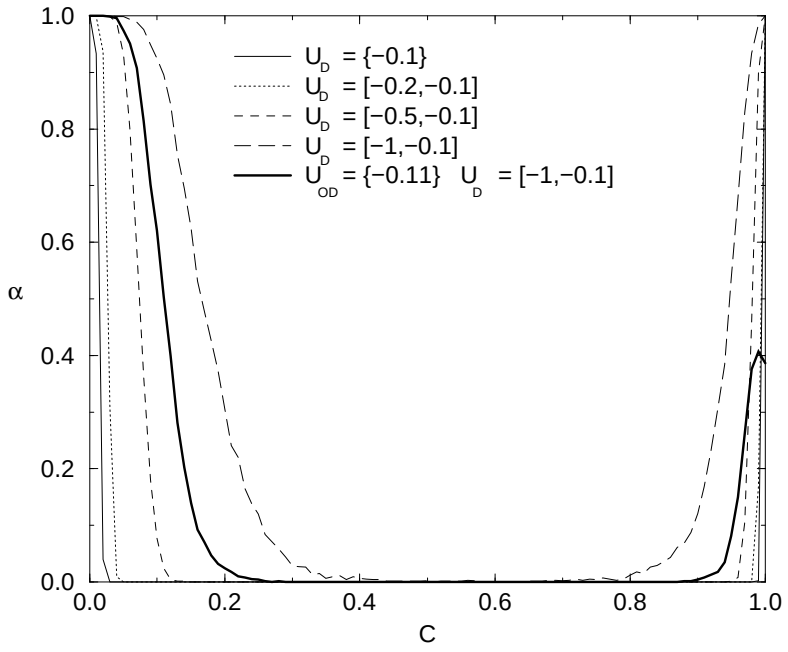

Figure 5.7: Probability of stability $\alpha(C)$ for $n = 100$. Light lines: $U_{OD} = \{-0.09\}$ and four diagonal intervals $U_D = [a_1, -0.1]$ with $a_1 = -0.1, -0.2, -0.5, -1$ (from solid to long dashed lines). Dark solid line: $U_{OD} = \{-0.11\}$ and $U_D = [-1, -0.1]$.

Moreover, extending the possible diagonal values to more negative numbers widens the range of C for which α is sensibly different from 0. Conversely, when $a_2 > b$ this result does not hold anymore, the probability of stability for $C = 1$ being about 0.98 for $b = -0.101$ (not shown) and only about 0.37 for $b = -0.11$ (Figure 5.7, dark curve). On these grounds, we will concentrate in the following on the case of intervals $U_D = [a_1, a_2]$ and $U_{OD} = [b_1, b_2]$ with $a_2 < b_1$, for which $\alpha(1)$ is likely to be maximal.

We investigate now the effect of widening the off-diagonal interval, by keeping the same diagonal elements equal to $a = -0.1$. We analyze here for simplicity the case $C = 1$. For $n = 100$, we take $U_{OD} = [-0.09, -0.09 + \beta]$ with $0 < \beta \leq 0.09$. The stability is rapidly lost when increasing β, such that already for $\beta = 0.02$ the fraction of stable matrices at C=1 is 0 (see Figure 5.8).

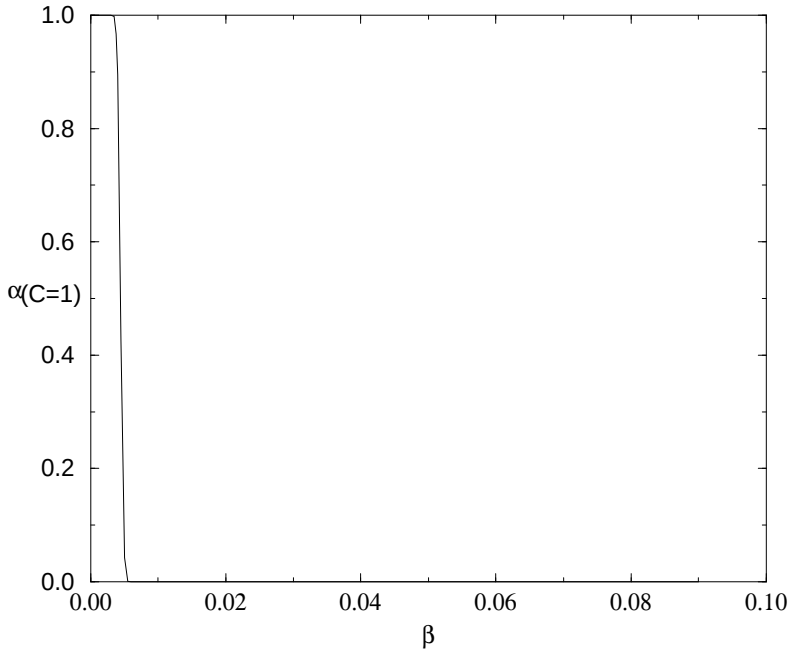

Figure 5.8: Diagonal elements all equal to $a = -0.1$, off-diagonal interval $U_{OD} = [-0.09, -0.09 + \beta]$, $n = 100$. Probability of stability α for $C = 1$ as a function of β.

5.3.2 The distribution of the largest eigenvalue for $C = 1$ and fixed diagonal terms

To shade some light on the previous behaviour, we study in the same cases (diagonal terms equal to $a = -0.1$, $U_{OD} = [-0.09, -0.09 + \beta]$ with $0 < \beta \leq 0.09$, $n = 100$) the distribution of the largest eigenvalue λ_{max}, which determines the stability and is equal to $\lambda_{max,0} = -0.01$ when $\beta = 0$. For a better statistics we use only for this experience a set of 10^5 matrices. A few histograms are plotted in Figure 5.9 for different values of β. The distribution of λ_{max} has a bell-shape with a higher tail on the right side, and its mean value $\bar{\lambda}_{max}$ is consistent with a law of the kind:

$$\bar{\lambda}_{max} - \lambda_{max,0} = \kappa\beta/2 \tag{5.9}$$

where κ is a proportionality factor depending on the matrix size n. This experimental law is plotted in Figure 5.10 (top). The coefficient κ respects an approximate scaling

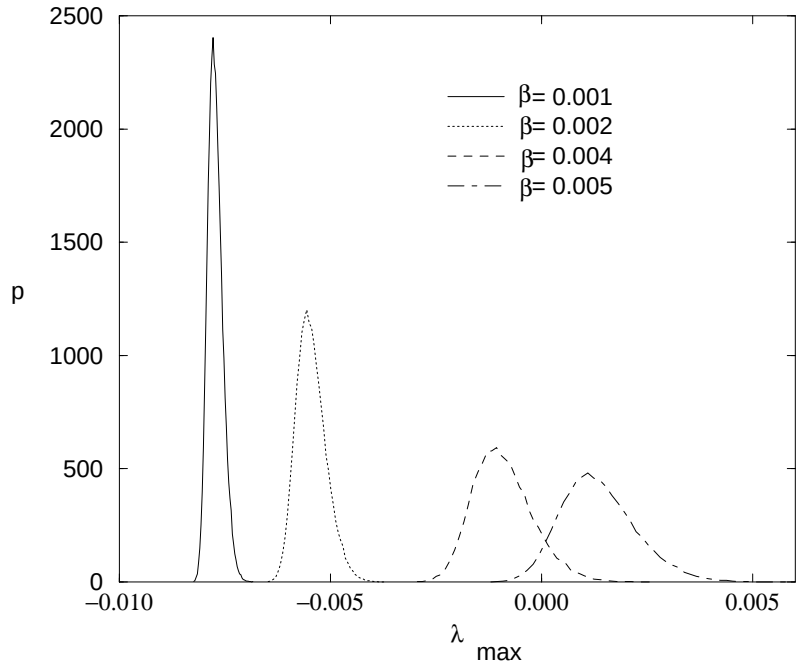

Figure 5.9: Diagonal elements all equal to $a = -0.1$, off-diagonal interval $U_{OD} = [-0.09, -0.09 + \beta]$, $n = 100$. Probability density $p(\lambda_{max})$ for the distribution of the real part of the largest eigenvalue for $\beta = 0.001, 0.002, 0.004, 0.005$.

$\kappa \propto \sqrt{n}$, as shown in Figure 5.10 (bottom) where $\bar{\lambda}_{max} - \lambda_{max,0}$ is plotted against $\sqrt{n}$ keeping β constant ($U_{OD} = [-0.09, -0.07]$).

Widening the off-diagonal interval corresponds then to destroy the stability for $C = 1$, making impossible a stability recover at high connectance. One can try to recover stability by taking lower values for the diagonal terms.

5.3.3 Stability properties when varying both the diagonal and the off-diagonal intervals

On the previous grounds we now go back to a diagonal interval $U_D = [-1, -0.1]$, considering the whole dependence on C. The probability of stability $\alpha(C)$ is plotted in Figure 5.11 for $U_{OD} = [-0.09, -0.09 + \beta]$ and $\beta = 0, 0.02, 0.04, 0.05, 0.07, 0.09$.

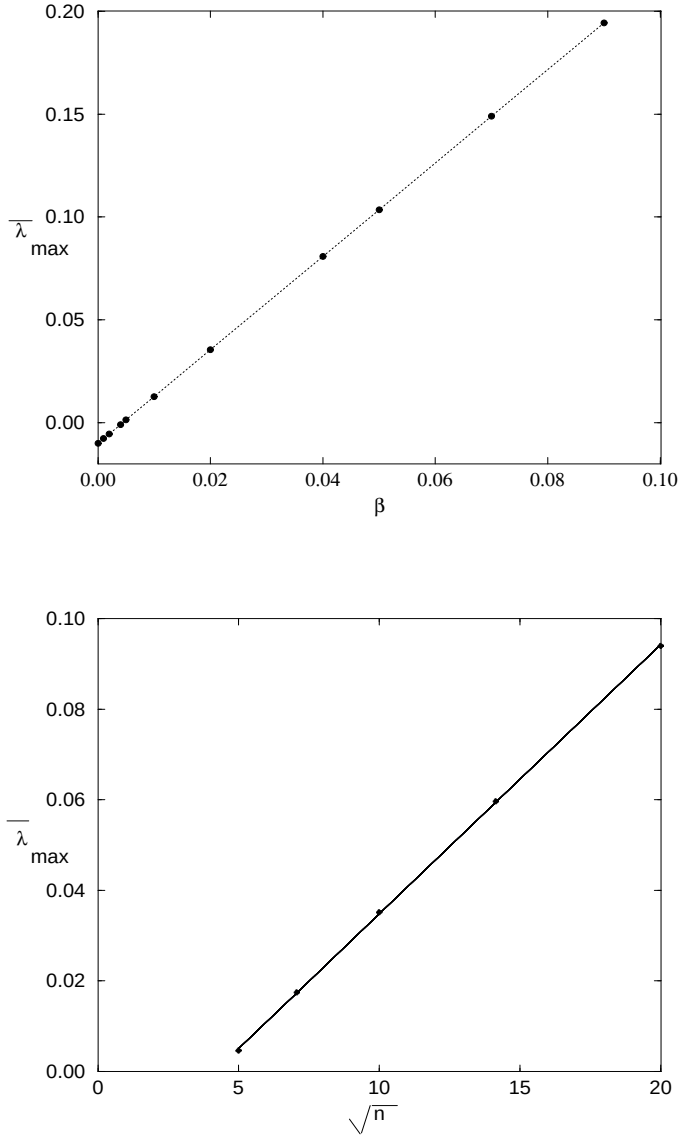

Figure 5.10: Diagonal elements all equal to $a = -0.1$, off-diagonal interval $U_{OD} = [-0.09, -0.09 + \beta]$. Top: for $n = 100$, values of $\bar{\lambda}_{max}$ as a function of β and corresponding linear fit. Bottom: values of $\bar{\lambda}_{max}$ as a function of $\sqrt{n}$ for $\beta = 0.02$ and corresponding linear fit.

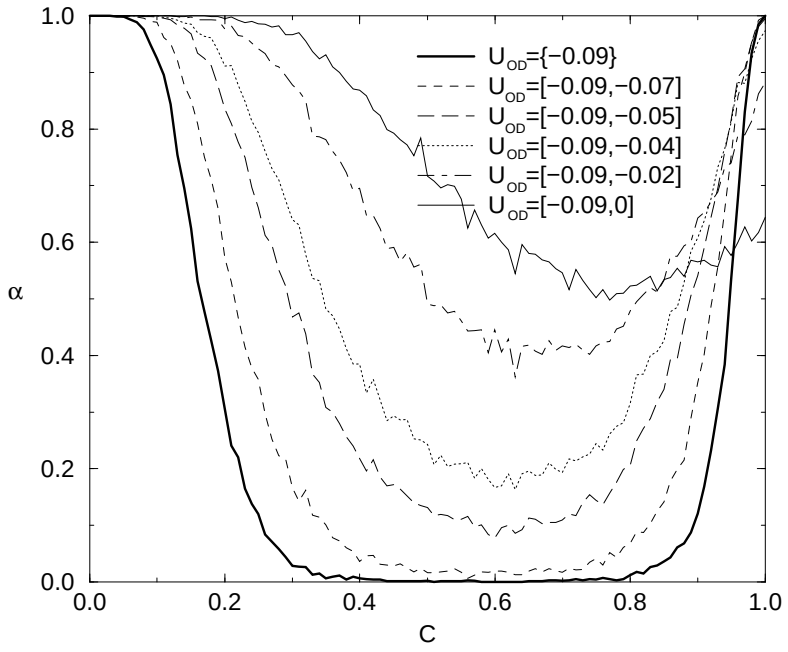

Figure 5.11: Probability of stability $\alpha(C)$ for $n = 100$, $U_D = [-1, -0.1]$ and six off-diagonal intervals $U_{OD} = [-0.09, -0.09 + \beta]$. From the dark solid line to the light solid line (bottom to top), $\beta = 0, 0.02, 0.04, 0.05, 0.07, 0.09$.

Taking a more negative diagonal a partial stability is recovered for $C = 1$, while the fast decreasing of α at low C persists. The net effect is a minimum of stability for intermediate values of C.

We conclude that even in non-trivial situations in which the diagonal and the off-diagonal coupling coefficients are distributed in a given interval, one can increase the probability of stability at high connectance by choosing *non-overlapping intervals* U_D, U_{OD}, such that U_D be wide enough and U_{OD} be narrow enough, both containing only negative terms.

We now proceed by refining this rule of thumb. To stress the importance of the non-superposition criterion between diagonal and off-diagonal intervals as a way to recover stability at high C, we perform two series of experiences with $U_{OD} = [-0.2, 0]$. We first take $U_D = [-1 - \delta_1, -0.1]$ varying δ_1 from 0 to 0.4 to widen the

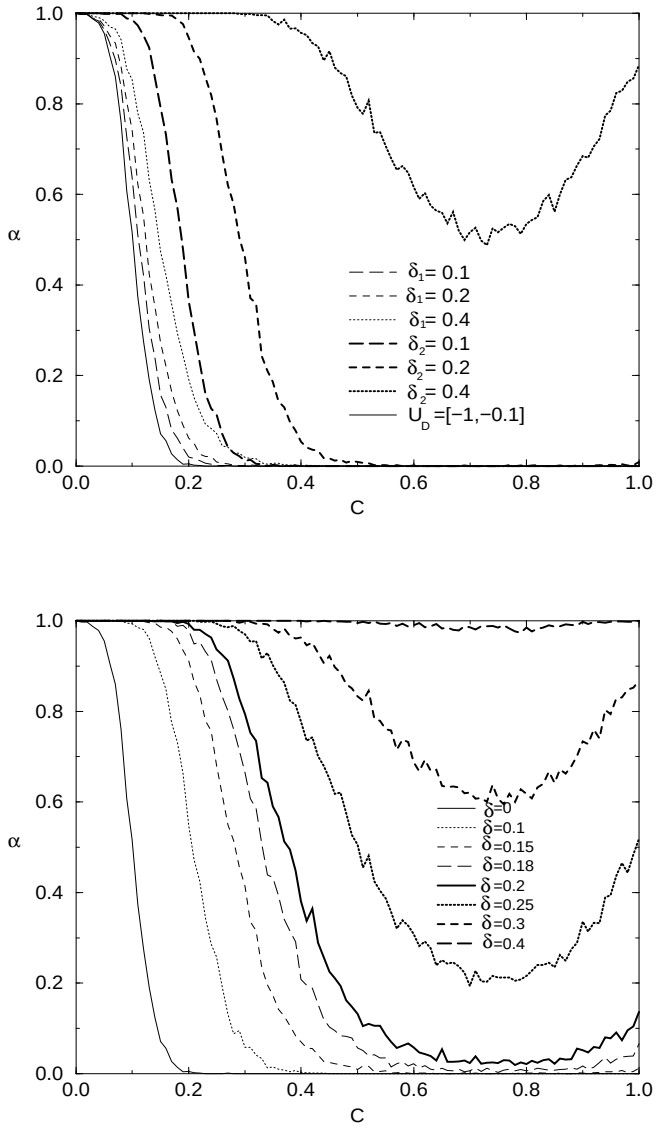

Figure 5.12: Probability of stability $\alpha(C)$ for $n = 100$ and off-diagonal interval $U_{OD} = [-0.2, 0]$. Top: $U_D = [-1, -0.1]$ (light solid line); $U_D = [-1 - \delta_1, -0.1]$ and $\delta_1 = 0.1, 0.2, 0.4$ (light respectively long-dashed, dashed and dotted lines); $U_D = [-1, -0.1 - \delta_2]$ and $\delta_2 = 0.1, 0.2, 0.4$ (dark respectively long-dashed, dashed and dotted lines). Bottom :$U_D = [-1-\delta, -0.1-\delta]$ and $\delta = 0, 0.1, 0.15, 0.18, 0.2, 0.25, 0.3, 0.4$ (from light solid to dark long-dashed lines).

diagonal interval but keeping a partial superposition with U_{OD}. We take next $U_D = [-1, -0.1 - \delta_2]$, thus making narrower the diagonal interval but progressively non-superposed with U_{OD}. The results are shown in Figure 5.12 (top) for $n = 100$. While increasing δ_1 alone has almost no effect on the probability of stability, increasing δ_2 alone allows a quick stability recover at large C.

On the other hand, it is necessary to precise that the non-superposition criterion is only necessary but evidently non sufficient to increase the stability at large C, being related in a complicated way to the size of the intervals themselves. This can be put in evidence by taking still $n = 100$, $U_{OD} = [-0.2, 0]$ and by simply shifting U_D towards the left as $U_D = [-1 - \delta, -0.1 - \delta]$ with $0 \leq \delta \leq 0.4$. For $\delta = 0.1$ the intervals do not superpose anymore, but the stability recover is not yet present, appearing for $\delta = 0.18$ and becoming more and more relevant when the separation between the intervals is increased (Figure 5.12 (bottom)).

When allowing some off-diagonal terms to be also positive, the increase of stability at large C is quickly lost, recovering the more trivial result of α monotonically decreasing with C. This can be seen in Figure (5.13), in which $\alpha(C)$ is plotted for $n = 100$, $U_D = [-1, -0.1]$ and $U_{OD} = [-0.09, b_2]$ with $b_2 = 0, 0.02, 0.045, 0.07, 0.09$, corresponding to a probability of having a fraction between 0% and 50% of non-competitive interactions. As conspicuous in Figure 5.13, already one tenth of positive off-diagonal terms is sufficient to destroy the stability recover at large C.

5.4 The influence of the matrix size

The problem can be made even more complicated by taking into account the influence of the matrix size n. As an example, we plot the stability curves $\alpha(C)$ for $U_D = [-1, -0.1]$ and varying both n and U_{OD}. We take $U_{OD} = [-0.09, 0]$ for $n = 50, 100, 200$ and $U_{OD} = [-0.05, 0]$ for $n = 200$. When $U_{OD} = [-0.09, 0]$ one can see that for an intermediate value of n ($n = 100$) the stability increases at large C, while if n is too large ($n = 200$) α decreases monotonically with C (Figure 5.14, light lines). Nevertheless, almost total stability everywhere can be recovered when the off-diagonal interval is reduced to $U_{OD} = [-0.05, 0]$ (Figure 5.14, dark line).

To investigate the dependence of stability on both n and the size of the off-diagonal interval, we calculate $\alpha(C)$ for $U_D = [-1, -0.1]$, taking different intervals $U_{OD} = [b_1, 0]$ ($b_1 < 0$) and different values of n but keeping constant the product $|b_1|\sqrt{n} = \sqrt{2/3}$. The values of the dimension are $n = 150, 200, 400, 600$. The stability curves plotted in Figure 5.15 do not superpose but are comparable, the stability slightly increasing when n is made larger.

We deduce that a situation of overall stability, for U_D and U_{OD} non-overlapping,

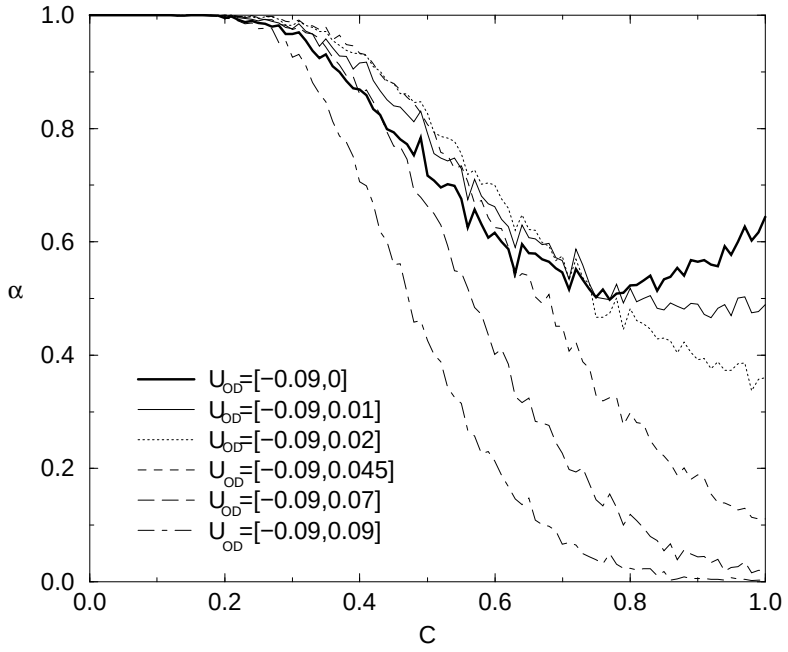

Figure 5.13: Probability of stability $\alpha(C)$ for $n = 100$, $U_D = [-1, -0.1]$ and six off-diagonal intervals $U_{OD} = [-0.09, b_2]$. From the dark solid line to the light dash-dotted line (top to bottom), $b_2 = 0, 0.01, 0.02, 0.045, 0.07, 0.09$.

can be maintained and even strengthened for larger and larger systems if the coupling coefficients are decreased as $1/\sqrt{n}$. This result contrasts with the case of positive off-diagonal terms, in which the stability curve $\alpha(C)$ does not vary when $|b_1|n$ is kept constant.

It is interesting to remark that for symmetric off-diagonal intervals $U_{OD} = [-b, b]$ (the diagonal elements being all equal) May [41] conjectured that the relevant parameter for stability was the product $b\sqrt{nC}$. In our case of non-symmetric intervals, we recover an approximate stability parameter $b\sqrt{n}$, but the connectance cannot enters in such a parameter with a monotonic function, which would prevent the stability recover phenomenon at large C to appear.

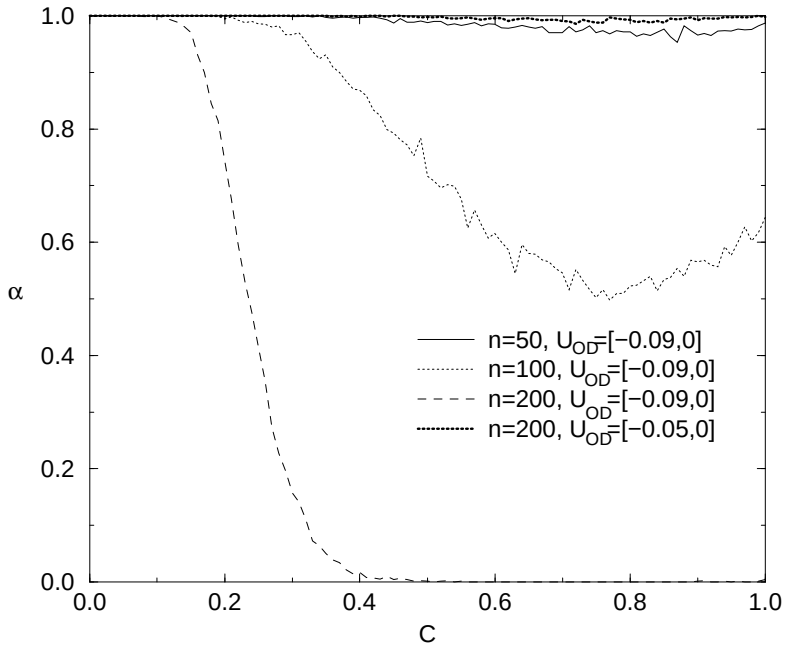

Figure 5.14: Probability of stability $\alpha(C)$ for $U_D = [-1, -0.1]$. Light lines: $U_{OD} = [-0.09, 0]$, $n = 50, 100, 200$ (respectively solid, dotted and dashed lines). Dark dash-dotted line: $U_{OD} = [-0.05, 0]$, $n = 200$.

5.5 Conclusions

The stability of a linear dynamical system is influenced both on the number of the degrees of freedom and on their mutual coupling (i.e. connectance), in a way which is far from being understood. In our work we investigated the relationship stability-versus-connectance by pointing out the role of the distribution of the diagonal and off-diagonal terms in the matrix defining the system.

We first discussed the applicability of the well-know sufficient condition of stability given by the quasi-diagonal dominance criterion, used in literature as a guide to build stable connected systems. This condition is shown to be far from optimal even when the system is only partially competitive (i.e. when some of the off-diagonal coefficients of the matrix M are negative).

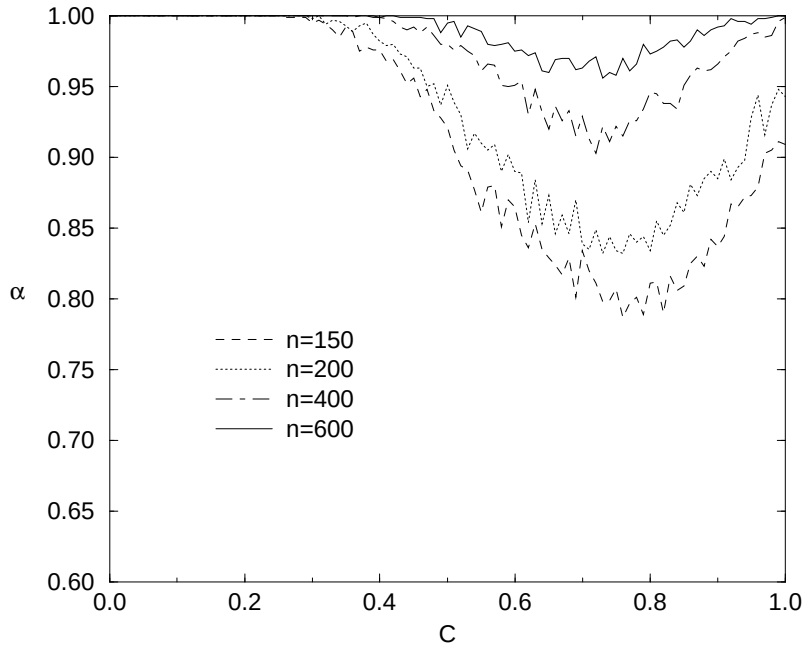

Figure 5.15: Probability of stability $\alpha(C)$ for $U_D = [-1, -0.1]$, $U_{OD} = [b_1, 0]$ and dimensions n such that $|b_1|\sqrt{n} = \sqrt{2/3}$. Dashed line: $n = 150$, $b_1 \approx 0.067$; dotted line: $n = 200$, $b_1 \approx 0.057$; dash-dotted line: $n = 400$, $b_1 \approx 0.041$; solid line: $n = 600$, $b_1 \approx 0.033$.

We then looked for different criteria of stability, by analysing in particular the possibility of restabilization at moderate or high connectance. We started our analysis with a specific fully connected system in which the matrix M is characterized by only two values (one for the diagonal terms and one for the off-diagonal ones), for which there exists an analytical necessary and sufficient condition of stability. For competitive systems, this condition is independent of the dimension of the matrix and less restrictive than the quasi-diagonal dominance theorem.

We then investigated numerically the effect of the connectance on stability in the more general case in which the elements of the matrix M are drawn from some intervals. We interpreted some results by studying the distribution of the largest eigenvalue of the matrix as a function of the overlapping among the intervals from

which diagonal and off-diagonal terms are drawn. We obtained this way a new operational criterion to increase the probability of stability at high connectance, which can be resumed this way: stability can be increased by choosing non-overlapping diagonal and off-diagonal intervals U_D, U_{OD}, such that U_D be wide enough and U_{OD} be narrow enough, both containing only negative terms.

Concerning the size of the system we showed that, for the competitive case, the stability rescales approximately with the square root of the dimension, in agreement with a conjecture concerning symmetric off-diagonal intervals [41].

Chapter 6

The nonlinear case

While in Chapter 5 we presented some results on the influence of the connectance on the linear stability of dynamical systems, we face here the problem of how the connectance affects the global nonlinear dynamics. We restrict to the problem of the stability of the actions in Hamiltonian systems, the theory of which has been resumed in Chapter 3. We analyse in particular how the emergency of chaos is related to the variation of the connectance in some nonlinear models. To this goal, we first discuss the general properties of Hamiltonian chaos and some methods used to detect it, concentrating on the notion of Lyapunov exponents and on some indicators giving an estimate of them. In the second part of this Chapter we apply these methods to two different many-dimensional nonlinear systems. We will see that the degree of connectance has a deep impact on the global chaoticity, even if every model has specific properties and the results are less generic than in the linear case. This results are resumed in a paper which is currently in preparation [37].

6.1 The detection of chaos

According to the classical results of the KAM and the Nekhoroshev theorems presented in Chapter 3, the structure of the phase space of a non-integrable dynamical system is characterized by orbits both lying on invariant tori and "chaotically" wandering among them. In this sense, one considers an orbit $(q(t), p(t))$ as *chaotic* when in a $2n$-dimensional phase space it does not exist a n-dimensional surface on which this orbit is contained. Two examples of chaotic trajectories are represented on Figure 6.1 for the standard map (3.29). In (a) for $\epsilon = 0.6$ we displayed a chaotic orbit generated around the hyperbolic point $(0, 0)$, the evolution of which is limited by the presence of many KAM tori, while in (b) for $\epsilon = 1.2$ a much more "wandering"

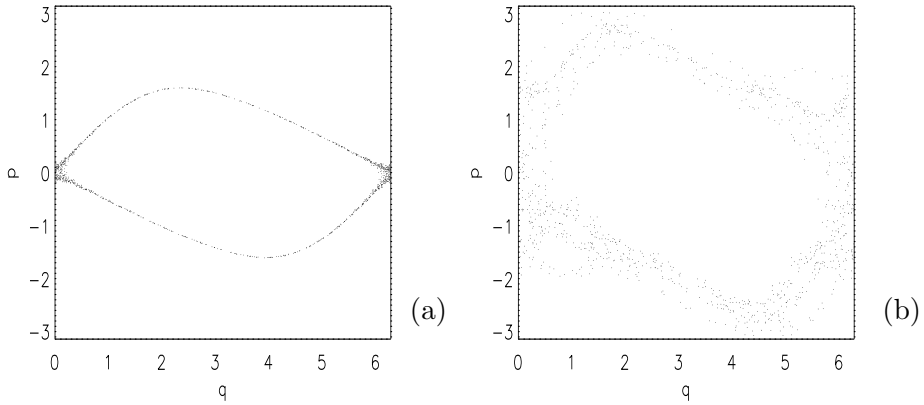

Figure 6.1: Chaotic orbits generated around the hyperbolic point $(0, 0)$ for the standard map. In (a) $\epsilon = 0.6$, while in (b) $\epsilon = 1.2$.

chaotic trajectory is shown. In both cases one has the visual impression that it does not exist a regular curve $p = p(q)$ over which these orbits can lie, even if this feeling is much more evident in the second case.

In fact, there exist many definitions of chaos, and the one we presented is just one among others. Moreover, it does not exist an operative procedure to establish whether a given orbit lies or not on a invariant surface. An iterative procedure has been developed by Milani and Knezevic [44], but its convergence is not guarantee.

A more operative criterion to decide whether an orbit is chaotic or not resides on the notion of exponential separation of close trajectories. One can say that an orbit is chaotic when, taking an infinitely close one, the two trajectories separate exponentially fast. This property, which is displayed by numerical simulations, derives from the hyperbolic character of the dynamics close to resonant regions. For more details, see for example [54]. On an invariant torus, on which the Hamiltonian is locally integrable, two nearby orbits separate instead at a linear rate.

The idea of exponential divergence between close orbits can be mathematically formalized with the notion of *Lyapunov characteristic exponents* (LCEs), the theory of which is resumed in the next Section. Positive Lyapunov exponents correspond to exponential separation. In compact manifolds the Lyapunov exponents always exist and can be iteratively calculated, so we can rely on them to give an operative definition of chaos. Moreover, an orbit which does not lie on an invariant surface has at least a positive Lyapunov exponent. The general theory of LCEs as well as the method to compute them was provided by Oseledec [48] in 1968.

6.1.1 Lyapunov exponents

Let us consider a compact Riemannian manifold W of dimension m, a probability measure μ on W and a measure–preserving flow Φ^t. $\Phi^t : W \to W$ is then a one parameter group of diffeomorphism with composition law $\Phi^{t+t'} = \Phi^t \circ \Phi^{t'}$ and $\mu(\Phi^{-t}(A)) = \mu(A)$ for any measurable set $A \subset W$. We consider a regular curve

$$\begin{aligned} y : W &\to W \\ s &\mapsto y(s) \end{aligned}$$

such that $y(0) = x$ and $y(s) = \tilde{x}$ for s fixed. If s is small one can consider x and $\tilde{x}$ as two near orbits and introduce the tangent vector to the curve y

$$\mathbf{w} = \frac{\partial y}{\partial s}|_{s=0} \in T_x W.$$

The Riemannian metric induces a distance on W that we indicate with $d(\cdot, \cdot)$. We calculate then the ratio among the initial distance between the two orbits and the distance after a time t on the action of the flow:

$$\Psi(x, y(s)) = d(\Phi^t(\tilde{x}), \Phi^t(x))/d(\tilde{x}, x),$$

where Ψ is a function $\Psi : W^m \times \mathbb{R}^2 \to \mathbb{R}$. Hence we have:

$$d(\tilde{x}, x) = s||\mathbf{w}|| + o(s),$$

$||\ ||$ being the norm on $T_x W$ induced by the metric on W. In the same way we have

$$d(\Phi^t(\tilde{x}), \Phi^t(x)) = s||D\Phi^t_x \mathbf{w}|| + o(s),$$

where $D\Phi^t_x$ is the linear tangent mapping which maps $T_x W$ into $T_{\Phi^t(x)} W$.

If the flow represents the family of the integral curves of a dynamical system in $\mathbb{R}^m$, i.e. $\dot{x} = F(x)$, the evolution of the tangent vector can be calculated by linearizing the equations of motion:

$$\frac{d\mathbf{w}}{dt} = \Big(\frac{\partial F}{\partial x}\Big)\mathbf{w}. \tag{6.1}$$

The limit of the distances ratio $\Psi(x, \tilde{x}, s, t)$ when $s \to 0$ is given by $\frac{||D\Phi^t_x \mathbf{w}||}{||\mathbf{w}||}$ and we define the Lyapunov characteristic exponent on the flow Φ^t_x relative to x and $\mathbf{w}$ as:

$$\lim_{t\to\infty} \frac{1}{t} \log \frac{||D\Phi^t_x \mathbf{w}||}{||\mathbf{w}||} = \chi(x, \mathbf{w}). \tag{6.2}$$

This quantity measures then the time ratio of the divergence between infinitely close orbits over an infinite time. It can be shown that the limit exists and is finite. Furthermore, there is a m-dimensional basis $\{\mathbf{e}_i\}$ of T_xW such that for any $\mathbf{w}$, $\chi(x, \mathbf{w})$ takes one of the m values $\chi(x, \mathbf{e}_i)$. These are independent of the choice of the metric and are called the Lyapunov characteristic exponents (LCEs) relative to x for the flow Ψ.

We say that two near orbits *diverge exponentially* if the largest LCE is positive, and that two near orbits *diverge linearly* if the largest LCE is zero.

In fact, for any choice of the vector $\mathbf{w}$, apart for a set of zero measure, $\chi(x, \mathbf{w})$ coincides with the largest LCE [48].

In the following we concentrate on the practical ways of measuring $\chi(x, \mathbf{w})$ (LCE hereafter), which, when positive, gives a measure of the "strength of the chaos" for a given orbit. Apart from very special cases (i.e. hyperbolic integrable orbits), the simple fact of having a positive value for χ is sufficient for characterizing an orbit as chaotic.

6.1.2 Numerical computation of the LCE

To calculate the LCE, in principle one has to integrate the equation of motion and of the tangent vector, for a sufficiently long time to be sure that the convergence in the limit (6.2) has been reached. Naive integration leads after a sufficiently long time to a computer overflow, as the norm of $\mathbf{w}$ increases exponentially with time. The difficulty is overcome making use of the linearity of the tangent map.

Taken an initial vector $\mathbf{w}$ of norm 1, one considers the time-advancing procedure at arbitrary times $j\tau$ ($i = 1, 2, \ldots$). Then, using the property of the composite map: $D\Phi_x^{t+t'} = D\Phi_{\Phi^t(x)}^{t'} \circ D\Phi_x^t$ we have:

$$||D\Phi^{n\tau}\mathbf{w}|| = ||D\Phi^{\tau} \ldots D\Phi^{\tau}\mathbf{w}||$$

Now, if at each step j we consider the amplification factor α_j of $\mathbf{w}$, we have

$$||D\Phi^{n\tau}\mathbf{w}|| = \alpha_1 \ldots \alpha_n ||\alpha_n^{-1} D\Phi^{\tau} \ldots \alpha_1^{-1} D\Phi^{\tau}\mathbf{w}|| \tag{6.3}$$

i.e. on the r.h.s. of equation (6.3) appear the renormalized vectors at each step. Because each renormalized vector has norm 1, one has simply $||D\Phi^{n\tau}\mathbf{w}|| = \alpha_1 \ldots \alpha_n$.

In practice, one renormalizes the evolved vectors at arbitrary times $j\tau$ and after n steps he has for the truncated value of χ at time $n\tau$

$$\tilde{\chi}(x, n, \mathbf{w}) \equiv \frac{1}{n\tau} \sum_{j=1}^{n} \log \alpha_j \tag{6.4}$$

where α_j is the renormalizing factor at time $j\tau$. For $n \to \infty$ this procedure converges to the LCE.

Actually the integration of the equation (6.2) is not really necessary if one wants to calculate only the largest Lyapunov exponent. As shown on Figure 6.2, let us consider two orbits starting at P_0 and P_0' and denote by $d(t)$ the distance between them at time t. After a time τ, let bring back the second orbit at the initial distance $d(0)$ from the first one and iterate the process n times, as displayed on Figure 6.2. It is demonstrated in [5] that the quantity

$$\gamma(P_0, d(0), \tau, n) \equiv \frac{1}{n\tau} \sum_{j=1}^{n} \log \frac{d(j\tau)}{d(0)} \tag{6.5}$$

converges to the LCE in P_0 as $n \to \infty$ and the distance $d(0)$ tend to 0.

In the case of a mapping in $\mathbb{R}^m$ defined by $M : \vec{X}_{n+1} = M(\vec{X}_n)$ the definition and the properties of the Lyapunov exponents are the same. We consider the application M, and the corresponding tangent mapping given by

$$\left\{ \begin{array}{lcl} \vec{X}_{n+1} & = & M\vec{X}_n \\ \vec{\mathbf{V}}_{n+1} & = & (\frac{\partial M}{\partial \vec{X}})_{\vec{X}_n} \vec{\mathbf{V}}_n \end{array} \right. \tag{6.6}$$

We iterate simultaneously these two mappings, taking as initial conditions a point $\vec{X}_0$ and a vector $\vec{\mathbf{V}}_0$ of norm 1. The vector is renormalized every h integration steps. According to equation (6.4) the LCE of an initial point $\vec{X}_0$ is given by

$$\chi(\vec{X}_0) = \lim_{n\to\infty} \frac{1}{nh} \sum_{j=1}^{n} \log \alpha_j = \lim_{n\to\infty} \frac{1}{n} \sum_{j=1}^{n/h} \log \alpha_j \tag{6.7}$$

where α_j is again the renormalization coefficient.

In practice, the computation is done on a finite number of iterations and we retain the truncated values of the LCE for a finite time. This value is called *Lyapunov Characteristic Indicator* (LCI) and we indicate it hereafter by $\tilde{\chi}(n)$, not mentioning the initial point x or the initial vector $\mathbf{w}$. For the case of a mapping, we have then for the LCI $\tilde{\chi}(n) = \frac{1}{nh} \sum_{j=1}^{n} \log \alpha_j$.

To investigate the convergence of the sum $\tilde{\chi}$ to its limit for $n \to \infty$, we study its behaviour as a function of the number of interactions for 3 different orbits in the case of the standard map, which is rewritten here for convenience:

$$\left\{ \begin{array}{lcll} p_{i+1} & = & p_i + \epsilon \sin(p_i + q_i) & (\mathrm{mod} 2\pi) \\ q_{i+1} & = & p_i + q_i & (\mathrm{mod} 2\pi) \end{array} \right. \tag{6.8}$$

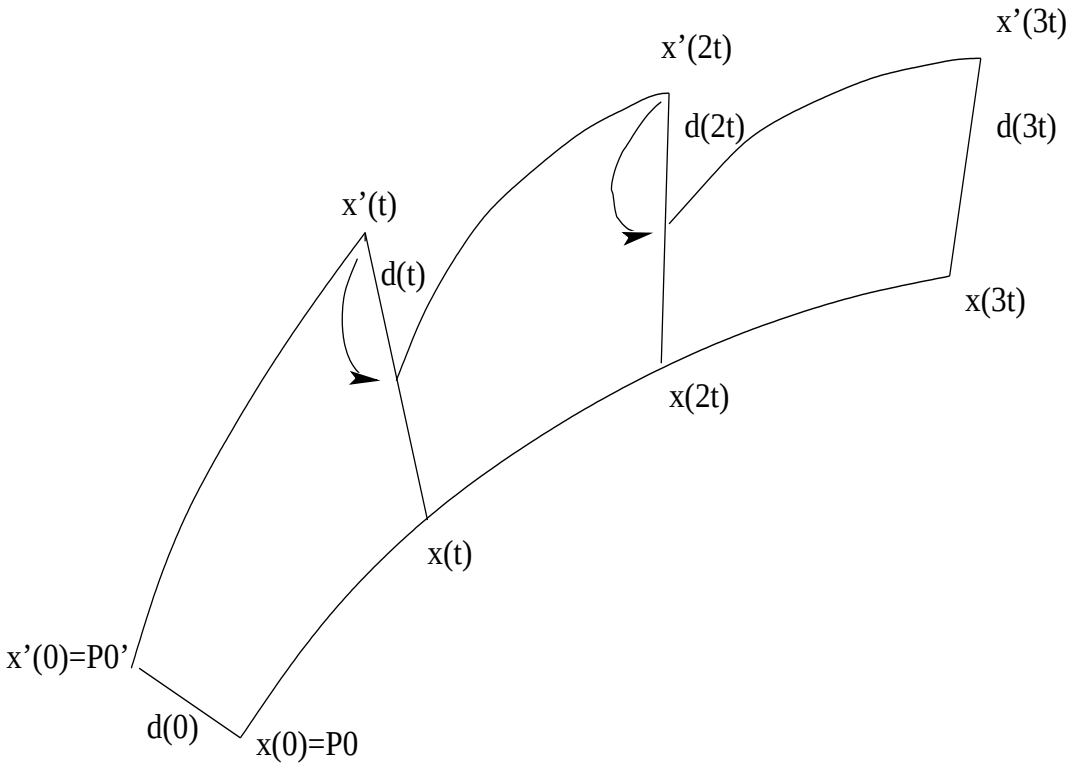

Figure 6.2: Renormalization procedure for the computation of the LCE using two close orbits. The second orbit is periodically brought back at the initial distance and re-integrated starting from its new location.

The orbits are calculated for $\epsilon = 0.6$ and are displayed on Figure 6.3. The corresponding time evolutions of the LCI are shown on Figure 6.4. We consider first an orbit lying on a torus, with initial condition $\vec{X_0} \equiv (q_0, p_0) = (0, 1)$, indicated as (a) on Figure 6.3. We note that the LCI tends to 0 in agreement with the fact that $\chi = 0$ for regular orbits (dotted line on Figure 6.4). Also in the case of $\vec{X_0} = (0.5, 0)$ the LCI goes to 0 (dashed line on Figure 6.4), but now the orbit is resonant, i.e. lies on an island (indicated as (b) on Figure 6.3). Moreover, in both cases $\tilde{\chi} \sim \log(n)/n$ in agreement with a linear rate of separation. The last initial condition $\vec{X_0} = (10^{-5}, 0)$ corresponds to a chaotic orbit (trajectory (c) on Figure 6.3). In this case the LCI is positive and converges to a constant value in agreement with the fact that for chaotic orbits the rate of separation is exponential and $\chi > 0$ (Figure 6.4, solid line).

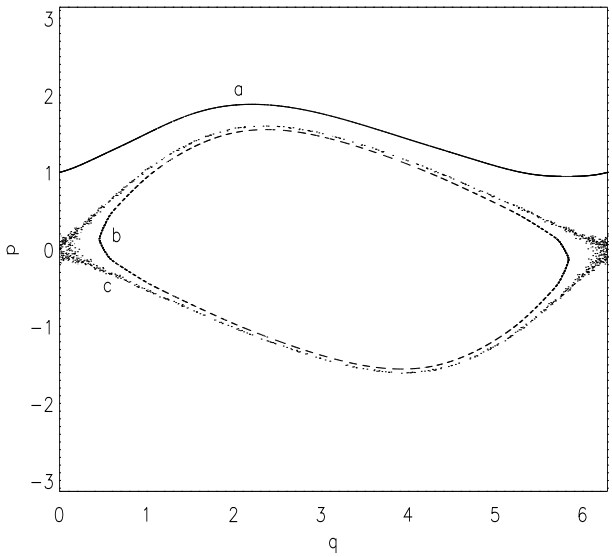

Figure 6.3: 3 different kinds of orbits of the standard map for $\epsilon = 0.6$. In (a) the initial condition is $\vec{X}_0 = (0, 1)$, in (b) $\vec{X}_0 = (0.5, 0)$, in (c) $\vec{X}_0 = (10^{-5}, 0)$.

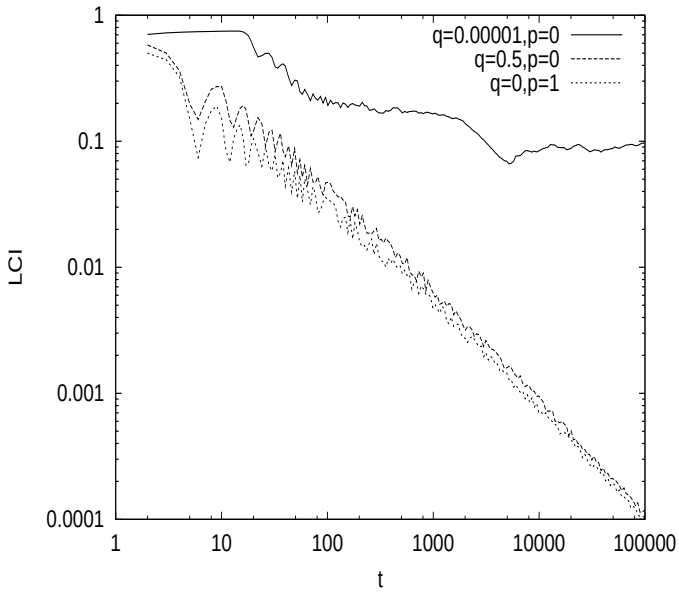

Figure 6.4: LCI for the three orbits displayed on Figure 6.3.

In this case it is not a problem to reveal the chaotic character of an orbit, since the LCI quickly stops to decrease and reaches a positive value. A similar case is called *strong chaos*.

A real difficulty to discriminate between a regular and a chaotic orbit arises for example for the two initial conditions $\vec{X}_0 = (0.2, 0)$ and $\vec{X}_0 = (10^{-10}, 0)$ when $\epsilon = 0.003$. The former orbit is regular and is shown on Figure 6.5. The latter looks very much to the former, as seen on Figure 6.6a, but it originates so close to the hyperbolic point $(0, 0)$ to have positive Lyapunov exponent even if ϵ is very small. In fact, its chaotic character is evident when zooming around the hyperbolic point, as seen on Figure 6.6b. The behaviour of the LCI is plotted on Figure 6.7, where we can see that 10^6 iterations are needed to reveal the chaotic character of the second orbit. In this case one talks of *weak chaos*. For weak chaotic orbits, it is clear that an arbitrary truncation of the computation can give misleading results. When the attention is focused on a single orbit, nothing prevents to integrate for a sufficiently long time to reach the convergence. The problem arises when we are interested in the analysis of a whole region of the phase space, for which it is practically impossible to integrate for too long times. Therefore, although the theory of LCI has a solid mathematical background, in order to overcome the computational difficulties which can arise in particular for the case of weak chaos, other indicators have been developed.

6.2 The case of weak chaos: some indicators

We summarize in this Section some indicators used for a fine identification of large sets of orbits, and we give some examples of their application on the two-dimensional standard map.

6.2.1 Frequency map analysis

Introduced by Laskar in 1988 [34] to understand the long-time evolution of the Solar System, this method was then successfully used in two-dimensional mappings to determine the critical value for which the last invariant torus disappears [35], as well as for the study of global dynamics and diffusion in multi-dimensional systems [36]. Moreover, it has been used by Celletti, Lega and Froeschlé to explore the structure around an invariant KAM torus [7],[38].

The basic idea of the frequency map analysis is to obtain directly, in a numerical manner, the quasi-periodic approximation of the solution of an n-dimensional quasi-integrable Hamiltonian system (and therefore the set of associated frequencies ω_i,

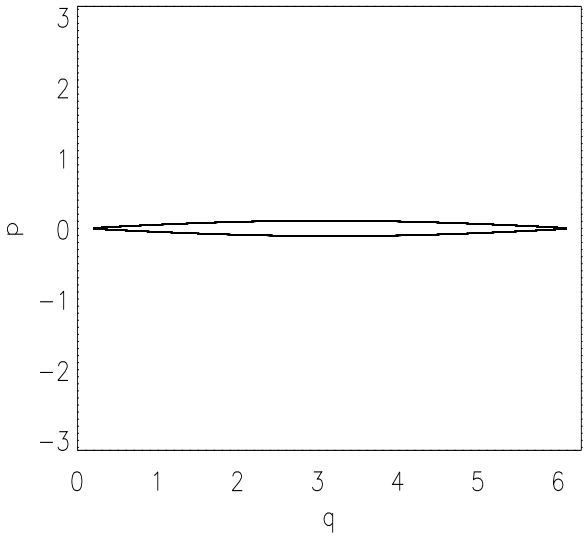

Figure 6.5: Regular orbit of the standard map for $\epsilon = 0.003$, with initial condition $\vec{X}_0 = (0.2, 0)$.

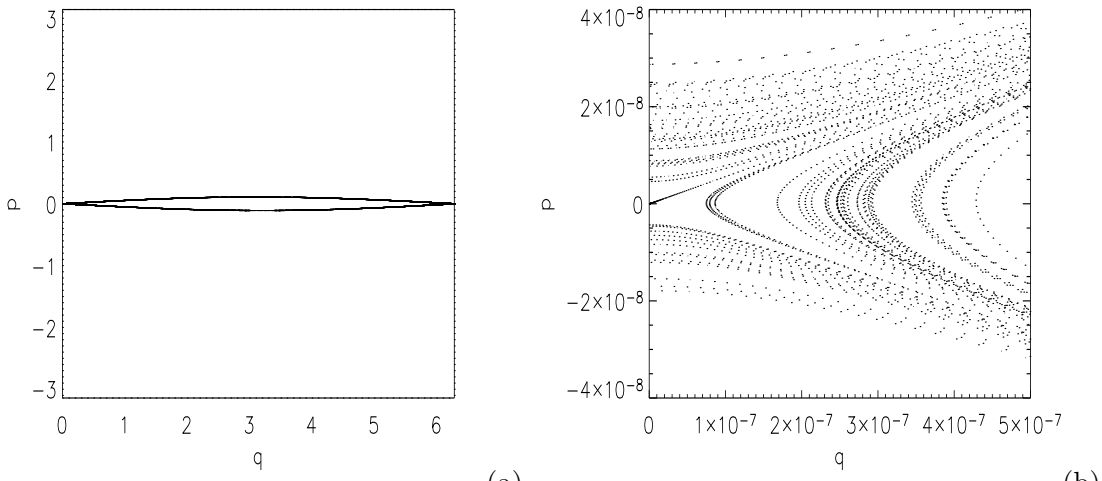

(a) (b)

Figure 6.6: (a): Weakly chaotic orbit of the standard map for $\epsilon = 0.003$, with initial condition $\vec{X}_0 = (10^{-10}, 0)$. (b): zoom around the hyperbolic point $(0, 0)$.

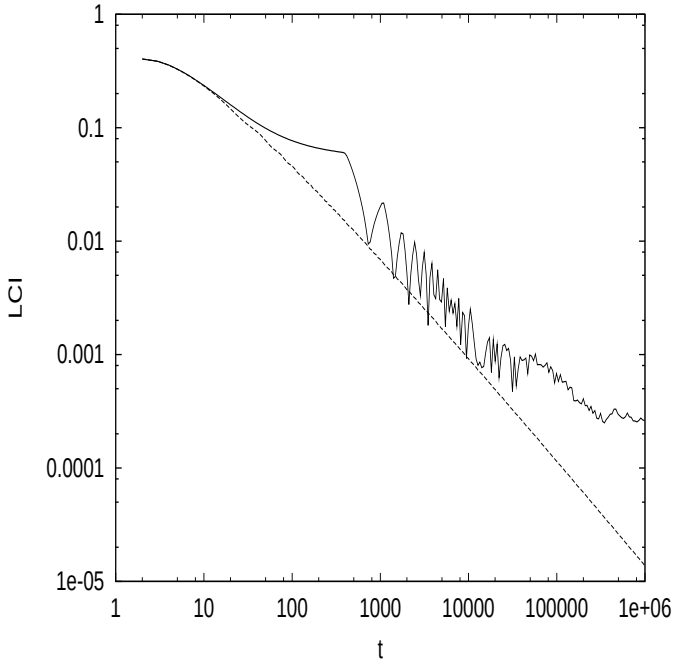

Figure 6.7: LCI for the two orbits displayed on Figure 6.5.

$i = 1, ..n$) without searching for an explicit change of coordinates to action-angle variables.

Different methods have been developed in order to compute the frequencies associated to the quasi-periodic motion [34],[35]. Let us suppose to have computed the quasi-periodic approximation for a given non-degenerated Hamiltonian system with n degrees of freedom. Following Laskar, the frequency map F is defined as the application which associates to a vector of initial action-like variables $p_j(0)$, $j = 1, .., n-1$, the frequency vector ω_j, $j = 1, .., n$ as follows:

$$F: \ (p(0)_1, p(0)_2, ...p(0)_{n-1}) \rightarrow (\frac{\omega_1}{\omega_n}, \frac{\omega_2}{\omega_n}, ..., \frac{\omega_{n-1}}{\omega_n}). \tag{6.9}$$

The angles are fixed to arbitrary values $q_j(0) = q_{j0}$ and the last action p_n is determined by the condition: $H(p, q) = \text{const}$.

One important remark is that, although frequencies are defined only on invariant tori, the frequency analysis algorithm computes numerically the frequency vector for any initial condition. On the KAM tori, this frequency vector will be a very accurate

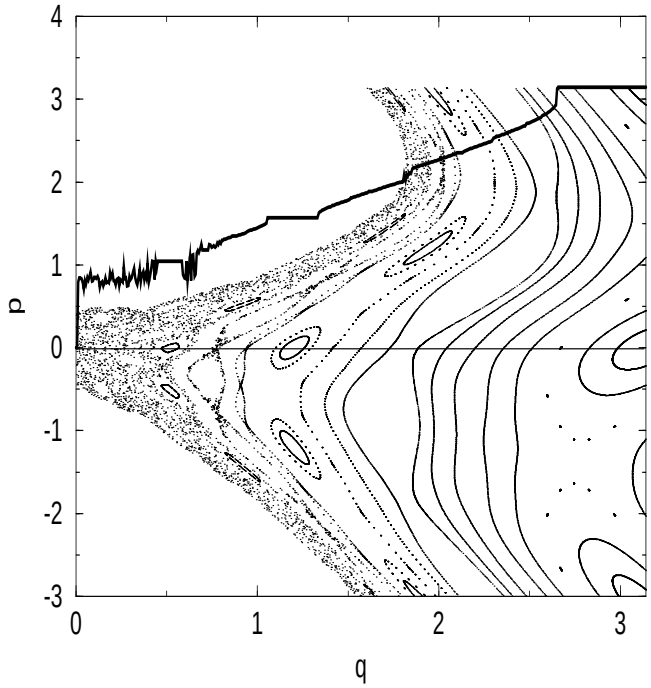

Figure 6.8: Standard map for $\epsilon = 0.8$. Orbits on the phase plane and value of the frequency map on the cross-section $p = 0$ (curtesy of Froeschlé and Lega [19]).

approximation of the actual frequencies, while in the weakly chaotic regions, it will provide a natural interpolation between these fixed frequencies.

As an example, we take the standard map and we consider a cross-section of the phase plane at $p = 0$. The frequency map associates to each orbit its corresponding frequency $\omega = \omega_1$ ($\omega_2 = 1$).

We can clearly see in Figure 6.8 that noisy variations of the frequency correspond to chaotic regions, while the set of rotational tori are revealed by a monotonic variation of ω and the crossing of islands is identified by a constant value of the frequency.

The algorithm for the calculation of the frequency map developed by Laskar relies in a sophisticated use of the Fourier transform. The details can be found in [35].

As far as two-dimensional mappings are concerned, an easier method of compu-

tation was developed by Hénon [27] and then used and extended by Celletti et al. in 1996. [8].

6.2.2 The Fast Lyapunov indicator (FLI)

When computing the LCI the attention is focused on the length of time necessary to get a reliable value of its limit, but very little importance has been given to the first part of the computation. Actually, this part was considered as a kind of transitory regime depending, among other factors, on the choice of an initial vector of the tangent manifold.

Already in 1997, Froeschlé et al. [18] remarked that the intermediate value of the LCI, taken at equal times for chaotic, even weakly chaotic, and ordered motion, allows to distinguish between them. In fact, we noticed that the LCI tends to 0 for regular orbits and to a non-zero constant for chaotic orbits, but in some cases one must wait for long times to discriminate clearly among the two regimes. If one takes instead the LCI multiplied by the time, he visually can separate more easily the two cases, but the presence of oscillations still makes difficult to distinguish the two regimes. If one now takes not only the LCI multiplied by the time, but its largest value over a given time interval, he can eliminate the time oscillations. From this observation, Froeschlé et al [39] defined a new indicator, called *fast Lyapunov indicator* (FLI), which consists in the largest value, over a time T, of the LCI multiplied by the time at which the LCI is calculated.

For a given mapping $M : \mathbb{R}^m \to \mathbb{R}^m$, along with its tangent map:

$$\begin{cases} \vec{x}_{i+1} &= M\vec{x}_i \\ \vec{v}_{i+1} &= \frac{\partial M}{\partial \vec{x}}(\vec{x}_i)\,\vec{v}_i\,. \end{cases} \tag{6.10}$$

the FLI after n iterations is defined, for an initial tangent vector of norm 1, as

$$\psi(\vec{x}_0, \vec{v}_0, n) = \sup_{0<i\leq n} \log ||\vec{v}_i||. \tag{6.11}$$

It turns out that the fact of multiplying the LCI by the time elapsed, and taking the largest value over this time, gives to this indicator a surprisingly good sensitivity. A main characteristic of the FLI is that it allows not only to distinguish among strong and weak chaos using shorter integration times, but also to distinguish between non-chaotic orbits of different origin, like resonant and non-resonant motion [26]. In both cases the LCI tends to zero when t goes to infinity, while the FLI grows linearly with time, but over a finite time it reaches a different value on a torus than on an island.

The linear growth of the FLI with time can be easily seen for the case of a torus in a continuous system. Take the quasi-integrable Hamiltonian

$$H = H_0(\mathbf{p}) + \epsilon H_1(\mathbf{p}, \mathbf{q}), \tag{6.12}$$

where $\mathbf{p}$ and $\mathbf{q}$ are canonically conjugate variables and ϵ is a small parameter. The equations (6.1) for the tangent vector $(\mathbf{V_p}, \mathbf{V_q})$ now read

$$\begin{cases} \dfrac{dV_{p_j}}{dt} &= -\epsilon \displaystyle\sum_{i=1}^{n} \frac{\partial^2 H_1}{\partial q_j \partial p_i} V_{p_i} - \epsilon \sum_{i=1}^{n} \frac{\partial^2 H_1}{\partial q_i \partial q_j} V_{q_i} \\ \dfrac{dV_{q_j}}{dt} &= \displaystyle\sum_{i=1}^{n} \frac{\partial^2 H_0}{\partial p_i \partial p_j} V_{p_i} + \epsilon \sum_{i=1}^{n} \frac{\partial^2 H_1}{\partial p_i \partial p_j} V_{p_i} + \epsilon \sum_{i=1}^{n} \frac{\partial^2 H_1}{\partial p_j \partial q_i} V_{q_i} \end{cases}$$

These are immediately integrated in the case $\epsilon = 0$: for any initial tangent vector $(\mathbf{V_p}(0), \mathbf{V_q}(0))$ the solution is

$$\begin{cases} \mathbf{V_p}(t) &= \mathbf{V_p}(0) \\ \mathbf{V_q}(t) &= \mathbf{V_q}(0) + \dfrac{\partial^2 H_0}{\partial^2 p}(\mathbf{p}(0), \mathbf{V_p}(0))t = \mathbf{V_q}(0) + \dfrac{\partial \omega}{\partial p}(\mathbf{p}(0), \mathbf{V_p}(0))t \end{cases} \tag{6.13}$$

In the integrable case, the norm of the tangent vector grows at most linearly with the time and $||\mathbf{V}(t)|| \sim \frac{\partial \omega}{\partial p} t$, so the FLI behaves like $\log |\partial \omega / \partial p| + \log t$. For most Hamiltonians (at most quadratic in $\mathbf{p}$) $\partial \omega / \partial p$ is constant over the phase space, so all the tori have the same value for the FLI.

If one considers the perturbation, he can demonstrate [26] that for tori

$$||\mathbf{V}(t)|| \sim \frac{\partial \omega}{\partial p} t + \mathcal{O}(\epsilon^{\alpha} t)$$

for some α. For resonant motion instead the norm of the tangent vector is still linear with time, but with a different coefficient, which turns out to be lower than for tori [26].

If one looks at the frequency map displayed on Figure 6.8, he can see that even in the perturbed case the detected frequency varies linearly with p on tori and is constant inside islands. $\frac{\partial \omega}{\partial p}$ is a non-zero constant on tori and zero inside islands. With this simple observation one can understand why at the lowest order, for which $||\mathbf{V}(t)|| \sim \frac{\partial \omega}{\partial p} t$, the growing factor of the tangent vector is lower on islands than on tori.

We now test the sensitivity of the FLI on the two-dimensional standard map (6.8).

Figure 6.9 shows the variation of the FLI with the time for three different kinds of orbits plotted on Figure 6.3. The upper curve, with initial conditions $(10^{-5}, 0)$ in a chaotic zone, shows an exponential variation of the FLI with time. The second curve corresponds to a regular invariant torus of initial conditions $(0.5, 0)$ and the lowest one to a resonant curve of initial conditions $(0, 1)$. We can observe a little difference between the regular and the resonant curve. The FLI grows linearly with $\log t$ for both kinds of regular orbits but with a different constant which turns out to be lower for resonant regular motion than for tori. Moreover, such a constant is the same for all tori, while changes smoothly for resonant regular orbits.

Figure 6.10 shows instead the variation of the FLI with the time for the two orbits plotted on Figure 6.5, for which the LCI has to be evaluated over a very long time to discriminate among the two orbits. The FLI instead allows to distinguish much more easily among a resonant orbit (lower curve, with initial conditions $(0.2, 0)$ and a weakly chaotic one (upper curve, with initial conditions $(10^{-10}, 0)$.

If we want to analyse many orbits, a good tool is the computation of the FLI-map, i.e. a mapping which associates to each initial condition the corresponding value of the FLI, for a fixed time T. On Figure 6.11 we have computed the FLI for a set of 1000 initial conditions of the standard map , regularly spaced on the q-axis in the interval $[0, \pi]$. For each orbit $p(0) = 0$, and $T = 1000$. Many orbits appear to have a value of FLI very close to $\log T = 3$. Actually, they all appear to be regular invariant tori. Values slightly greater than $\log T$ indicate either very thin chaotic layers or invariant tori close to very thin chaotic zones. The orbits having an FLI value lower than $\log T$ correspond to chains of islands.

6.2.3 The FLI charts: transition from the Nekhoroshev to the Chirikov regime

We saw that the Nekhoroshev theorem provides a "practical" result for the stability of Hamiltonian dynamical systems, and under a certain point of view it can be more useful that the KAM theorem. The Nekhoroshev theorem gives estimates of stability over an exponential long time provided that the perturbation is small enough. This result is valid for any trajectory: resonant, chaotic or non-resonant. Actually, the Nekhoroshev mechanism is associated with the existence of a large domain of the phase space filled by invariant tori. Of course, for conservative systems with two degrees of freedom, or for a two-dimensional area-preserving mapping, stability is ensured as far as the last torus remains, but this result is no more true when the dimension of the system increases and in this case we rely on the Nekhoroshev theorem for stability. The transition from the Nekhoroshev to the Chirikov regime is a smooth process involving the progressive superposition of resonances. The system

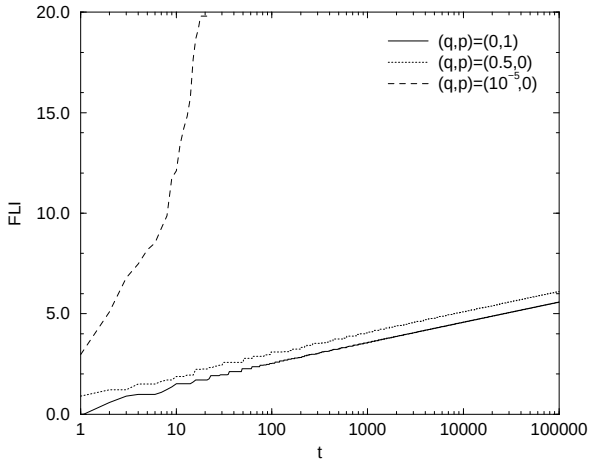

Figure 6.9: Variation of the FLI with time for three orbits of the standard map with $\epsilon = 0.6$. Upper curve: chaotic orbit with initial conditions $\vec{X_0} = (10^{-5}, 0)$. Middle curve: non-resonant orbit with $\vec{X_0} = (0.5, 0)$. Lowest curve: resonant orbit with $\vec{X_0} = (0, 1)$.

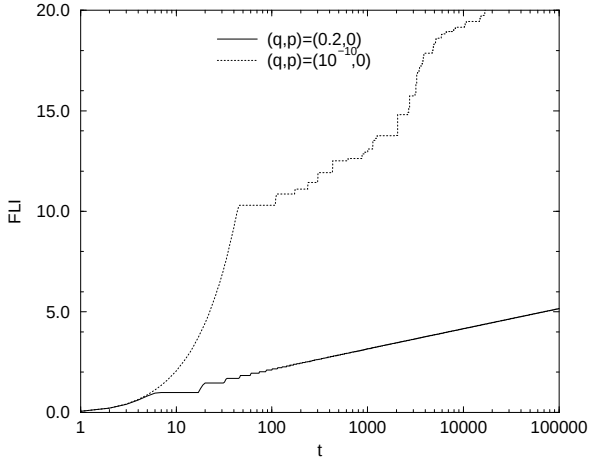

Figure 6.10: Variation of the FLI with time for two orbits of the standard map with $\epsilon = 0.003$. Upper curve: weakly chaotic orbit with initial conditions $\vec{X_0} = (10^{-10}, 0)$. Lowest curve: resonant orbit with $\vec{X_0} = (0.2, 0)$.

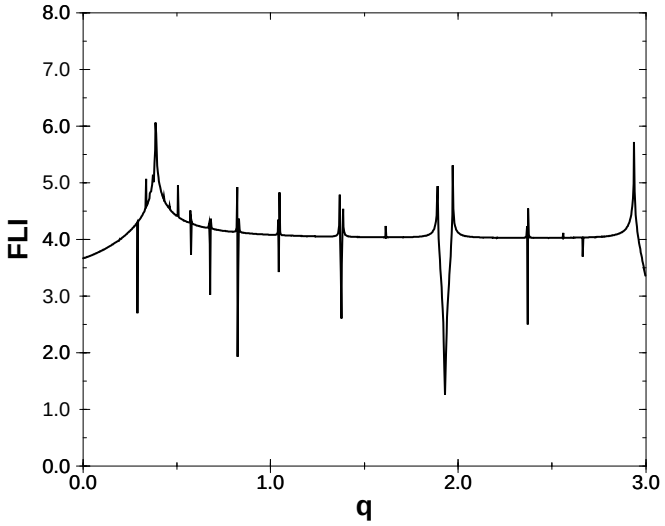

Figure 6.11: Value of the FLI at $T = 1000$ as a function of the initial angle on the line $p(0) = 0$ for the standard map with $\epsilon = 0.3$.

switches from a regime in which the diffusion of the actions among the regular region is slow, to a regime of fast diffusion in which the phase space is almost completely chaotic.

For systems with a low number of degrees of freedom, this transition can be represented and studied by means of FLI-charts. In the m-dimensional action space spanned by $(p_1, \ldots, p_n)$ one takes $m - 2$ actions constant and calculates the FLI on the plan mapped by the remaining two, let's say p_1 and p_2. This map $\psi(p_1, p_2)$ gives a very informative description of the action space, allowing to identify regular, resonant and chaotic zones and to see the transition among the mostly regular and the chaotic regimes.

We give here an example of this technique, applied to a four-dimensional symplectic mapping given by

$$\begin{cases} P_1 &= q_1 + \mu_1 \sin(p_1 + q_1) + \\ & \epsilon \sin(p_1 + q_1 + p_2 + q_2) + \\ & \epsilon \sin(p_1 + q_1 - p_2 - q_2) + \qquad (\mathrm{mod}\, 2\pi) \\ Q_1 &= p_1 + q_1 \\ P_2 &= q_2 + \mu_2 \sin(p_2 + q_2) + \\ & \epsilon \sin(p_1 + q_1 + p_2 + q_2) - \\ & \epsilon \sin(p_1 + q_1 - p_2 - q_2) + \qquad (\mathrm{mod}\, 2\pi) \\ Q_2 &= p_2 + q_2 \end{cases} \tag{6.14}$$

which is built with two coupled standard maps. We keep fixed the single-mappings perturbation parameters $\mu_1 = 0.4$ and $\mu_2 = 0.3$, and we progressively increase the chaoticity by increasing the coupling parameter ϵ. The FLI-charts on the plane (p_1, p_2) are displayed on Figure 6.12 for $\epsilon = 0.01, 0.02, 0.03, 0.05$, where $\log(\psi)$ after $n = 1000$ iterations is displayed with color codes. The FLI for regular orbits behaves like $\log(n)$, for resonant orbits it is smaller and for the chaotic ones it is much larger than this value, being exponential with n. The FLI range is restricted to $[2, 5]$. The value 5 is assigned to all the orbits for which the FLI is larger 5. The value $\log(1000) = 3$ indicates then tori, a smaller one resonant orbits, while all chaotic orbits correspond to values larger than 3, and mainly close to 5.

Panel (a) on Figure 6.12 represents a situation in which the action space is mainly filled by tori. When increasing ϵ, the chaotic zones become larger and larger at the crossing of resonant lines. Further resonant lines appear and the volume occupied by the tori shrinks to 0 (Figure 6.12d). The system is in the Nekoroshev regime when a web of resonances is embedded in a large volume of tori, and the transition to the Chirikov one happens when resonance crossings overlap. This evolution is evident from panel (b) to panel (d).

When the number of degrees of freedom is large, the FLI-charts give just a qualitative picture of the geometry in the action space, but they are not representative of the full complexity of the system. In this case one must discard the precise geometrical representation and can give just a statistical description, using histograms for the distribution of the FLI.

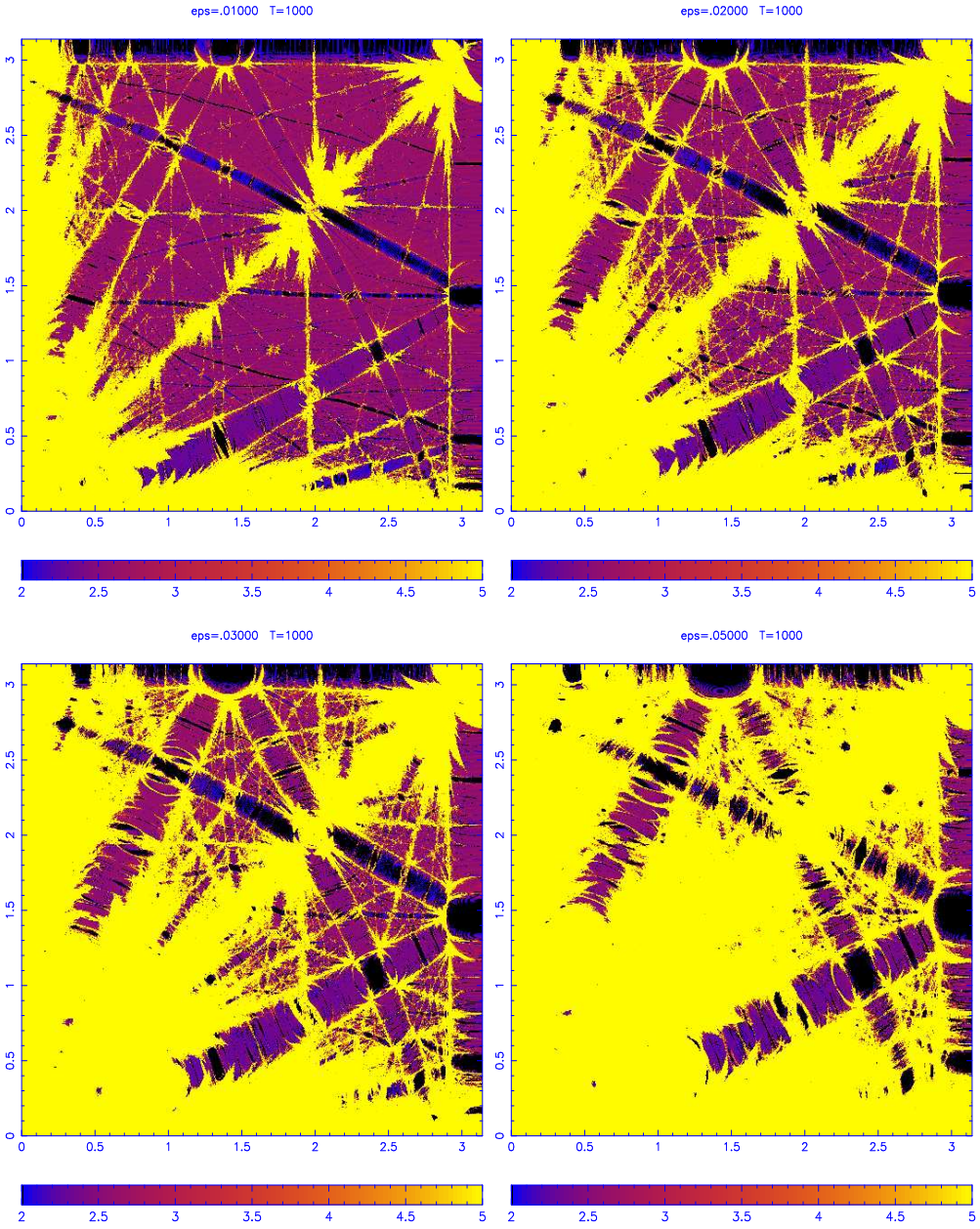

Figure 6.12: Graphical representation of the values of the FLI in the action plane (p_1, p_2) for the four-dimensional mapping (6.14) when $\mu_1 = 0.4$, $\mu_2 = 0.3$ and $n = 1000$ iterations. The values of ϵ are 0.01 (a), 0.02 (b), 0.03 (c), 0.05 (c).

6.3 Connectance and nonlinear dynamics

We want now to investigate the influence of the connectance on the stability of coupled nonlinear systems, using the tools discussed in the first part of this Chapter. As introduced in Chapter 4, the role of the connectance in some nonlinear models was investigated first by Froeschlé in 1978. His attempt has remained almost isolate until now. The original question can be resumed as follows: taken n dynamical systems, integrable or quasi-integrable, does (and how fast) the fraction of chaotic orbits increase with their degree of coupling? We analyse this issue on two different nonlinear systems, the first one deriving from the original Froeschlé model.

6.4 The Froeschlé model revisited

We consider here the model already used by Froeschlé in 1978, but with some differences. Starting with the Hamiltonian of the pendulum for the j^{th} degrees of freedom

$$H_j = \frac{p_j^2}{2} + \epsilon_j \cos q_j \tag{6.15}$$

one can introduce couplings among the angles and consider the n-degrees of freedom Hamiltonian

$$H = \sum_{j=1}^{n} \frac{p_j^2}{2} + \sum_{j=1}^{n} \epsilon_j \cos\Big(\sum_{k=1}^{n} \alpha_{jk} q_k\Big) \tag{6.16}$$

for which the equations of motion are

$$\begin{cases} \dfrac{\partial p_i}{\partial t} = \displaystyle\sum_{j=1}^{n} \epsilon_j \alpha_{ji} \sin\Big(\sum_{k=1}^{n} \alpha_{jk} q_k\Big) \\ \dfrac{\partial q_i}{\partial t} = p_i \end{cases} \tag{6.17}$$

We discretize in time with the leap-frog integrator. Taking a time step Δt, one approximates the equations (6.17) as follows:

$$\begin{cases} p_i^{t+\Delta t} = p_i^t + \Delta t \displaystyle\sum_{j=1}^{n} \epsilon_j \alpha_{ji} \sin\Big(\sum_{k=1}^{n} \alpha_{jk} q_k^{t+\Delta t}\Big) \\ q_i^{t+\Delta t} = q_i^t + \Delta t\, p_i^t \end{cases} \tag{6.18}$$

With the change of variables $\tilde{p}_i^t = \Delta t\, p_i^t$ and defining $\tilde{\epsilon} = \Delta t^2 \epsilon$ one obtains then, by

suppression of the tildes and using capital letters for the time-advanced variables:

$$\begin{cases} P_i = p_i + \sum_{j=1}^{n} \epsilon_j \alpha_{ji} \sin\Big[\sum_{k=1}^{n} \alpha_{jk}(q_k + p_k)\Big] \\ Q_i = q_i + p_i \end{cases} \tag{6.19}$$

This is a symplectic mapping which can be taken as a model to study the behaviour of a n-degrees of freedom interacting system. The interactions are switched on or off by setting to 0 or 1 the elements α_{ij}. When the matrix $A = [\alpha_{ij}]$ is diagonal, the mapping (6.19) reduces to n uncoupled standard maps, which are immediately integrated in the limit $\epsilon_j \to 0$. We recall that for $\epsilon \neq 0$ the uncoupled mappings are non-integrable, but the chaotic region is still small for ϵ as large as $1/4$ (see Section 3.2). The α_{ij} are taken symmetric. This model is the same as the one used by Froeschlé, apart for a further nonlinear self-coupling term which makes his model non-integrable already for $\epsilon = 0$. To switch on the couplings, Froeschlé took

$$\begin{cases} \alpha_{ij} = 1 & \text{for } j - i < N_c \\ \alpha_{ij} = 0 & \text{for } j - i \geq N_c \end{cases} \tag{6.20}$$

with $j \geq i$ and defined N_c as the connectance number.

In our work we progressively increase the couplings by filling the matrix A both in ordered and non-ordered way, and define the connectance as *the fraction of non-zero elements α_{ij} outside of the main diagonal*. This definition of connectance is exactly the same as in the linear case (Chapter 5). In the ordered case, we proceed as Froeschlé by progressively filling the upper and lower diagonals. For a given $N_c > 1$, the number of non-zero off-diagonal terms is given by $2\sum_{i=2}^{N_c}(n - i + 1)$, so the connectance C is related to N_c by

$$C = \frac{(N_c - 1)(2n - N_c)}{n(n-1)}.$$

In the non-ordered case, the position of the non-zero elements outside the main diagonal are taken at random, still enforcing the symmetry $\alpha_{ij} = \alpha_{ji}$.

Taking now a set of initial conditions, we iterate the mapping (6.19) for given values of C and ϵ_j. In particular, all the ϵ_j will be equal to the same value ϵ. For every orbit we detect whether it is chaotic or not by calculating its FLI (Section 6.1) and calculate the *probability of regularity* ρ, defined as the percentage of regular orbits (lying on both tori and island). In all numerical experiments, we take 500 initial conditions chosen at random and we iterate the mapping 10000 times.

6.4.1 Numerical experiments: the regularity recover

As a first experiment, we calculate the probability of regularity for the ordered connectance with $n = 10, 20, 30, 50, 100$ and $\epsilon = 10^{-3}$. To compare our definition of connectance to Froeschlé connectance number, we plot both ρ versus N_c (Figure 6.13) and ρ versus C (Figure 6.14). It is evident that when comparing systems with different number of degrees of freedom, it is better to measure the connectance with a quantity whose range is independent of n, then we discard N_c and keep using C.

The perturbation strength ϵ is chosen in such a way that for $C = 0$ the uncoupled mappings are almost completely integrable. When C increases, the measure of the phase space filled by chaotic orbits increases quickly, the faster the larger is n. A surprising fact is that if n is sufficiently small the probability of regularity reaches a minimum for a given C and then increases, reaching values close to 1 when the coupling matrix is completely full.

We fix now the dimension $n = 10$ and vary the perturbative parameter ϵ. The corresponding curves $\rho(C)$ are plotted on Figure 6.15 for 4 values of ϵ between 10^{-3} and 10^{-1}. Even in this case, ρ increases at high connectance for ϵ sufficiently small.

This phenomenon is analogous to the stability recover seen in the linear case (Chapter 5). To investigate it, we study the behaviour of the coupled mapping (6.19) for $C = 1$, i.e when $\alpha_{ij} = 1 \,\forall\, i, j$. In this case the mapping reads

$$\begin{cases} P_i = p_i + \sum_{j=1}^{n} \epsilon_j \sin\Big[\sum_{k=1}^{n}(q_k + p_k)\Big] \\ Q_i = q_i + p_i \ . \end{cases} \tag{6.21}$$

Introducing the summed variables

$$\begin{cases} z = \sum_{i=1}^{n} p_i \\ w = \sum_{i=1}^{n} q_i \end{cases} \tag{6.22}$$

the equations (6.21) become

$$\begin{cases} P_i = p_i + \sum_{j=1}^{n} [\epsilon_j \sin(z + w)] = p_i + \epsilon n \sin(z + w) \\ Q_i = q_i + p_i \end{cases} \tag{6.23}$$

where the last equality in the upper equation (6.23) holds only when $\epsilon_i = \epsilon \,\forall\, i$, which is the case we considered. Now, summing up over the index i one gets for the

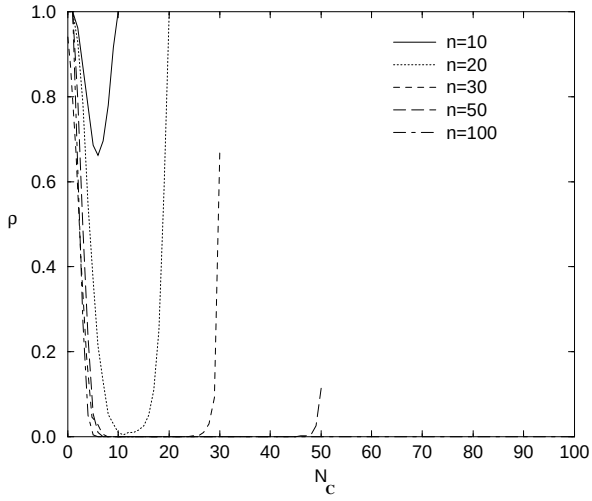

Figure 6.13: Probability of regularity ρ as a function of N_c for $n = 10, 20, 30, 50, 100$ and $\epsilon = 10^{-3}$ with ordered connectance.

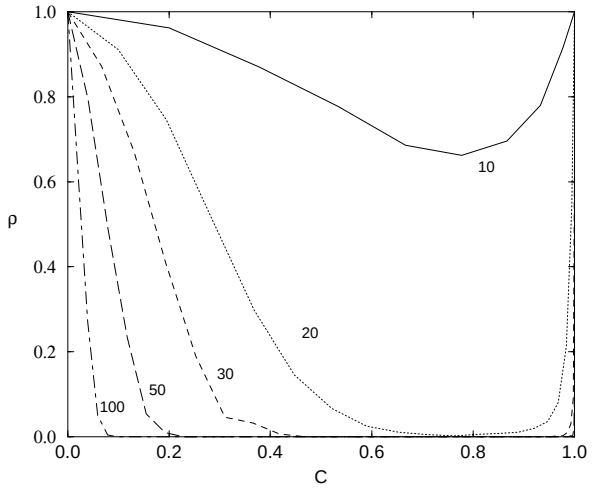

Figure 6.14: Probability of regularity ρ as a function of C for $n = 10, 20, 30, 50, 100$ and $\epsilon = 10^{-3}$ with ordered connectance.

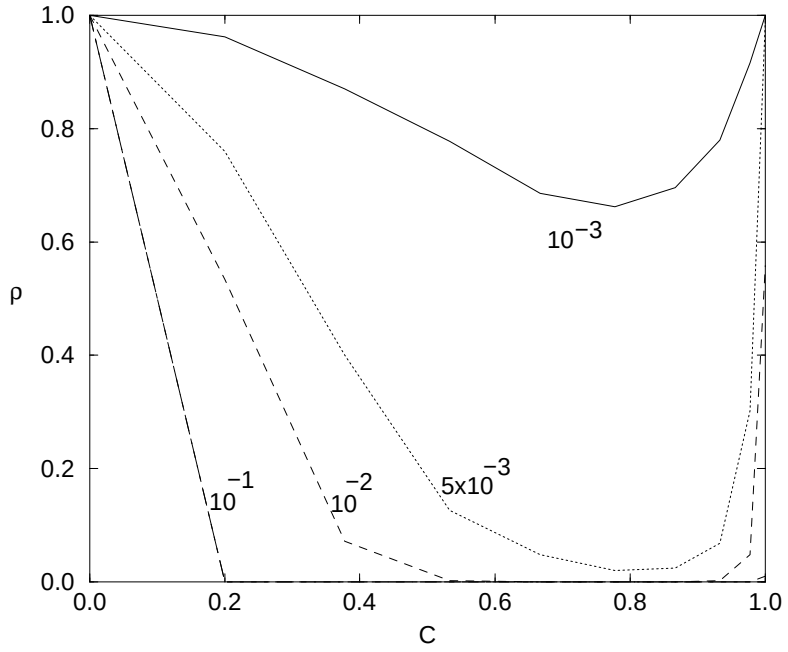

Figure 6.15: Probability of regularity ρ as a function of C for $n = 10$ and $\epsilon = 10^{-3}, 5 \cdot 10^{-3}, 10^{-2}, 10^{-1}$ with ordered connectance.

evolution of the summed variables

$$\begin{cases} Z = z + \epsilon n^2 \sin(z + w) \\ W = z + w \end{cases} \tag{6.24}$$

The dynamics of the i^{th} variable is then given by the four-dimensional mapping

$$\begin{cases} P_i = p_i + \epsilon n \sin(z + w) \\ Q_i = q_i + p_i \\ Z = z + \epsilon n^2 \sin(z + w) \\ W = z + w \end{cases} \tag{6.25}$$

so each couple (p_i, q_i) has the same dynamical evolution, slaved to the dynamics of the summed variables (z, w) and integrable once the evolution of z and w is known. Then the fully coupled system reduces in fact to a 4-dimensional mapping, of which

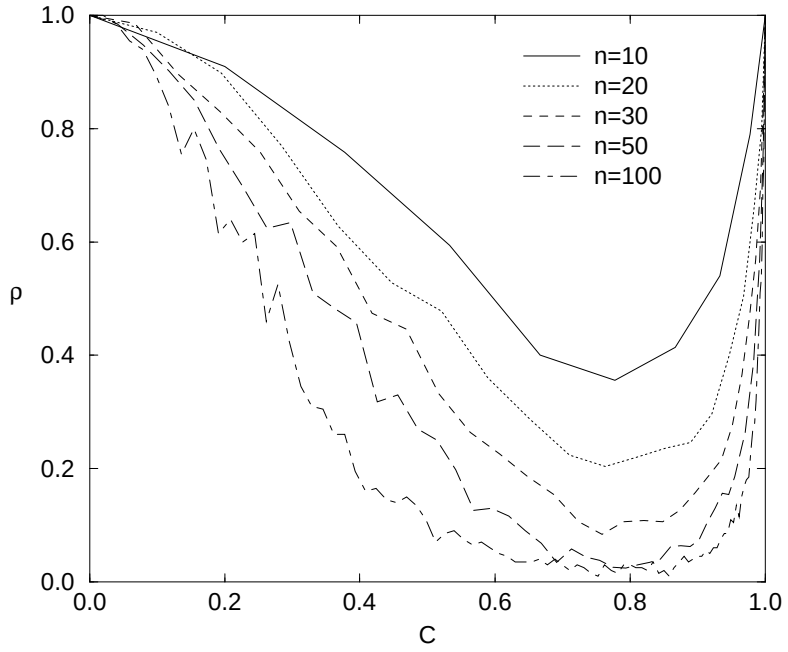

Figure 6.16: Probability of regularity ρ as a function of C for $\epsilon n^2 = 0.2 = \text{constant}$ and $n = 10, 20, 30, 50, 100$ with ordered connectance.

two equations are integrable. The parameter controlling the fraction of chaotic orbits is the one driving the non-integrable part of the system, i.e. ϵn^2. We display on Figure 6.16 the curves $\rho(C)$ obtained when both n and ϵ are varied by keeping the product ϵn^2 constant. We take $n = 10, 20, 30, 50, 100$ and $\epsilon n^2 = 0.2$. For this value of the perturbation parameter the system (z, w) is in fact almost integrable, then for $C = 1$ the probability ρ is practically equal to 1. ϵn^2 does not prescribe completely the dynamics when $C \neq 1$, but it is still a relevant control parameter.

We remark that the value of C for which the probability of regularity $\rho(C)$ is minimal is approximately the same when n is varied, and it is independent of ϵ, when sufficiently small. To put in evidence this property we recalculate $\rho(C)$ for $\epsilon = 10^{-4}$, a value for which a minimum can be individuated even for n quite large ($n = 50$ in this case). The corresponding curves for $n = 10, 20, 30, 50$ are displayed on Figure 6.17.

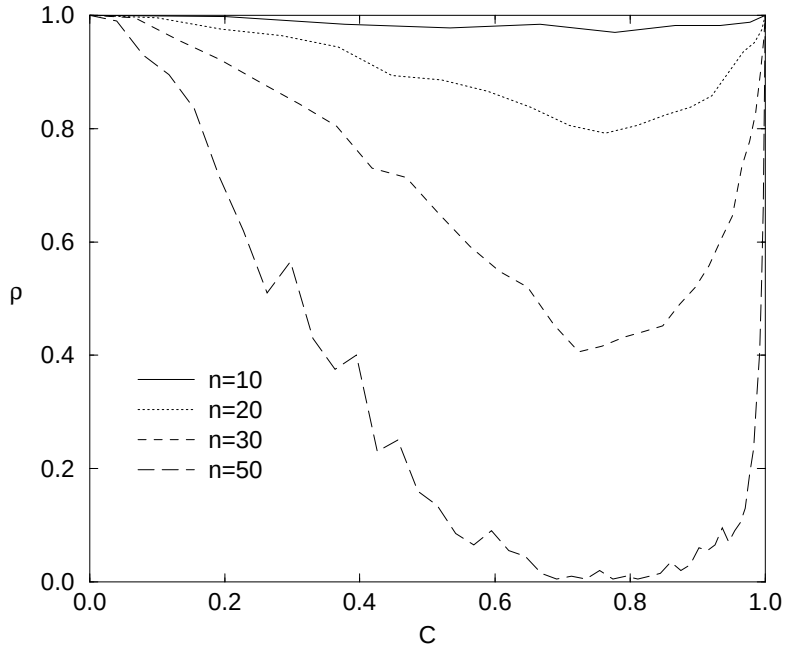

Figure 6.17: Probability of regularity ρ as a function of C for $\epsilon = 10^{-4}$ and $n = 10, 20, 30, 50$ with ordered connectance. The position of the minimum is almost constant.

6.4.2 Connectance and number of direct couplings. Reduction of the number of degrees of freedom

To comment the previous results, we must point out some special features of the model. First of all, the connectance previously defined does not correspond to the *fraction of direct couplings in the equations of motion*, as it was in the linear case. This can be seen by examining the equations for the momenta, which contain the coupling terms:

$$P_i = p_i + \sum_{j=1}^{n} \epsilon_j \alpha_{ji} \sin\Big[\sum_{k=1}^{n} \alpha_{jk}(q_k + p_k)\Big]. \tag{6.26}$$

It is evident that the i^{th} variable is coupled with some others if $\alpha_{ji} \neq 0$ for some j. In this case it is coupled with all the variables k for which $\alpha_{jk} \neq 0$. To list

immediately all the variables coupled with the i^{th} one, the following procedure can be used: take the matrix $A = [\alpha_{ij}]$ (which is symmetric) and in the line i look for all the columns j such that $\alpha_{ij} \neq 0$. In any such column j, look then for all $\alpha_{kj} \neq 0$. Then the variable i is coupled with all these variables k. We point out that this method is valid both for ordered and non-ordered connectance, because it concerns the structure of the equations and not the way of filling the matrix A. Take for example the following matrix (6.27), in which we indicated only the non-zero α_{ij} (they are of course present on the main diagonal). We can see that the variable i is coupled with the variables 1(from column 1), 2, 4, $n-1$ (from column 2), 2, 3, 4, $n-2$ (from column 4), 1, 2, 4, $n-1$, n (from column i), 2, $n-1$ (from column $n-1$), and n (from column n).

$$A = \begin{pmatrix} \alpha_{11} & 0 & 0 & 0 & 0 & \alpha_{1i} & 0 & 0 & \alpha_{2,n-1} & 0 \\ 0 & \alpha_{22} & 0 & \alpha_{24} & 0 & \alpha_{2i} & 0 & 0 & 0 & 0 \\ 0 & 0 & \alpha_{33} & \alpha_{34} & 0 & 0 & 0 & 0 & 0 & 0 \\ 0 & \alpha_{42} & \alpha_{43} & \alpha_{44} & 0 & \alpha_{4i} & 0 & \alpha_{4,n-2} & 0 & 0 \\ 0 & 0 & 0 & 0 & \alpha_{55} & 0 & 0 & 0 & 0 & 0 \\ \boxed{\alpha_{i1}} & \boxed{\alpha_{i2}} & 0 & \boxed{\alpha_{i4}} & 0 & \boxed{\alpha_{ii}} & 0 & 0 & \boxed{\alpha_{i,n-1}} & \boxed{\alpha_{in}} \\ 0 & 0 & 0 & 0 & 0 & 0 & \alpha_{n-3,n-3} & 0 & 0 & 0 \\ 0 & 0 & 0 & \alpha_{n-2,4} & 0 & 0 & 0 & \alpha_{n-2,n-2} & 0 & 0 \\ 0 & \alpha_{n-1,2} & 0 & 0 & 0 & \alpha_{n-1,i} & 0 & 0 & \alpha_{n-1,n-1} & 0 \\ 0 & 0 & 0 & 0 & 0 & \alpha_{ni} & 0 & 0 & 0 & \alpha_{nn} \end{pmatrix} \tag{6.27}$$

It is clear that multiple couplings can exist, i.e. in the equation for the variable i the same variable k can appear many times. The fraction of direct couplings in the equations of motion (indicated hereafter as C_d) can then be counted once the matrix A is assigned. It is given by the number of direct couplings (multiple couplings being counted once) divided by the number of off-diagonal matrix element $n(n-1)$, which is equal in turn to the number of "connected" couples of variables in the equations divided by the number of total couples, i.e. $n(n-1)/2$.

When filling the matrix the ordered way, already Froeschlé pointed out that the system becomes fully coupled (i.e in the equation for every variable i all the others appear) when N_c equals a critical value $N_c^{\text{crit}} = \frac{1}{2}(n+2)$ if n is even and $N_c^{\text{crit}} = \frac{1}{2}(n+1)$ if n is odd. This corresponds to a value of C given by

$$C^{\text{crit}} = \frac{3n-2}{4(n-1)} = \frac{3}{4}\left(1 + \frac{1}{3n} + \mathcal{O}\Big(\frac{1}{n^2}\Big)\right)$$

for n even and

$$C^{\text{crit}} = \frac{3n-1}{4n} = \frac{3}{4}\left(1 - \frac{1}{n}\right)$$

for n odd. For this way of filling and for $N_c \leq N_c^{\text{crit}}$, C_d is in fact related to N_c by the relationship

$$C_d = 2(N_c - 1)(2n - 2N_c + 1). \tag{6.28}$$

For $n = 6$, the critical configuration is the following one:

$$A = \begin{pmatrix} 1 & 1 & 1 & 1 & 0 & 0 \\ 1 & 1 & 1 & 1 & 1 & 0 \\ 1 & 1 & 1 & 1 & 1 & 1 \\ 1 & 1 & 1 & 1 & 1 & 1 \\ 0 & 1 & 1 & 1 & 1 & 1 \\ 0 & 0 & 1 & 1 & 1 & 1 \end{pmatrix}$$

In fact, a sufficient condition to have full coupling is that every line intersects a completely full column. For symmetric ordered matrices, this is also a necessary request. In this case the critical configuration is the one with minimal connectance which presents full coupling.

On the basis of these results, we can see that the position of the minimum for $\rho(C)$ corresponds to the connectance C^{crit} for which one has full coupling (see again Figure 6.17). C^{crit} is weakly dependent on n for the values we take, varying between 0.76 and 0.78 for n between 10 and 50.

The existence of a minimum corresponding to full coupling can be explained by noticing that when the connectance is further increased, the effective number of degrees of freedom of the system decreases. This can be demonstrated as follows. Consider again the equation for the i^{th} momentum:

$$P_i = p_i + \sum_{j=1}^{n} \epsilon_j \alpha_{ji} \sin\Big[\sum_{k=1}^{n} \alpha_{jk}(q_k + p_k)\Big]. \tag{6.29}$$

When the matrix has m upper and lower diagonals filled, i.e. $N_c = m$ ($m = 1$ being the main diagonal), in the coupling terms $\Big(\alpha_{jk}(q_k + p_k)\Big)$ the α_{jk} are equal to:

$$
\begin{aligned}
&\alpha_{1,k} = 1 \text{ for } k = 1 \dots m\,,\ 0 \text{ otherwise}\\
&\alpha_{2,k} = 1 \text{ for } k = 1 \dots m+1\,,\ 0 \text{ otherwise}\\
&\alpha_{3,k} = 1 \text{ for } k = 1 \dots m+2\,,\ 0 \text{ otherwise}\\
&\dots\\
&\alpha_{n-m,k} = 1 \text{ for } k = 1 \dots n-1\,,\ 0 \text{ otherwise}\\
&\alpha_{n-m+1,k} = 1 \text{ for } k = 1 \dots n\,,\ 0 \text{ otherwise}\\
&\alpha_{n-m+2,k} = 1 \text{ for } k = 1 \dots n\,,\ 0 \text{ otherwise}\\
&\dots\\
&\alpha_{m-1,k} = 1 \text{ for } k = 1 \dots n\,,\ 0 \text{ otherwise}\\
&\alpha_{m,k} = 1 \text{ for } k = 1 \dots n\,,\ 0 \text{ otherwise}\\
&\alpha_{m+1,k} = 1 \text{ for } k = 2 \dots n\,,\ 0 \text{ otherwise}\\
&\alpha_{m+2,k} = 1 \text{ for } k = 3 \dots n\,,\ 0 \text{ otherwise}\\
&\dots\\
&\alpha_{n,k} = 1 \text{ for } k = n-m+1 \dots n\,,\ 0 \text{ otherwise.}
\end{aligned}
$$

In the combinations $\sum_{k=1}^{n} \alpha_{jk}(q_k + p_k) = \sum_{k=1}^{n} \alpha_{jk} q_k + \sum_{k=1}^{n} \alpha_{jk} p_k$ one can then define the summed variables:

$$
\begin{aligned}
&z_1^m = \textstyle\sum_{k=1}^{m} p_k \quad \text{using the } \alpha_{1,k}\\
&z_1^{m+1} = \textstyle\sum_{k=1}^{m+1} p_k \quad \text{using the } \alpha_{2,k}\\
&z_1^{m+2} = \textstyle\sum_{k=1}^{m+2} p_k \quad \text{using the } \alpha_{3,k}\\
&\dots\\
&z_1^{n-1} = \textstyle\sum_{k=1}^{n-1} p_k \quad \text{using the } \alpha_{n-m,k}\\
&z_1^{n} = \textstyle\sum_{k=1}^{n} p_k \quad \text{using the } \alpha_{n-m+1,k}\\
&z_1^{n} = \textstyle\sum_{k=1}^{n} p_k \quad \text{using the } \alpha_{n-m+2,k}\\
&\dots\\
&z_1^{n} = \textstyle\sum_{k=1}^{n} p_k \quad \text{using the } \alpha_{m-1,k}\\
&z_1^{n} = \textstyle\sum_{k=1}^{n} p_k \quad \text{using the } \alpha_{m,k}\\
&z_2^{n} = \textstyle\sum_{k=2}^{n} p_k \quad \text{using the } \alpha_{m+1,k}\\
&z_3^{n} = \textstyle\sum_{k=3}^{n} p_k \quad \text{using the } \alpha_{m+2,k}\\
&\dots\\
&z_{n-m+1}^{n} = \textstyle\sum_{k=n-m+1}^{n} p_k \quad \text{using the } \alpha_{n,k}
\end{aligned}
$$

and the same for the summed variables w_r^s using the q_k. It is evident that the same variables z_1^n and w_1^n appear $2m-n$ times, so globally one has $\nu = n-(2m-n)+1 = 2(n-m)+1$ different variables z_r^s and the same number of different variables w_r^s. By examination of the equations (6.29), it turns out that once the dynamics of the summed variables is solved, the system can be integrated for the p_i and q_i,

so the effective dimension of the system is 2ν. Such number decreases when m is increased, i.e. when increasing the connectance. For the case of full coupling, when $m = (n+2)/2$, $\nu = n-1$. For $C = 1$, i.e. $m = n$, $\nu = 1$, and one recovers again the result presented in the equation (6.25).

In this specific model, increasing the connectance beyond C^{crit} leads in fact to a *reduction of the effective number of degrees of freedom.* When the number of degrees of freedom is not reduced, i.e. for $C < C^{\text{crit}}$, the percentage of regular orbits ρ decreases to a minimum when the fraction of direct couplings C_d is increased. At this point, ρ starts to increase because the number of dynamically relevant variables is decreased, while C_d cannot further increase.

We want to see now whether this special "ordered" way of filling has some influence on the behaviour of $\rho(C)$. Given a value for C, we then fill the matrix A by assigning random positions for the non-zero coefficients α_{ij}, still enforcing the constraint $\alpha_{ij} = \alpha_{ji}$. We take 100 different realizations for the matrices A and the curve $\rho(C)$ is averaged over the set of all the matrices. We calculate $\rho(C)$ for $n = 10, 20, 30, 50, 100$ and $\epsilon = 10^{-3}$. The results are plotted on Figure 6.18, to compare with the ordered case displayed on Figure 6.14, for which the dimensions n and the value of ϵ are the same. We note that there are no evident qualitative changes between the two cases. In fact, at least for ϵn^2 small, $\rho(0)$ must be equal to 1, and $\rho(1)$ very close to 1 independently of the way of filling the matrix, so a minimum must be present.

While in this non-ordered case there is no explicit formula to evaluate the fraction of direct couplings C_d, we can still count it directly once a matrix A is given. We then study the position of the minimum as a function of the fraction of couplings averaged over all the matrices, still indicated as C_d. We consider the case $n = 10$, for which the minimum can be clearly identified. We plot on Figure 6.19 the curve $\rho(C)$ along with the function $C_d(C)$. The minimum of ρ is reached when C_d becomes maximal (i.e. equal to 1), exactly for $C = 0.82$ (even if the maximum of C_d is not clearly distinguishable on the Figure). At this point the matrix A is not yet full on average, but increasing further the connectance adds simply multiple couplings, while C_d remains constant. Now the dominant effect becomes probably the reduction of degrees of freedom, which leads to a rapid increase of ρ with C until the matrix is full. To better investigate this phenomenon, on Figure 6.20 we plot ρ as a function of C_d. The circles correspond to the values $\rho(C_d)$ for which C_d increases from 0 to 1, and the triangles to the values $\rho(C_d)$ for which C_d is equal to 1. It is evident that $\rho(C_d)$ becomes minimal when C_d reaches 1. In conclusion, the indicator C_d is still the meaningful one to give information on the probability of chaoticity, independently of the filling procedure.

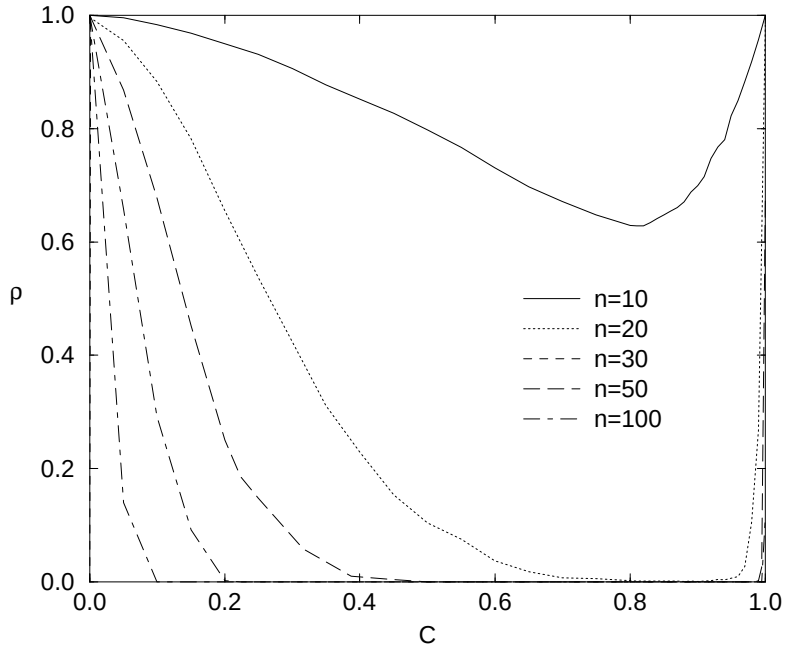

Figure 6.18: Probability of regularity ρ as a function of C for $n = 10, 20, 30, 50, 100$ and $\epsilon = 10^{-3}$ with non-ordered connectance.

6.5 The coupled Hamiltonian mean field model

We want to check now the influence of the connectance on a different model, for which the coefficients of a coupling matrix correspond exactly to the direct interactions among degrees of freedom.

Let's take the classical Hamiltonian mean field model [1] with a perturbative parameter ϵ

$$H = \sum_{j=1}^{n} \frac{p_j^2}{2} + \frac{\epsilon}{2n} \sum_{j=1}^{n} \sum_{k=1}^{n} (1 - \cos(q_j - q_k)). \tag{6.30}$$

Here all the degrees of freedom are coupled among them. This Hamiltonian describes a set of n particles moving on the unit circle, and has been used to model phase transitions. Let us introduce coupling coefficients α_{jk} which are still taken equal to

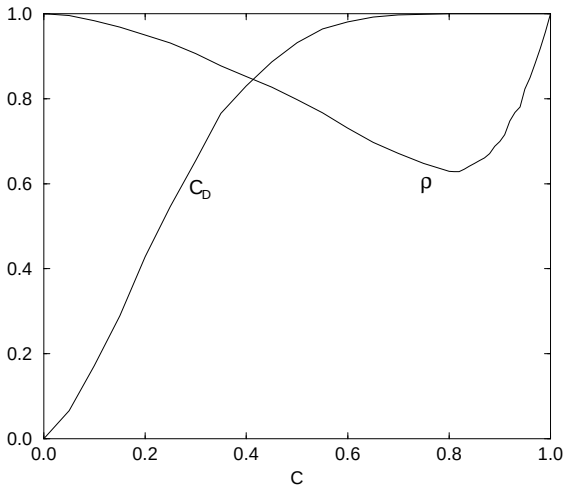

Figure 6.19: Probability of regularity ρ and fraction of direct couplings C_d as function of C for $n = 10$ and $\epsilon = 10^{-3}$ with non-ordered connectance.

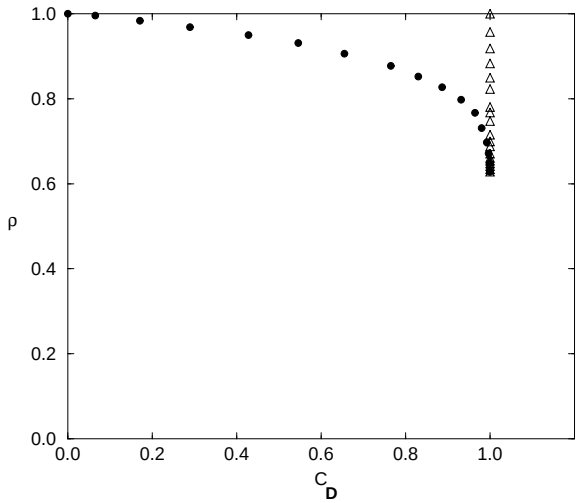

Figure 6.20: Probability of regularity ρ as a function of C_d for $n = 10$ and $\epsilon = 10^{-3}$ with non-ordered connectance.

0 or 1, and perturbative parameters depending on the particles:

$$H = \sum_{j=1}^{n} \frac{p_j^2}{2} + \frac{1}{2n} \sum_{j=1}^{n} \sum_{k=1}^{n} \epsilon_{jk} \cos[\alpha_{jk}(q_j - q_k)]. \tag{6.31}$$

When all the α_{jk} are equal to 1 the two models are the same. The equations of motion read

$$\begin{cases} \dfrac{\partial p_j}{\partial t} = & -\dfrac{1}{2n} \displaystyle\sum_{k=1}^{n} \epsilon_{jk}\alpha_{jk} \sin[\alpha_{jk}(q_j - q_k)] + \dfrac{1}{2n} \sum_{k=1}^{n} \epsilon_{kj}\alpha_{kj} \sin[\alpha_{kj}(q_k - q_j)] = \\ & -\dfrac{1}{n} \displaystyle\sum_{k=1}^{n} \epsilon_{jk}\alpha_{jk} \sin[\alpha_{jk}(q_j - q_k)] \\ \dfrac{\partial q_j}{\partial t} = & p_j \end{cases} \tag{6.32}$$

where the symmetries $\alpha_{ij} = \alpha_{ji}$ and $\epsilon_{ij} = \epsilon_{ji}$ have been imposed.

Once discretized the system with the leap-frog integrator as done for the first model, we obtain the following mapping:

$$\begin{cases} P_j = p_j - \dfrac{1}{n} \displaystyle\sum_{k=1}^{n} \alpha_{jk}\epsilon_{jk} \sin[\alpha_{jk}(q_j + p_j - q_k - p_k)]. \\ Q_j = q_j + p_j \ . \end{cases} \tag{6.33}$$

In this model it is clear that if $\alpha_{ij} = 0$ the i^{th} and the j^{th} degree of freedom are not directly coupled in the dynamical equations, while they are if $\alpha_{ij} = 1$.

We fill the coupling matrix the ordered way, with the same parameters taken for the Froeschlé model: $n = 10, 20, 30, 50, 100$ and $\epsilon = 10^{-3}$. The corresponding curves $\rho(C)$ are plotted on Figure 6.21. A first observation is that the probability of regularity still decreases with C, but more slowly compared to the first model. Second, no return to regularity appears when C approaches 1. We can explain the slower decrease by noticing that now the fraction of effective couplings C_d monotonically increases with C, and there is no intermediate situation in which the system is fully directly coupled. This means that as far as the dimension of the system cannot be reduced, it is really the indicator C_d which has a measurable effect on the dynamical properties. Moreover, the chaoticity increases quite regularly with this quantity. In this case there is no return to regularity because there is no simplification of the model at large C. In fact, the dynamical equations simplify when the system is fully coupled [1], but the model is still a real $2n$-dimensional one, and far from being quasi-integrable.

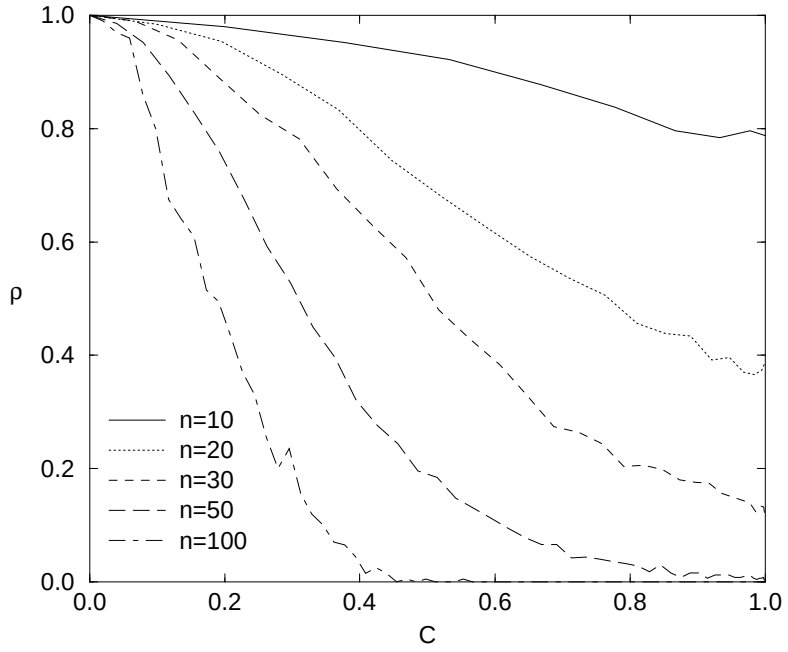

Figure 6.21: Probability of regularity ρ as a function of C for $n = 10, 20, 30, 50, 100$ and $\epsilon = 10^{-3}$ with ordered connectance in the Hamiltonian mean field model.

It turns out that the situation remains the same when the connectance is taken at random, still showing that for what concerns the probability of regularity the way of filling the matrix is not really important on average.

6.6 FLI charts and FLI histograms

To visualize the transition from order to chaos and the recover of regularity when the connectance is increased, we present here some FLI-charts in the action space calculated for the first model when $n = 20$ and $\epsilon = 10^{-3}$, for 10000 iterations. They are obtained by fixing $n - 2$ actions to given random values, and varying the remaining two. In fact, we explore a plane in a n-dimensional space, and give only a qualitative and limited representation of its full complexity. Nevertheless the results are consistent with the fact that regularity decreases with the connectance, reaches

a minimum and then increases again. Tori are represented in red by a value of the FLI close to $\log(10000) = 4$, while larger values correspond to chaotic orbits. We take an upper threshold for the FLI equal to $1.5\log(10000) = 6$, to which we set larger values. Four charts are plotted on Figure 6.22 for $C = 0.1, 0.195, 0, 284, 0.521$, the corresponding values of ρ being $0.928, 0.784, 0.546, 0.13$. One sees as the tori are progressively replaced by chaotic regions.

On Figure 6.23 we represent instead two charts corresponding to the regularity recover, for $C = 0.995$ and 1 ($\rho = 0.582, 0.996$). On the left panel one can see an example of transition between Chirikov and Nekhoroshev regimes, with some crossings among the main resonances. On the right panel an almost completely regular phase space is restored.

To give a statistical view of the transition between ordered and chaotic motions, histograms of the FLI are displayed on Figure 6.24 for the same values of the connectance. The histograms are calculated over a set of 5000 random initial conditions. One can see the transition from a situation dominated by tori (FLI distributed around the value 4) to a mainly chaotic regime (FLI equal to the threshold). When the regularity is recovered the FLI distribution, still centered around 4, presents a larger tail towards smaller values, indicating the presence of resonant orbits. They are in fact visible with blue color on the FLI-charts of Figure 6.23.

6.7 Conclusions

By comparison between two different models, we have shown that the connectance is a meaningful concept even when nonlinearity is taken into account. Nevertheless it has to be intended as *the fraction of direct dynamical couplings among degrees of freedom*, rather than the fraction of non-zero elements in a given matrix. This difference does not exist in the linear case, for which the two notions coincide. When the connectance is understood in such a way, we can say that the chaoticity increases with it until the system is fully coupled. It is not sufficient to add a few couplings to an uncoupled n-dimensional system to switch between regularity and chaoticity in a catastrophic way, at least when the perturbative parameters are small enough. When the model has some special features, such that its effective dimension is reduced by adding couplings, the number of such couplings is not anymore relevant. Instead, the amount of chaos depends on the true dimension of the system. These special situations are not captured by simple and economical statistical concepts like the connectance, but must be analysed case by case. This study can be a point of departure to apply the notion of connectance to ecology and economics in nonlinear models as well.

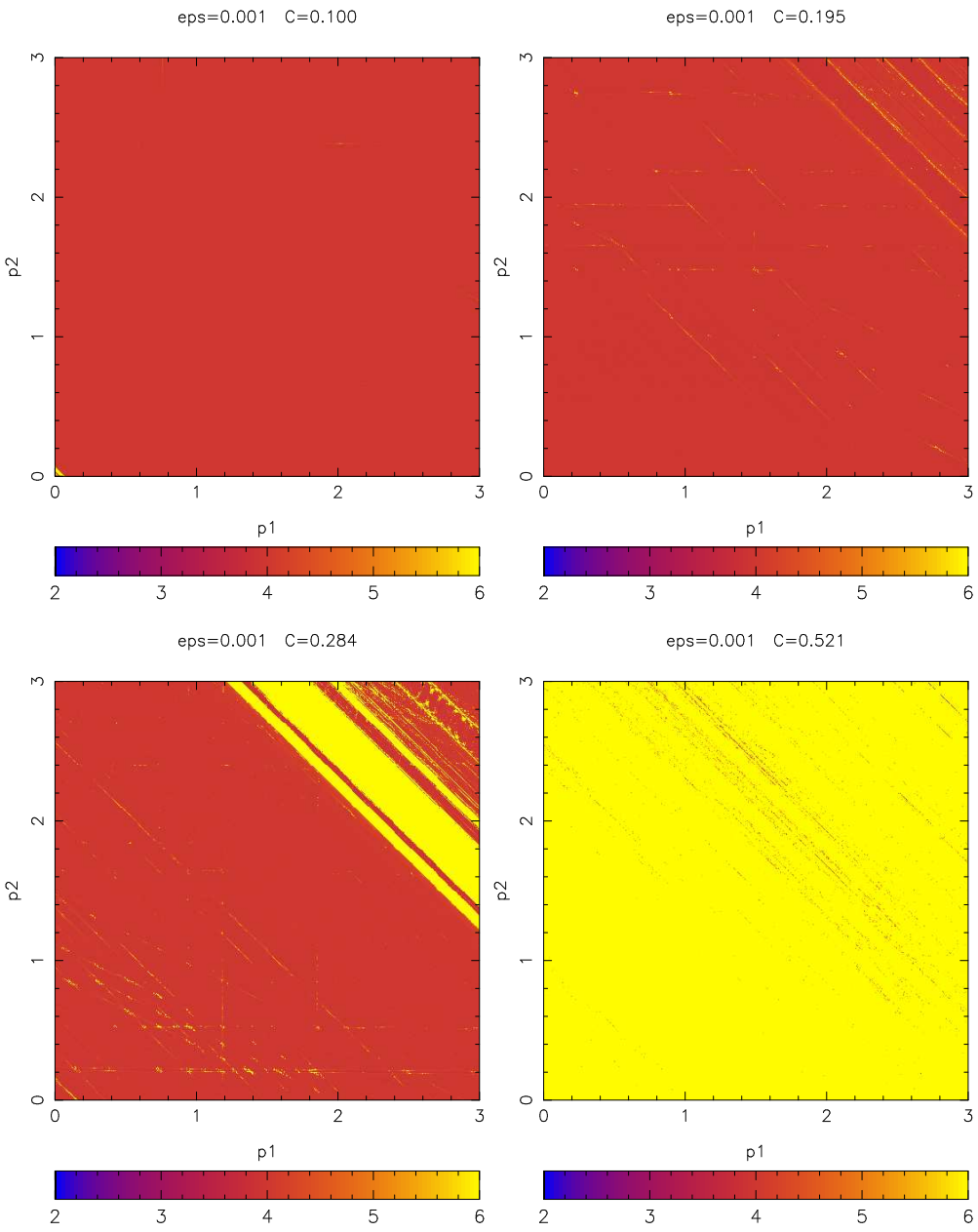

Figure 6.22: Graphical representation of the values of the FLI in the action plane (p_1, p_2) for the model (6.19) with $C = 0.1, 0.195, 0, 284, 0.521$.

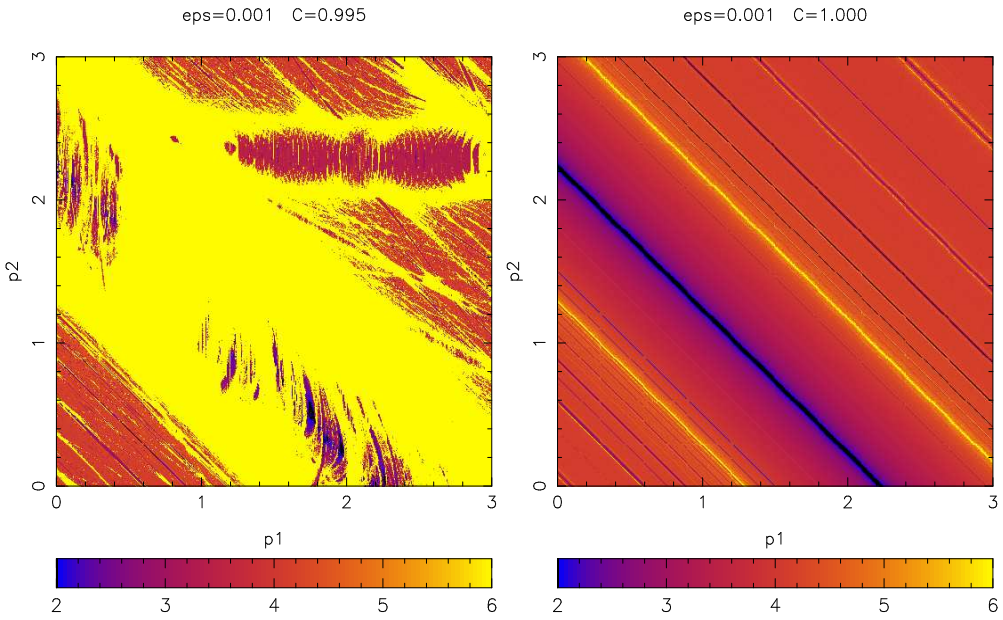

Figure 6.23: Graphical representation of the values of the FLI in the action plane (p_1, p_2) for the model (6.19) with $C = 0.995, 1.0$.

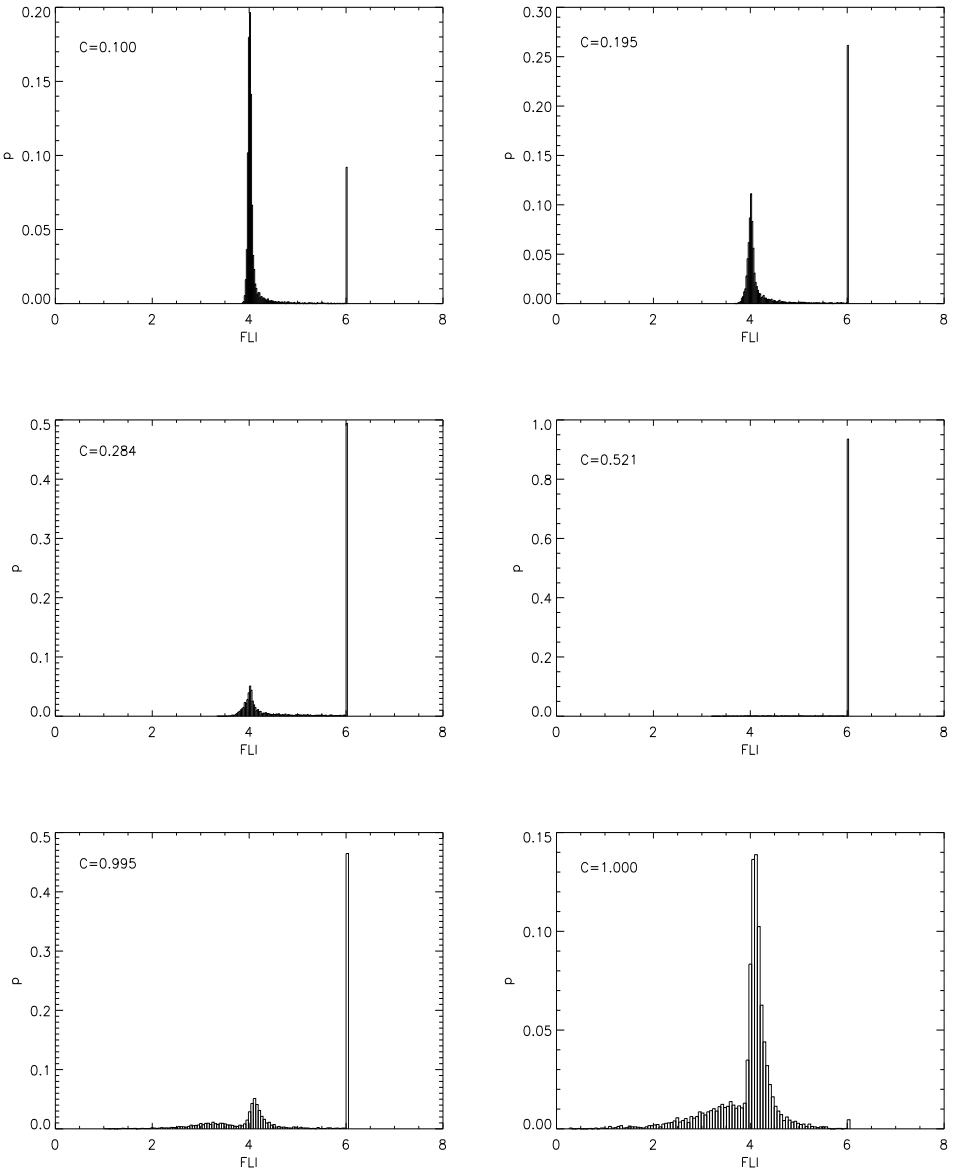

Figure 6.24: Histograms of the values of the FLI for the model (6.19) with $C = 0.1, 0.195, 0, 284, 0.521, 0.995, 1.0$. The probability $p(FLI)$ is plotted against the FLI value.

Bibliography

[1] Antoni, M. and Ruffo, S.: 1995, *Clustering and relaxation in Hamiltonian long-range dynamics*, Phys. Rev. E **52(3)**, pp. 2361–2374

[2] Arnold, V.I.: 1963, *Proof of a theorem by A.N. Kolmogorov on the invariance of quasi-periodic motions under small perturbations of the Hamiltonian*, Usp. Math. Nauk **18(5)**, pp. 13–40

[3] Arnold, V.I.: 1963, *A theorem of Liouville concerning integrable dynamics*, Siberian Math. J. **4**, pp. 471–474

[4] Benettin, G., Froeschlé, C. and Scheidecker, J.P.: 1979, *Kolmogorov entropy of a dynamical system with an increasing number of degrees of freedom*, Phys. Rev **A19**, pp. 2454–2460

[5] Benettin, G., Galgani, L. and Strelcyn, J.M.: 1976, *Kolmogorov entropy and numerical experiments*, Phys. Rev **A14**, pp. 2338

[6] Casartelli,M., Diana, E., Galgani, L. and Scotti, A.: 1976, *Numerical computation on a stochastic parameter related to the Kolmogorov entropy*, Phys. Rev. **A13**, pp. 1921–1925

[7] Celletti, A. and Froesché, C.: 1995, *On the determination of the stochasticity threshold of invariant curves*, Int. J. of Bif. and Chaos **5(6)**, pp. 1713–1719

[8] Celletti, A., Froesché, C. and Lega, E.: 1996, *Determination of the frequency vector in the four dimensional standard mapping*, Int. J. of Bif. and Chaos **6(6)**, pp. 1579–1585

[9] Chirikov, B.V.: 1979, *An universal instability of many dimensional oscillator systems*, Phys. Rep. **52**, pp. 263–379

[10] Cosentino, M., Laveder, D., Lega, E. and Froeschlé, C.: 2006, *Connectance and stability of dynamical systems*, in "Detection, measure and consequences of chaos. Applications to dynamics of celestial bodies", Lecture notes in Physics (Springer-Verlag), submitted

[11] Cosentino, M., Lega, E. and Froeschlé, C.: 2007, *Rapport sur "Organisation des marchés en lignes: interactions cognitives et émergence"*, Rapport finale du "Programme Complexité en SHS", in press.

[12] Daniels, J. and Mackay, A.L.: 1974, *The stability of connected linear systems*, Nature **251**, pp. 49–50

[13] De Luca, J., Lichtenberg, A.J. and Ruffo, S.: 1995, *Energy transition and time scale to equipartition in the Fermi-Pasta-Ulam oscillator chain*, Phys. Rev. E **51**, pp. 2877–2884

[14] Fermi, E., Pasta, J. and Ulam, S.: 1955, *Studies of nonlinear problems*, Los Alamos document LA-1940

[15] Froeschlé, C.: 1970, *A numerical study of the stochasticity of dynamical systems with two degrees of freedom*, Astron. Astrophys. **9**, pp. 15–23

[16] Froeschlé, C. and Scheidecker, J.P.: 1975, *Stochasticity of dynamical system with increasing number of degrees of freedom*, Phys. Rev **A12**, pp. 2137–2143

[17] Froeschlé, C.: 1978, *Connectance of dynamical systems with increasing number of degrees of freedom*, Phys. Rev **A18**, pp. 277–281

[18] Froeschlé, C., Gonczi, R. and Lega, E.: 1997, *The fast Lyapunov indicator: a simple tool to detect weak chaos. Application to the structure of the main asteroidal belt*, Planetary and Space Science **45**, pp. 881–886

[19] Froeschlé, C. and Lega, E.: 1998, *Weak chaos and diffusion in Hamiltonian systems. From Nekhoroshev to Kirkwood*, in "The Dynamics of small bodies in the Solar system: a major key to Solar system studies", A.E. Roy eds., NATO/ASI series

[20] Froeschlé, C., Lega, E. and Lohinger, E.: 2000, *Connectance and Stability. Application to linear and nonlinear dynamical systems with increasing number of degrees of freedom*, Nonlinear Phenomena in Complex Systems **3(3)**, pp. 247–252

[21] Froeschlé, C. and Longhi, A.: 1987, *Connectance et stabilité locale d'un équilibre général*, Economie appliquée **XL**, pp. 49–78

[22] Galgani, L. and Giorgilli, A.: 2005, *Recent results on the Fermi-Pasta-Ulam problem*, Journal of Mathematical Sciences **128(2)**, pp. 2761–2766

[23] Gardner, M.R. and Ashby , W.R.: 1970, *Connectance of large dynamical (cybernetic) systems: critical values for stability*, Nature **228**, p. 784

[24] Geršgorin, S.: 1931, *Über die abgrenzung der eigenwerte einer matrix*, Isv. Akad Nauk USSR Ser. Mat. **7**, pp. 749–754

[25] Giansanti, A., Pettini, M. and Vulpiani, A.: 1985, *Connectance and equipartition thresholds in Hamiltonian systems*, Phys. Lett. **109A/9**, pp. 451–453

[26] Guzzo, M., Lega, E. and Froeschlé, C.: 2002, *On the numerical detection of the effective stability of chaotic motions in quasi-integrable systems*, Physica D **106**, pp. 1–25

[27] Hénon, M., private communication

[28] Hénon, M.: 1969, *Numerical study of quadratic area-preserving mappings*, Quarterly of Appl. Math. **27**, pp. 291–312

[29] Hénon, M.: 1974, *Integrals of the Toda Lattice*, Phys. Rev. **B 9**, pp. 1921–1925

[30] Hénon, M. and Heiles, C.: 1964, *The applicability of the third integral of motion: some numerical experiments*, Astron. J. **1**, pp. 73–79

[31] Hirsch, M.W. and Smale, S.: 1974, *Differential equation, dynamical systems, and linear Algebra*, (Academic Press, San Diego, CA)

[32] Izrailev, F.M. and Chirikov, B.V.: 1966, *Statistic properties of a nonlinear string*, Dokl. Akad. Nauk. SSSR **166**, pp. 57–59

[33] Kolmogorov, A.N.: 1954, *On the conservation of conditionally periodic motions under small perturbation of the Hamiltonian*, Dokl. Akad. Nauk. SSSR **98**, p. 524

[34] Laskar, J.: 1988, *Secular evolution of the Solar system over 10 million years*, Astron. Astrophys. **198**, pp. 341–362

[35] Laskar, J., Froeschlé, C. and Celletti, A.: 1992, *The measure of chaos by the numerical analysis of the fundamental frequencies. Application to the standard mapping*, Physica D **56**, p. 253

[36] Laskar, J.: 1993, *Frequency analysis for multi-dimensional systems. Global dynamics and diffusion*, Physica D **67**, pp. 257–281

[37] Laveder, D., Cosentino, M., Lega, E. and Froeschlé, C.: *The effect of the connectance on nonlinear systems with increasing number of degrees of freedom*, in prep.

[38] Lega, E. and Froeschlé, C.: 1996, *Numerical investigations of the structure around an invariant KAM torus using the frequency map analysis*, Physica D **95**, pp. 97–106

[39] Lega, E. and Froeschlé, C.: 2001, *On the relationship between fast Lyapunov indicator and periodic orbits for symplectic mappings*, Celest. Mech. Dyn. Astr. **81**, pp. 129–147

[40] Martens, B.: 1987, *Connectance in linear and Volterra systems*, Ecological Modelling, **35**, pp. 157–163

[41] May, R.M.: 1972, *Will a large complex system be stable?*, Nature **238**, pp. 413–414

[42] May, R.M.: 1999, *Unanswered questions in ecology*, Phyl. Trans. R. Soc. London B **354**, pp. 1951–1959

[43] Mckenzie, L.: 1959, *Matrices with dominant diagonals and economic theory*, Mathematical Methods in the Social Sciences, eds. K. J. Arrow, L. S. Karlin, and L. P. Suppes (Stanford University Press, Stanford), pp. 47–62

[44] Milani, A. and Knezevic, Z.: 1990, *Secular perturbation theory and computation of asteroids proper elements*, Celestial Mechanics **49**, pp. 347–411

[45] Morbidelli, A. and Giorgilli, A.: 1995, *Superexponential stability of KAM tori*, J. Stat. Phys. **78**, pp. 1607–1617

[46] Moser, J.K.: 1958, *New aspects in the theory of stability of Hamiltonian systems*, Comm. on Pure and Appl. Math **11**, pp. 81–114

[47] Nekhoroshev, N.N.: 1977, *Exponential estimates of stability time of near-integrable hamiltonian systems*, Russ. Math. Surveys **32**, pp. 1–65

[48] Oseledec, V.I.: 1968, *A multiplicative ergodic theorem: the Lyapunov characteristic numbers of dynamical systems*, Trans. Moscov Mat. Soc. **19**, p. 197

[49] Paladin, G. and Vulpiani, A.: 1985, *The role of connectance on the chaoticity of Hamiltonian Systems*, Phys. Lett. **111/7**, pp. 333–335

[50] Poincaré, H.: 1892, *Les méthodes nouvelles de la mécanique céleste*, (Gauthier-Villar, Paris)

[51] Šiljak D.D.: 1978, *Large-scale dynamic systems. Stability and structure*, (North Holland, New York), Chap. 4, p. 230

[52] Stoka, M: 1981, *Corso di Geometria* (Cedam, Padova)

[53] Varga, R.: 2004, *Geršgorin and his circles* (Springer-Verlag, Berlin)

[54] Wiggins, S.: 1988, *Global bifurcations and chaos* (Springer-Verlag, New York)

[55] Wilmers, C., Sinha, S. and Brede, M.: 2000, *Evolving stable ecological networks*, Proceeding of "2000 Complex Systems Summer School", Santa Fe (USA)

Ringraziamenti

Desidero ringraziare il Prof Milani per i suoi prezioni consigli e per aver accettato il ruolo di Supervisor della tesi.

Un grazie al Prof Claude Froeschlé che mi ha accolto una seconda volta all'Osservatorio della Costa Azzurra e mi ha permesso di portare a termine il mio travagliato lavoro di tesi.

Un grazie speciale ai miei due codirettori, Dimitri e Elena.

In particolare ringrazio mio marito Dimitri per avermi scientificamente guidata giorno dopo giorno, accompagnata in maniera spropositata e sostenuta con amore, pazienza e tenacia...insomma senza di lui questa tesi non ci sarebbe!

Ringrazio Elena per il suo prezioso aiuto e per aver saputo appoggiare fraternamente le mie scelte anche se sembravano un po' pazze! A volte la testa dura aiuta...

Un grazie va ai miei genitori che ancora una volta mi sono stati vicino e mi hanno sostenuta in maniera esemplare in questo lungo e faticoso cammino.

Grazie a Eli, Fede e alla mia figlioccia Martina per essermi stati vicini nonostante la lontananza!

Ringrazio Ire e Dani, miei sostenitori e incoraggiatori morali e materiali nella mia avventura pisana.

Grazie a Fra' e Nicla...quante mangiate e quante risate in casa carducce!

Grazie a Mario, Elisa, Gianpaolo e Francesca per avermi accolto come figlia e sorella durante la mia breve permanenza a Padova.

Ringrazio Fathi per le sue lunghe chiacchierate "filosofiche" e per le sue "corte" passeggiate in montagna!

Un grazie di cuore va a Mara per avermi spalancato le porte dell'insegnamento! Quando il gioco si fa duro...i duri non mollano! Grazie Collega!

Ringrazio Eloisa per avermi sostenuta moralmente durante la mia permanenza a Padova.

Ringrazio Renza e Claudio per avermi incoraggiata e sostenuta in questa mia avventura!

Un grazie collettivo (ma non meno importante) a Sonia (che bei pranzetti!), Cri, Chiara di Coldirodi, gli amici pisani, gli amici di Sanremo e di Biella, gli amici della Fraternità, Alejandra, Don Pino e Don Camillo.